

Politecnico di Torino

Corso di Laurea Magistrale in Ingegneria dell'Autoveicolo A.a. 2024/2025 Sessione di Laurea Ottobre 2025

Mechanical characterisation for the development of advanced tyres in the motorcycle sector

Relatori:

Gianfranco Genta Giacomo Maculotti Roberto Cagliero Candidato:

Manuel Alberto Barale

Ringraziamenti

Vorrei ringraziare tutte le persone che mi sono state vicine durante gli anni universitari e durante la scrittura di questa tesi.

Innanzitutto ringrazio LBN Ricerca per avermi permesso di svolgere il tirocinio e la tesi in azienda. In particolare, ringrazio il tutor aziendale Roberto e il collega Giulio per tutti gli insegnamenti utili che mi hanno fornito durante il tirocinio in LBN Ricerca e per i momenti divertenti passati insieme durante le pause caffè.

Ringrazio il Professor Genta per avermi dato la possibilità di svolgere questa tesi e per avermi seguito durante la scrittura.

Ringrazio mia mamma Milena e mio papà Davide per avermi permesso sempre di studiare e di inseguire i miei sogni, mio fratello Andrea, le mie nonne Pai e Gegia, mio nonno Beppe e tutto il resto della mia famiglia per essere sempre stati presenti e per aver creduto in me.

Un ringraziamento speciale va alla mia ragazza Rubi, che da quando ci conosciamo mi ha sempre supportato e ha sempre fatto il tifo per me.

Infine, ringrazio i miei amici per i bei momenti passati insieme durante questi anni.

Manuel Alberto Barale

Table of contents

1	Intro	duction	5
	1.1	Companies	5
	1.2	Aim of the thesis	5
2	Tyre	s in the motorcycle sector	7
	2.1	Inner tube tyre	7
	2.2	Tubeless tyre	8
	2.3	Non-pneumatic tyre	9
	2.4	Tyre mousse	16
	2.5	Company proposal	17
3	Mec	hanical characterisation	18
	3.1	Hardness Shore test	18
	3.2	Tensile test	20
	3.3	Tear test	22
4	Expe	erimental set up	26
	4.1	Elastomeric compound	26
	4.2	Laboratory specimens and oven	26
	4.3	Hardness Shore test	29
	4.4	Tensile test	29
	4.5	Tear test	31
5	Data analysis		32
	5.1	Statistical methodologies	32
	5.1.1	Descriptive statistics	32
	5.1.2	Outlier identification	33
	5.1.3	ANOVA	34
	5.1.4	Response surface regression	37
	5.2	Hardness Shore test	38
	5.2.1	Descriptive statistics	38
	5.2.2	Outlier identification	40
	5.2.3	ANOVA	41
	5.2.4	Response surface regression	42
	5.3	Tensile test: stress at break.	47
	5.3.1	Descriptive statistics	47
	5.3.2	Outlier identification	49
	5.3.3	ANOVA	50
	5.4	Tensile test: strain at break	51
	5.4.1	Descriptive statistics	51
	5.4.2	Outlier identification	53
	5.4.3	ANOVA	54

	5.4.4	Response surface regression	55
	5.5 T	Cear test: tear strength at break	60
	5.5.1	Descriptive statistics	60
	5.5.2	Outlier identification	62
	5.5.3	ANOVA	63
	5.5.4	Response surface regression	64
6	Post-c	uring effect analysis	69
	6.1 F	Hardness Shore test	69
	6.1.1	Descriptive statistics	69
	6.1.2	Outlier identification	70
	6.1.3	ANOVA	70
	6.2 T	Fensile test: stress at break	72
	6.2.1	Descriptive statistics	72
	6.2.2	Outlier identification	
	6.2.3	ANOVA	74
	6.3 T	ensile test: strain at break	75
	6.3.1	Descriptive statistics	75
	6.3.2	Outlier identification	76
	6.3.3	ANOVA	77
	6.4 T	Cear test: tear strength at break	78
	6.4.1	Descriptive statistics	78
	6.4.2	Outlier identification	79
	6.4.3	ANOVA	80
7	Conclu	usions	82
R	Refere	ences	83

1 Introduction

1.1 Companies

This Master's thesis was carried out in the LBN Ricerca laboratory, which is a company associated with AGLA Power Transmission. The specimens of elastomers used for the laboratory tests are produced by Bottino Girardi.

LBN Ricerca is a multi-disciplinary research group dedicated to the study of correlations between production processes and advanced materials through the integration of laboratory tests with finite element analysis and experiments on pilot plants or specific test benches. L.B.N. RICERCA S.r.l. was established in July 2002 with the purchase of a pre-existing research laboratory founded in 1994 in Avigliana (TO). Today the laboratory is a point of reference for any problem concerning the introduction of new materials and the definition of innovative production processes in the following branches of activity:

- production systems for plastic deformation of metallic materials;
- development of special production machines and systems;
- industrial automation;
- testing, inspections and trials.

A peculiarity of the LBN Ricerca laboratory is the presence of specific test benches for tests accredited by the main players in the international automotive market (VOLKSWAGEN-AUDI, PSA GROUP, FCA, MASERATI). [1]

AGLA Power Transmission was founded in 1962. The company is specialized in sheet metal stamping and component assembly. Today AGLA is a global leader in cold plastic deformation of steel, expertise that translates into innovative technological solutions dedicated to components for engines and automatic transmissions. AGLA is known throughout the world for its torsional vibration dampers and pulleys, bestsellers in a range that includes components for automatic transmissions, flexplates and other stamped components. [2]

Fondazione Bottino Girardi & C was founded in 1957 in Turin. The production, initially focused on motorcycle components, extended to automotive components, metal and rubber components, rubber bushings as vibration isolators, filter gaskets and spare parts for Piaggio and Fiat. The headquarters moved to Moncalieri (TO). Today Bottino Girardi boasts a large-scale production of gaskets, o-rings for the automotive sector, shock absorbers and torsional vibration dampers, filters, soundproof bumpers, and a series of rubber components for windshields, handlebars and eyelets. The company also provides solutions with high-quality materials for commercial vehicles and large cars, such as tractors and commercial vehicles; standardized or highly customized solutions based on customer requests or drawings. The products made of NBR, HNBR, NR, SBR, EACM, EPDM, VMQ, FVMQ, EAM, FKM are part of a process that starts from a well-defined preventive analysis of the customer's need or design, up to an accurate design analysis according to highly technological standards, ending with a whole series of proposals to submit to the customer. [3]

1.2 Aim of the thesis

The aim of this Master's thesis is to investigate how the mechanical properties of elastomers change depending on the position of the specimen inside the die and inside the oven. Indeed, to produce the elastomers, the elastomeric compound is vulcanised inside a die and subsequently post-cured inside an oven. As the temperature inside the oven is not homogeneous, the mechanical properties, such as hardness, tensile stress and strain at break and tear strength at break, can be affected by the position of the elastomer inside the oven. Moreover, the post-curing effect is analysed by comparing the mechanical properties of the elastomers before and after entering the oven.

To measure the mechanical properties of the elastomers, different tests are carried out in laboratory following the corresponding norms: hardness Shore test, tensile test and tear test. After collecting the data, they are analysed using statistics tools.

The elastomers analysed in this thesis will be used by AGLA Power Transmission to produce advanced tyres for motorcycle sector, in particular for enduro races, without an inner tube, with an anti-puncture system and able to guarantee a long life with a view to the circular economy.

2 Tyres in the motorcycle sector

2.1 Inner tube tyre

There are different types of tyres. The simplest type is the inner tube tyre, which can be seen in Figure 2.1.1. It is composed mainly by two parts: the carcass, which is the external part and stays in contact with the ground, and the inner tube, which is the internal part and contains pressurized air. The air pressure is variable depending on the scenario and on the type of vehicle. This type of tyre is very good at staying inflated even with cracked or mildly bent rims and it is the cheapest solution. On the other hand, it suffers from punctures and if there is the necessity to be repaired, it is needed to remove the carcass in order to gain access to the inner tube.



Figure 2.1.1: Inner tube tyre

The inner tube is made of butyl rubber, also known as Isobutylene-isoprene (IIR), which is a synthetic rubber, a copolymer of isobutylene with isoprene. Butyl rubber is produced by polymerization of about 98% of isobutylene with about 2% of isoprene. Structurally, polyisobutylene resembles polypropylene, but has two methyl groups substituted on every other carbon atom, rather than one. Polyisobutylene is a colorless to light yellow viscoelastic material. It is generally odorless and tasteless, though it may exhibit a slight characteristic odor. Butyl has outstanding resistance to attack by oxygen and ozone, and good chemical resistance to a large number of organic and inorganic media. Butyl rubber is the only known elastomer that is impervious to gases. It is flexible, with good room temperature damping characteristics. Figure 2.1.2 shows the atomic structure of this polymer. [4]

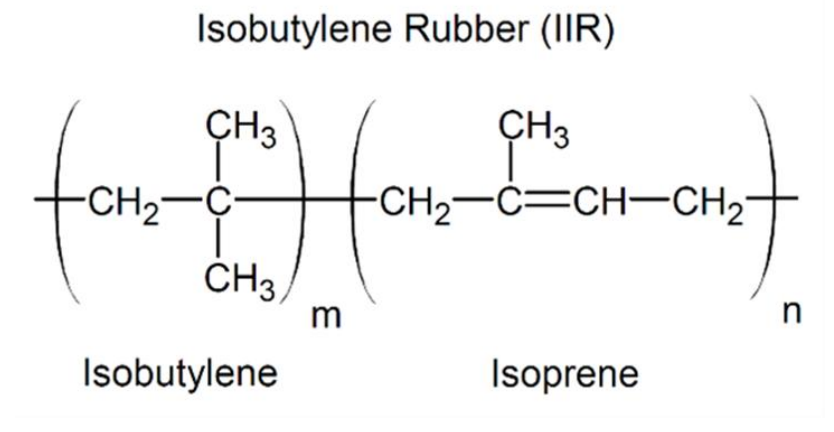


Figure 2.1.2: Atomic structure of butyl rubber

2.2 Tubeless tyre

Another type of tyre which is more popular nowadays is the tubeless tyre. This type of tyre, which is showed in Figure 2.2.1, does not need the inner tube because it has continuous ribs moulded integrally into the bead of the tyre that are forced by air pressure into a flange on the metal rim of the wheel, sealing the tyre to the rim. Traditional designs of pneumatic tyres required a separate inner tube which could fail for a number of reasons, such as incorrect tyre fit, friction between the tyre wall and inner tube generating excess heat, or a puncture. Tubeless tyre technology does away with the need for an inner tube thereby increasing safety. In a tubeless tyre, the tyre and the rim of the wheel form an airtight seal, with the valve being directly mounted on the rim. If a tubeless tyre gets a small puncture, air escapes only through the hole, leading to a gentle deflation. Conversely, a tubed tyre, with an inner tube, could burst like a balloon, leading to deflation of the tyre which could result in sudden loss of control of the vehicle. Tubeless tyres provide several advantages, such as remaining operational at lower air pressure. Due to their high width, tubeless tyres are less likely to get punctured than regular tube tyres. Air leakage is also reduced as the rubber in the tyre keeps the air trapped for longer, giving an extra time to drive safely and pull over. In addition, mending a tubeless tyre is easier than a traditional one: a simple liquid sealant poured over the puncture is often enough to patch it. Furthermore, the higher air pressure inside a tubeless tyre provides more stability and comfort while driving. Lastly, the lack of a tube also boosts fuel efficiency due to reduced tyre friction.



Figure 2.2.1: Tubeless tyre

Tyre sealant is made of glycol or latex. Glycol, which is showed in Figure 2.2.2, is a water based substance made of ethylene or propylene, while latex is a non-water based substance. Latex has a limited life span and dries in the tyre after about 15,000 km, it adheres to the tyre and the rim and it's often impossible to remove. Propylene glycol has an indefinite shelf life and can be reused. It is easily washed out with water. [5]

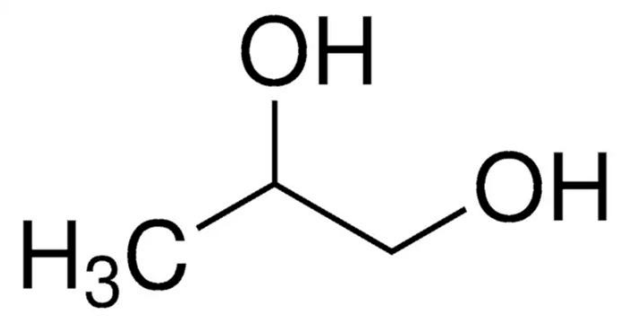


Figure 2.2.2: Atomic structure of glycol

2.3 Non-pneumatic tyre

An innovative type of tyre is the non-pneumatic tyre (NPT), also known as an airless tyre, which represents a cutting-edge technology designed to replace traditional pneumatic tyres. Pneumatic tyres suffer from common drawbacks, with the most critical being the risk of getting flattened or damaged during use. If a flat occurs while driving, it can hinder the vehicle from reaching its destination safely, potentially causing catastrophic damage and endangering the lives and property of passengers. Although many vehicles are equipped with a spare tyre as a precaution, there is still a risk involved in replacing it during critical situations. Moreover, traditional tyre solutions such as run flat systems and temporary repair methods often fall short in heavy-duty usage scenarios. Therefore, NPTs have attracted significant interest from various tyre manufacturers, offering a promising solution for demanding applications.

The core concept behind NPTs is to substitute the air in a pneumatic tyre with a polymeric spoke structure, usually constructed from poly urethane (PU). NPTs typically consist of three key components:

- 1) an elastomeric shear band;
- 2) a polymeric spoke structure;
- 3) a steel hub.

The shear band resembles a solid tyre composed of rubber and layers of steel belts/cables. These layers confine the elastomer from expanding in the circumferential direction, causing the rubber to deform mainly in shear: thus the term "shear band". Its primary function is to support the load of the vehicle by mimicking the inflation pressure in a pneumatic tyre. The spokes play a crucial role in transferring the load of the vehicle from the steel hub to the shear band. Additionally, the spoke structure determines the deformation and load distribution characteristics of the NPT. It is important to design the spoke structure meticulously because it significantly influences the performance and behaviour of NPTs. [6]

The companies who have worked in making airless tyres are: Michelin, Uniroyal, Yokohama, Bridgestone, Britek, Toyo, Hankook, Polaris, Amerityre, Boeing, Resilient Technologies. These tyres cannot be used for high speeds. The Uptis (Unique Puncture-Proof Tyre System) technology developed by Michelin (Figure 2.3.1) is an example of the utilization of airless tyre for automobiles.

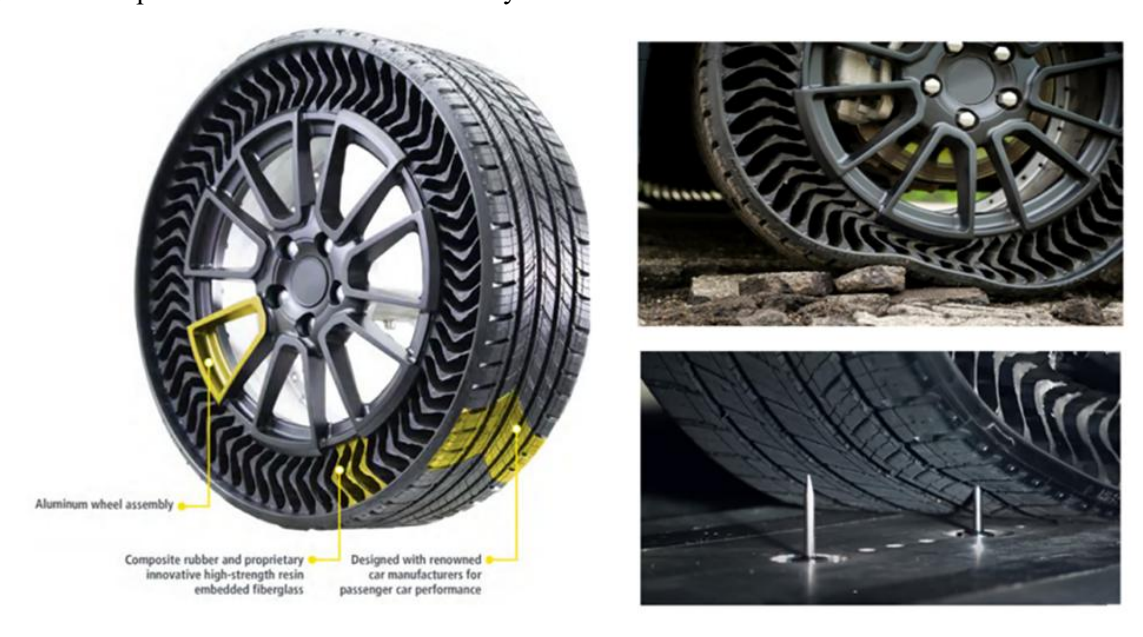


Figure 2.3.1: Michelin Uptis

Michelin has launched its Tweel family of products (Figure 2.3.2) that has non-pneumatic tyres that can be used in light weight construction equipment. They can be used in a broad range of surfaces. The unique design will give better stability and reduces the fatigue to driver due to bounce back effects and these tyres lasts 2–3 rimes longer than conventional pneumatic tyres.



Figure 2.3.2: Michelin X Tweel

Michelin is now working towards producing 3D printed airless tyre using completely biodegradable material (Figure 2.3.3) and bi-inspired design. Also, it has onboard sensors to collect real time tyre data.

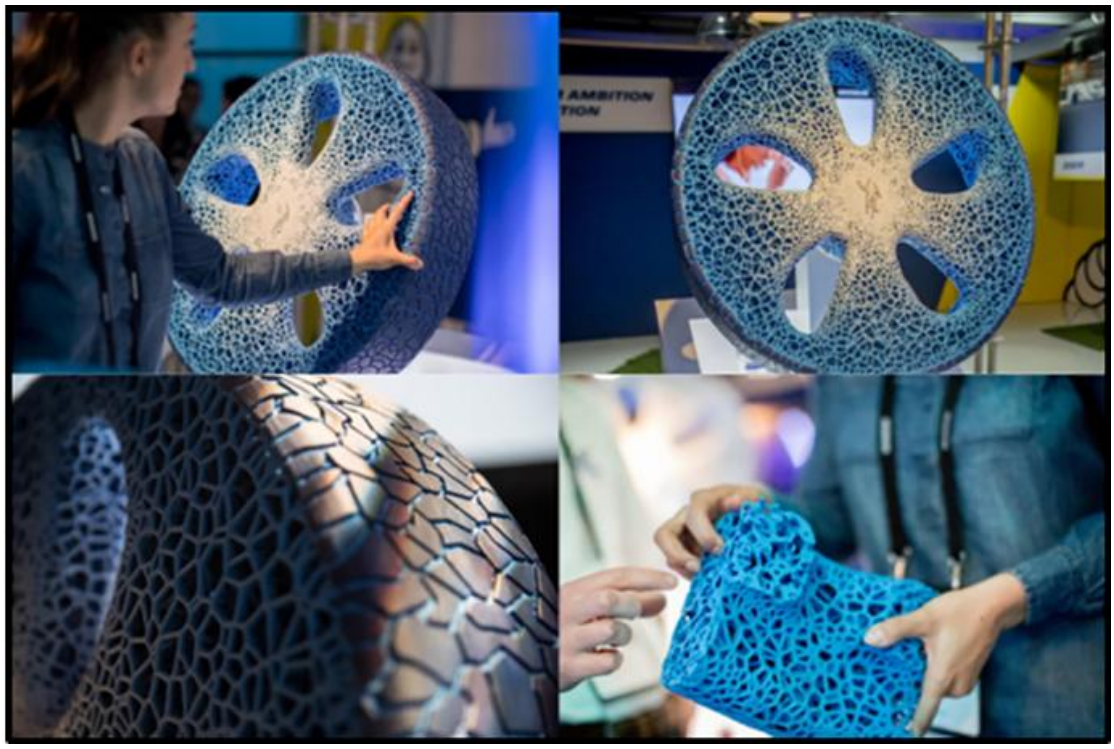


Figure 2.3.3: Michelin 3D Printed Concept tyre

Synthetic bio rubbers are made from ethanol which is derived from the sugar that is extracted from molasses. Goodyear 3D printed eco-friendly airless tyres (Figure 2.3.4) from recycled powder rubber from old tyres using selective laser sintering technique. Goodyear unveiled its latest concept tyre that has living moss that grows in the side walls, and it grows by doing photosynthesis and thus it takes carbon dioxide as intake and it exhales oxy gen. If this concept is used in all the vehicles in a city like Paris, 4000 tons of CO₂ will be converted into 3000 tons of oxygen.

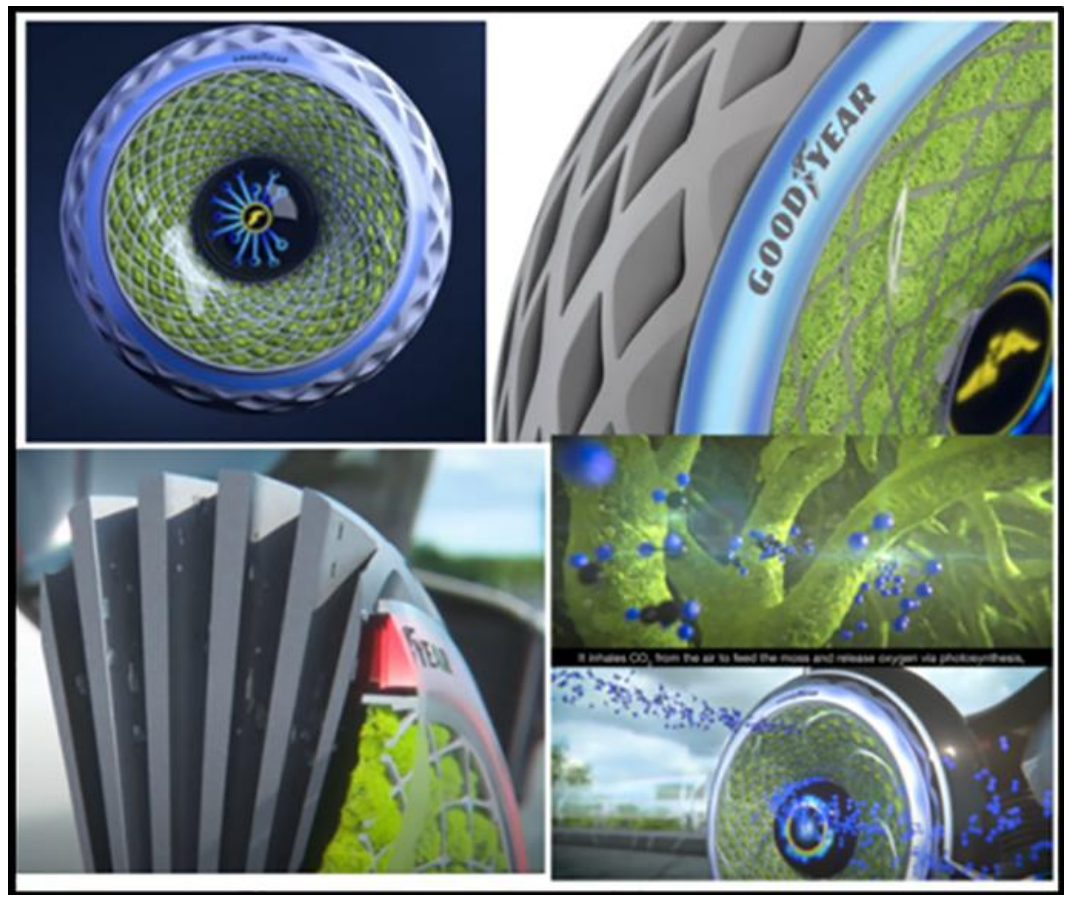


Figure 2.3.4: Goodyear 3D Printed Concept tyre

BigRep, a 3D printer manufacturer based in Germany has 3D printed airless tyres for bicycles Figure 2.3.5. This tyre prototype utilizes BigRep's Pro FLEX filament which has high durability and temperature resistance. These tyres have bio-inspired honeycomb structures, that reduces the weight by 40% when compared to conventional rubber tyres. This weight reduction is a significant advantage to the fuel economy of any vehicle. Also, the extreme durability of airless tyres will bring smile in the face of the user due to big cost savings.



Figure 2.3.5: Bigrep 3D printed Bicycle tyre

Polaris, the largest ATV manufacturer has used airless tyres in its military grade ATV as shown in Figure 2.3.6 and demonstrated the awesome capacity of the airless tyres. They keep on running 8000 km distance even after taking bursts from AK47 and it travelled 1800 km after inserting a railroad spike. Hence Polaris decided to focus on airless tyres for military applications.



Figure 2.3.6: Airless tyres in Polaris Military grade ATV

The UK tyre manufacturer Kumho Tyres won IDEA award, 2017 for its concept tyre called BON (Born on nature) with its bio-inspired design (Figure 2.3.7). The manufacturer has won the Platinum A'Design award 2015 for its Maxpolo tyre (Figure 2.3.8a) that has treads to self-adjust for all weather conditions from wet to snow. It has both 3D grooves and circumferential grooves which pumps the water from the contact patch. In slippery roads spikes will be unveiled to decrease the dangers faced due to ice and snow. The same manufacturer collaborated with Ssang Yong Motor Company and surprised the IAA Motorshow 2015 with a tyre model called Smasher (Figure 2.3.8b). The tyre has optimal designs meant to be used in all extreme weather conditions. It has suction plates which helps the vehicle to ascend and descend steep slopes. It also has tread blocks in the shape of grinder, which crushes the uneven areas of the terrain and helps the vehicle to drive through very tough terrains.



(a) (b)

Figure 2.3.8: (a) Maxpolo, (b) Smasher

Kenda Rubber Industrial Co., Ltd has launched an airless tyre (Airless tyre 3003) for the Asian market for lawn mowers. It has spokes that are flexible, and they will absorb all the impact loads and the design pattern used gives better durability and stability (Figure 2.3.9).



Figure 2.3.9: Airless tyres by Kenda Rubber Industrial Co., Ltd

Autovector has sustainable transportation as its mission statement and it launched "Absolut Airless". It has spokes made of elastomers in the longitudinal direction, acting as beams between the rigid spoke in outer loop and the rim spokes in the inner loop as shown in Figure 2.3.10. This design will always make the beams to be in tension unlike the tension-compression cyclic load, which gives increased cushioning.



Figure 2.3.10: Absolut Airless

NEXEN Tyre South Korea has introduced a bio-inspired airless tyre called Dandelion that was designed like a flower. It has 72 pins that are cantered from a spherical nucleus as shown in Figure 2.3.11. Each pin moves independently vertically upwards and downwards based on the road condition, this arrangement allows the tyre to be used in any rough terrain. This design has won the 2019 Reddot award.

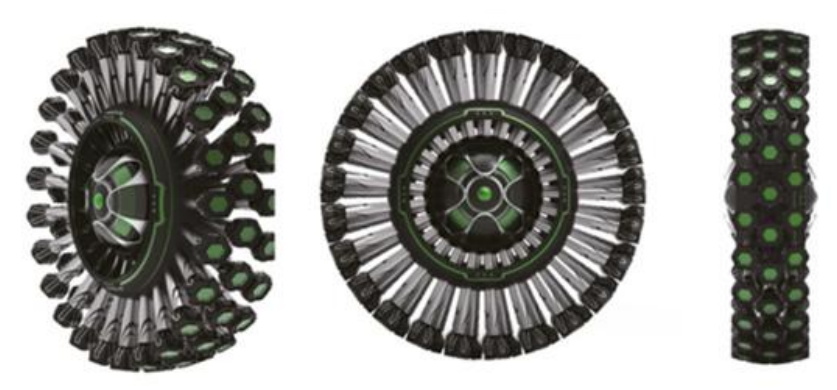


Figure 2.3.11: Dandelion

Bretek has launched a separate segment of Energy Return Wheels (ERW) which transforms the elastic potential energy that was stored in the wheel into useful forward momentum. It has a series of carbon fibre reinforced rods that has stretched rubber: this rod can be adjusted to vary the cushioning levels based on the terrain (Figure 2.3.12). [7]



Figure 2.3.12: ERW

The vertical mechanical performance of non-pneumatic tyres is related to their load capacity. Most non-pneumatic tyres adopt the top load-bearing mechanism, and each component participates in load bearing with uniform stress. However, rigid non-pneumatic tyres, such as honeycomb tyres, continue to use the bottom load bearing mode and rely on the grounding area. Compared with ordinary pneumatic tyres, the vertical stiffness of non-pneumatic tyres is greater and negatively related to the load. Theoretically, due to the special support structure of non-pneumatic tyres, their load-carrying capacity is greater than that of pneumatic tyres. The shape, thickness, and density of the spokes of the support structure significantly affect the vertical stiffness of non-pneumatic tyres. Proper vertical stiffness can not only ensure the comfort of drivers and passengers but also reduce the damage caused by road turbulence. In contrast to the close coupling between the vertical stiffness and inflation pressure of traditional pneumatic tyres, the vertical stiffness of non-pneumatic tyres is easier to adjust. This aids researchers in implementing optimisation according to different road conditions and user experience.

The study of the longitudinal mechanical properties of tyres is vital for analysing envelope characteristics, transient response, and rolling resistance. Rolling resistance is the most critical factor that increases vehicle fuel consumption and tyre temperature. The rolling resistance of non-pneumatic tyres is calculated using the total viscoelastic energy loss per unit rolling distance at maximum stable speed. Non-pneumatic tyres are found to exhibit excellent rolling resistance under general medium and low loads. Similar to traditional pneumatic

tyres, the rolling resistance of non-pneumatic tyres is a result of the interaction of various components. However, owing to the flexible structural design and wide material selection, more means are available for optimising the rolling resistance of non-pneumatic tyres. Researchers have found that the structural parameters of the support and shear layer can significantly affect the rolling resistance of non-pneumatic tyres. The increase in rolling resistance is an important indicator of performance optimisation.

The lateral mechanical characteristics of tyres are the most important characteristics that determine the handling stability of a vehicle. Because the support of non-pneumatic tyres is mainly arranged laterally in a circumferential manner, their lateral deformation under lateral loads is negligible. Therefore, non-pneumatic tyres typically have greater lateral stiffness than pneumatic tyres.

Improving the distribution of ground pressure such that it is uniform and reasonable directly affects the performance of non-pneumatic tyres. The ground pressure and vertical stiffness of pneumatic tyres are directly and closely coupled with air pressure. In contrast, the ground pressure of non-pneumatic tyres is primarily related to the tread profile size and shear zone parameters. Thus, the ground pressure and vertical stiffness of a relatively independent non-pneumatic tyre may be high or low. However, the grounding and air pressure of traditional pneumatic tyres are significantly coupled. Generally, optimising the grounding pressure of nonpneumatic tyres during design is easier. The grounding characteristics of different non-pneumatic tyres vary; however, their overall performance is satisfactory. The deformation of the Tweel tyre in the grounding area is larger than that of the pneumatic tyre of the same specification, forming a special structure of "contact piece" at the grounding point. This feature is conducive to reducing the grounding pressure and energy loss of the Tweel tyre during rolling. Under medium and low loads, the grounding pressure of honeycomb tyres was slightly higher than that of pneumatic tyres; however, with an increase in load, the grounding pressure of the honeycomb tyres was smaller. The contact mark of the mechanical elastic wheel was approximately rectangular. Under heavy loads, the mechanical elastic wheel does not have a stress concentration on the tyre shoulder. Compared with pneumatic tyres with the same specifications, the ground pressure distribution of mechanically elastic wheels was more uniform.

The vibration characteristics of non-pneumatic tyres are essential factors and must be investigated to improve tyre quality and design. At high speeds, the spokes of the non-pneumatic tyres enter the grounding area and produce bending deformation. When the spokes leave the grounding area, they quickly return from bent state to tensioned state. During the process of entering and leaving the grounding area, the spokes generate self-excited vibrations owing to deformation, causing overall tyre vibration and noise. Current research indicates that the vibration of the support is an important factor affecting the mechanical properties of non-pneumatic tyres. Researchers have analysed the vibration and noise mechanisms generated by non-pneumatic tyres. When non-pneumatic tyres run at high speeds, the deformation of the support structure causes self-excitation, causing vibration and noise throughout the tyre. This defect directly affects the stability and riding comfort of the vehicle as well as limits the use of non-pneumatic tyres. Researchers have also proposed a scheme to reduce vibration and noise by increasing the thickness and curvature of supporting spokes. However, no accurate data indicate whether the vibration characteristics of optimised non pneumatic tyres are comparable to those of pneumatic tyres. In summary, the vibration characteristics of non-pneumatic tyres considerably differ from those of traditional pneumatic tyres. To improve these characteristics, several aspects must be optimised.

Reliability and durability are essential indices of non-pneumatic tyres and are directly related to the safe operation of vehicles. The primary failure mode of non-pneumatic tyres is fatigue failure caused by alternating stresses. In the rolling process of non-pneumatic tyres, the flexible spokes bear an enormous alternating stress of extrusion and tension and a single alternating stress for a long time, resulting in the fatigue failure of flexible spokes. Research on the fatigue characteristics of non-pneumatic tyres is important for achieving the goals in the design stage, optimising the configuration in the improvement stage, and avoiding potential safety hazards. Under the action of alternating stress over an extended time, the fatigue performance of the support structure is unsatisfactory. At high speeds, the deformation of the support easily generates significant heat, further affecting the fatigue performance of non-pneumatic tyres and even leading to the failure of the support structure as conformed by experimental results. The driving mileage of traditional pneumatic tyres is approximately 50,000 km and that of non-pneumatic tyres of the same specification is less than half of this distance. Presently, the main problem restricting the use of non-pneumatic tyres in general passenger vehicles is their poor fatigue durability. This concern must also be resolved by researchers. The fatigue durability of the different non-pneumatic tyres is compared in Figure 2.3.13.

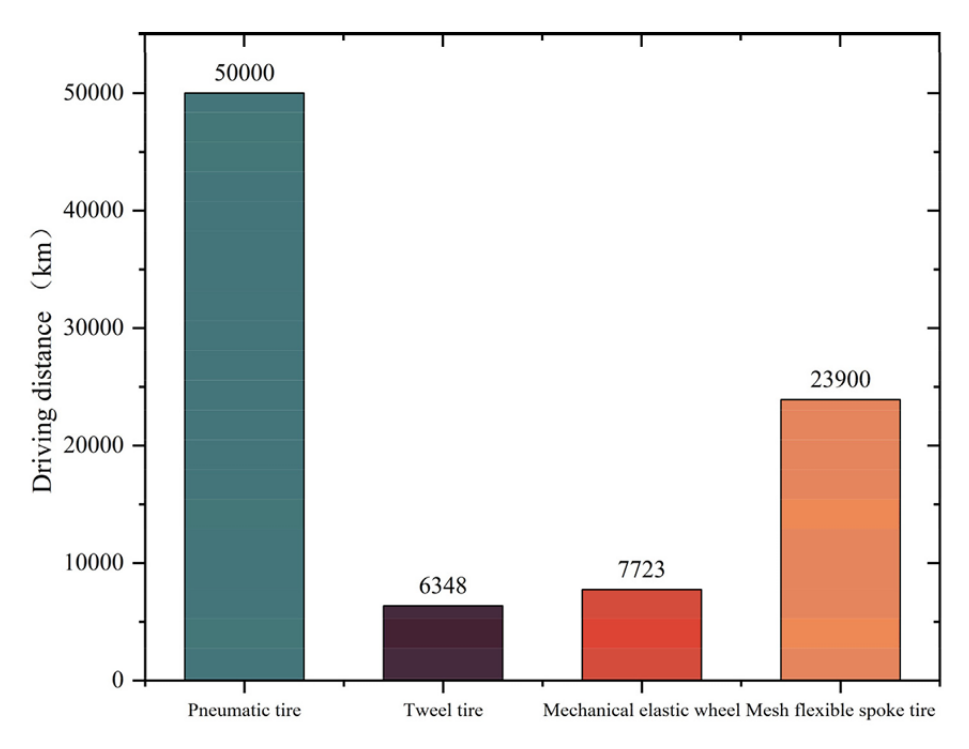


Figure 2.3.13: Comparison of tyre fatigue durability

Although non-pneumatic tyres possess several excellent properties and have considerable potential in the civil, military, and aerospace fields, they are still in the exploratory stage. To date, the application range of non-pneumatic tyres is limited. Because the support structure of non-pneumatic tyres is exposed, foreign matter can easily enter and cause damage. Moreover, when the vehicle passes areas, such as muddy and snow-covered sections, soil or snow can accumulate in the gaps of the structure and affect tyre performance. The difference in durability between non pneumatic and traditional pneumatic tyres is considerable. Accordingly, non-pneumatic tyres must be further optimised considering multiple perspectives. The aspects that must be improved to promote the application non-pneumatic tyres to vehicles and realise industrialisation are as follows:

- 1) improve structural design, and optimise tyre performance;
- 2) develop high-performance composites;
- 3) simplify the assembly process, and reduce the production cost;
- 4) develop an appropriate moulding technology for non-pneumatic tyres;
- 5) combine non-pneumatic tyre technology and frontier technologies. [8]

2.4 Tyre mousse

In off-road race vehicles, such as enduro motorcycles, where punctures are a great issue, air is replaced by tyre mousse. Tyre mousse is a component in certain types of off-road run-flat tyres, designed to allow them to maintain functionality despite a puncture. It is a ring of flexible foam that is placed inside a tyre before it is fitted on the rim. The original run-flat mousse, called Bib-Mousse, was developed in 1984 by Michelin, for use on motorbikes in enduro, rally-raid and motocross events. Bib-Mousse, which can be seen in Figure 2.4.1, is a tyre mousse made by French tyre manufacturer Michelin. The Bib-Mousse was named after Michelin's well-known mascot, Bibendum. It is a ring of butyl honeycomb foam with its cells filled with nitrogen. It has a smooth-moulded outer skin that is designed to slip into specific size off-road motorcycle tyres. [9]



Figure 2.4.1: Michelin Bib-Mousse

2.5 Company proposal

AGLA Power Transmission is investigating a new type of tyre for enduro motorcycle sector. The main problem of mousse is that it degrades quickly, so it lasts only one race and then it has to be changed: this leads to higher costs and environmental impacts. The idea is to create a non-pneumatic tyre suitable for enduro races. In this way, the internal structure does not need to be changed at every race.

3 Mechanical characterisation

To study the elastomeric compounds in the LBN Ricerca laboratory, different tests are carried out: hardness Shore test, tensile test and tear test. The procedures to carry out these tests are described respectively in norms ISO 48-4, DIN 53504 and ISO 34. These norms give details about the dimensions of the specimens and the functioning of the measure instruments used in laboratory.

3.1 Hardness Shore test

During the hardness test, a durometer with an indentor penetrates a surface of the specimen and the hardness of the material is measured depending on the protrusion depth. There are several types of hardness tests. In this thesis, Shore method is used.

Norm ISO 48-4 specifies a method for determining the indentation hardness (Shore hardness) of vulcanised or thermoplastic rubber using durometers with the following scales:

- the A scale for rubbers in the normal-hardness range;
- the D scale for rubbers in the high-hardness range;
- the AO scale for rubbers in the low-hardness range and for cellular rubbers;
- the AM scale for thin rubber test pieces in the normal-hardness range.

The rubbers analysed in this thesis belong to A scale.

An indentor of specified dimensions is pressed into a test piece under a specified load and the depth of indentation is measured. This indentation is converted to a hardness value by means of a specified relation.

When using durometers, the scale should be chosen as follows:

- for values less than 20 with a type D durometer: type A;
- for values less than 20 with a type A durometer: type AO;
- for values over 90 with a type A durometer: type D;
- for thin test pieces (less than 6 mm thick): type AM.

As described by this norm, the durometers for the different scales have slightly different dimensions and shapes. The following description is about type A durometer because it is the one used in this thesis.

The pressure foot shall have a diameter of 18 mm \pm 0,5 mm and a central hole of diameter 3 mm \pm 0,1 mm. The indentor shall be formed from a hardened-steel rod of diameter 1,25 mm \pm 0,15 mm to the shape and dimensions shown in Figure 3.1.1.

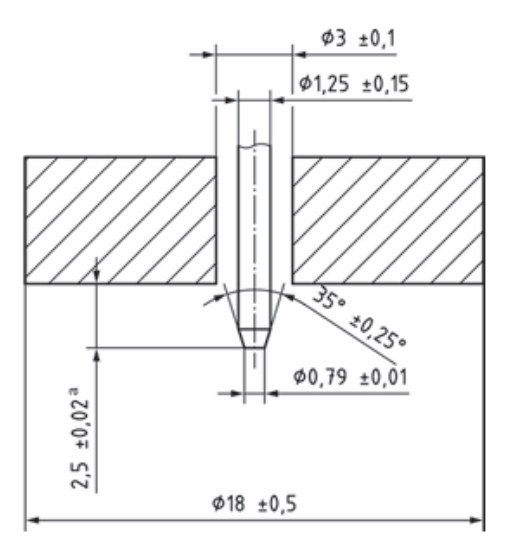


Figure 3.1.1: Indentor for type A durometer (dimensions are given in millimetres)

The indicating device allows the extent of protrusion of the point of the indentor beyond the face of the pressure foot to be read. It shall be calibrated directly in terms of units ranging from 0 for the maximum protrusion of $2,50 \text{ mm} \pm 0,02 \text{ mm}$ to $100 \text{ for zero protrusion obtained by placing the pressure foot and indentor in firm contact with a suitable flat, hard surface (e.g. glass).$

The calibrated spring is used to apply a force F, expressed in millinewtons, to the indentor in accordance with Equation (3.1.1):

$$F = 550 + 75H_A \tag{3.1.1}$$

where H_A is the hardness reading taken from the type A durometer.

The automatic timing device shall be automatically activated when the pressure foot is in contact with the test piece and shall indicate the end of the test time or lock the test value at its completion. Use of a timing device for the test time improves precision. When the instrument is used on a stand, the time tolerance shall be \pm 0,3 s.

The original concept of a durometer was a portable instrument that could be used, for example, on a product in service. However, better precision can be expected by using a stand with a weight centred on the axis of the indentor to apply the pressure foot to the test piece. The operating stand shall be capable of supporting the pressure-foot surface of the durometer parallel to the test piece support table. The stand shall be capable of applying the test piece to the indentor, or vice versa, without shock. The total mass of the durometer and extra mass to overcome the spring force shall be $1_0^{+0.1}$ kg.

The force values shall be in accordance with Table 3.1.1.

Spring force mN Indicated durometer value Type A and AO Type AM Type D 0 324 550 10 368 1300 4 450 20 412 2 0 5 0 8 900 30 456 2800 13 350 40 500 3 5 5 0 17 800 50 544 4300 22 250 60 588 5 0 5 0 26 700 70 632 5 8 0 0 31 150 80 676 6 5 5 0 35 600 7 3 0 0 90 720 40 050 100 764 8 050 44 500 Millinewtons (mN) per unit 4,4 75 445 Spring force tolerance ±8,8 ±37,5 ±222,5

Table 3.1.1: Durometer spring forces

The thickness of the test piece shall be at least 6 mm. The other dimensions of the test piece shall be sufficient to permit measurements at least 12 mm away from any edge. The surface of the test piece shall be flat and parallel over an area sufficient to permit the pressure foot to come into contact with the test piece over an area having a radius of at least 6 mm from the indentor point. Satisfactory hardness determinations cannot be made on rounded, uneven or rough surfaces using durometers.

For all test purposes, the minimum time between vulcanization and testing shall be 16 h.

To measure the hardness with Shore method, the test piece is placed on a flat, hard, rigid surface (e.g. glass). Subsequently, the pressure foot is applied to the test piece, or vice versa, as rapidly as possible but without shock, keeping the foot parallel to the surface of the test piece and ensuring that the indentor is normal to the rubber surface. The applied force must be sufficient only to obtain firm contact between the pressure foot and the test piece and the reading is taken at the specified time after the pressure foot is in firm contact with the test piece. The standard test time is 3 s for vulcanised rubber, which is analysed in this thesis.

The instrument shall be calibrated regularly using suitable instruments for measuring force, indentation depth and indenter geometry. To do the calibration, the instrument is pressed against a suitable flat, hard surface (e.g. glass) and adjusted, where possible, the reading on the scale to give a value of 100. Subsequently, the instrument check is continued using a set of standard rubber blocks covering the measurement range. All adjustments shall be made in accordance with the manufacturer's instructions. The set of standard rubber blocks used shall consist of at least three reference blocks in a suitable covered container away from light, heat, oil and grease. The reference blocks shall be recalibrated once a year, or if the mean value deviates more than one unit compared with the certificate of the reference blocks. The calibration of the reference blocks needs to be done with a reference measurement device of an accredited laboratory. Instruments in regular use shall be checked at least each week against standard rubber blocks. [10]

3.2 Tensile test

During the tensile test, the grips of the testing machine clamp the specimen and they stretch it at a constant speed until it breaks, while the extensometer measures how much the specimen is stretched. The machine measures the force. In this way, the curves of force-extension and stress-strain can be plotted and the values of stress and strain at break are obtained.

The test method specified in norm DIN 53504 serves to determine the tensile strength at break, tensile stress at yield, elongation at break and stress at a given strain of rubber test pieces of specified shape when these are stretched to rupture at a constant rate of traverse. It is advisable that the full force-extension curve or at least part of it be plotted, since the behaviour of rubber when subjected to tensile stress cannot be adequately characterized by the tensile strength at break and elongation at break.

The norm describes the procedures to test rings and dumb-bells. The specimens of rubbers used in this thesis are dumb-bells-shaped, so the following description is about testing dumb-bells.

The tensile testing machine is equipped with two grips designed to enable the longitudinal axis of the test piece to be aligned to coincide with the strain axis of the machine at any time. The dumb-bell shall be held so as to prevent slip relative to the grips as far as possible. Suitable grips are those which maintain or even increase the pressure on the dumb-bell as the stress increases. The grips shall not cause premature rupture of the dumb-bell.

The testing machine permits both force-extension curves and stress-strain curves to be plotted. The extensometer is suitable for determining the change in test length of the test piece at any moment during the test and shall have as low an inertia as possible. When an extensometer attached to the test piece is used instead of a contact-free extensometer, there shall be no sign of damage to the test piece nor any slippage between the extensometer grips and the test piece.

There are different types of dumb-bells with different dimensions. In this thesis, the S3A type, which is showed in Figure 3.2.1, is used and its dimensions are specified in Table 3.2.1.

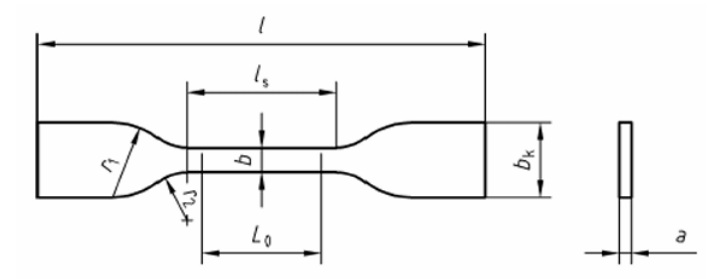


Figure 3.2.1: Dumb-bell

Table 3.2.1: Dimensions of dumb-bell (dimensions are given in millimetres)

Dimension		Dumb-bell type				
		S 1	S 1A	S 2	S 3	S 3A
Minimum overall length	l	115	100	75	35	50
Width of ends	b_{k}	25	25	12,5	6	8,5
Length of narrow portion	l_{s}	33	5	25	12	16
Width of narrow portion ± 0,05	b	6	5	4	2	4
Transition radius inside	<i>r</i> ₁	25	20	12,5	3	10
Transition radius outside	r_2	14	11	8	3	7,5
Thickness	а	2 ± 0,2	2 ± 0,2	2 ± 0,2	1 ± 0,1	2 ± 0,2
Initial test length	L_0	25	25	20	10	10

NOTE 1 The dimensions given relate to the dies. Although the width of the ends of dumb-bells and the transition radii may deviate from the dimensions specified, the symmetry shall be maintained.

NOTE 2 The dies shall be inspected regularly for sharpness and damage.

NOTE 3 Type S 2 dumb-bells shall preferably be used.

Where test pieces are prepared separately, choose the sheet form. The thickness of the sheets shall be equal to the thickness of the final test pieces. If the test pieces cannot be cut directly from finished components, cut out sheets of appropriate thickness so that test pieces can be taken from these. Remove any unevenness by grinding.

The test is carried out at (23 ± 2) °C (referred to as ambient temperature). Prior to the test, the test pieces should be conditioned for at least 20 minutes at the test temperature. Testing shall not be carried out less than 16 hours after vulcanization.

Prior to testing, measure the test piece thickness at ambient temperature at not less than three points, that of dumb-bells within the initial test length L_0 , preferably at the two ends and in the centre. Calculate the initial cross-sectional area from the median thickness and the width of the narrow portion.

The test piece is inserted in the grips in such a way that its longitudinal axis coincides with the strain axis. An area as large as possible should be gripped, but it must not include any region having a width less than b_k . Then, the grips are tightened evenly so as to prevent slippage of the test pieces. Afterwards, an initial stress of < 0,1 MPa is applied at a rate of traverse of < 50 mm/min and then the machine is stopped. At this point, the extensometer is brought into contact with the test piece. Finally, the machine starts to stretch the dumb-bell specimen with a rate of transverse equal to 200 mm/min. This method gives slightly falsified results owing to the initial stress applied. Accordingly, the selected initial stress shall be as small as possible while still sufficient to tauten the dumb-bell. Tests where the rupture occurs outside the test length must not be evaluated.

The tensile strength at break is calculated using Equation (3.2.1):

$$\sigma_R = \frac{F_R}{A_0} \tag{3.2.1}$$

where:

- σ_R is the tensile strength at break in MPa or N/mm²;
- F_R is the force at break in N;
- A_0 is the initial cross-sectional area in mm².

The tensile stress at yield is calculated using Equation (3.2.2):

$$\sigma_{max} = \frac{F_{max}}{A_0} \tag{3.2.2}$$

where:

- σ_{max} is the tensile stress at yield in MPa or N/mm²;
- F_{max} is the force at yield in N;
- A_0 is the initial cross-sectional area in mm².

The elongation at break is calculated using Equation (3.2.3):

$$\varepsilon_R = \frac{L_R - L_0}{L_0} \times 100 \tag{3.2.3}$$

where:

- ε_R is the elongation at break in %;
- L_R is the test length at break in mm;
- L_0 is the initial test length in mm.

The tensile stress at a given strain is calculated using Equation (3.2.4):

$$\sigma_i = \frac{F_i}{A_0} \tag{3.2.4}$$

where:

- σ_i is the tensile stress at a given strain *i* in MPa or N/mm²;
- F_i is the force at a given strain i in N;
- A_0 is the initial cross-sectional area in mm². [11]

3.3 Tear test

During tear test, an initial cut is created on the specimen, then the grips of the testing machine clamp the specimen by the two extremities of the cut and they stretch it at a constant speed to propagate the cut until the specimen is torn up. In this way, the curve of force as a function of displacement of the crosshead of the testing machine is obtained and the tear strength can be calculated.

Norm ISO 34-1 specifies three test methods for the determination of the tear strength of vulcanised or thermoplastic rubber, namely the following:

- method A, using a trouser test piece;
- method B, using an angle test piece, with or without a nick of specified depth;
- method C, using a crescent test piece with a nick.

The value of tear strength obtained depends on the shape of the test piece, speed of stretching, and temperature of test. It can also be susceptible to grain effects in rubber.

In this thesis, the trouser-shaped specimen is used, so the following description is about method A.

The trouser tear strength is defined as the median force required to propagate a cut in a specified trouser-shaped test piece by tearing, divided by the thickness of the test piece. The force is acting in a direction substantially in the plane of the cut.

The test consists in measuring the force required to tear a specified test piece, in continuation of the cut or nick already produced in the test piece. The tearing force is applied by means of a tensile testing machine, operated without interruption at a constant rate of traverse until the test piece breaks.

Method A, using the trouser test piece, is not sensitive to the length of the cut, unlike the other two test pieces in which the nick has to be very closely controlled. In addition, the results obtained are more easily related to the fundamental tear properties of the material and are less sensitive to modulus effects (provided that the leg extension is negligible) and the rate of propagation of the tear is directly related to the rate of grip separation.

The die used for cutting trouser test pieces shall have the dimensions shown in Figure 3.3.1.

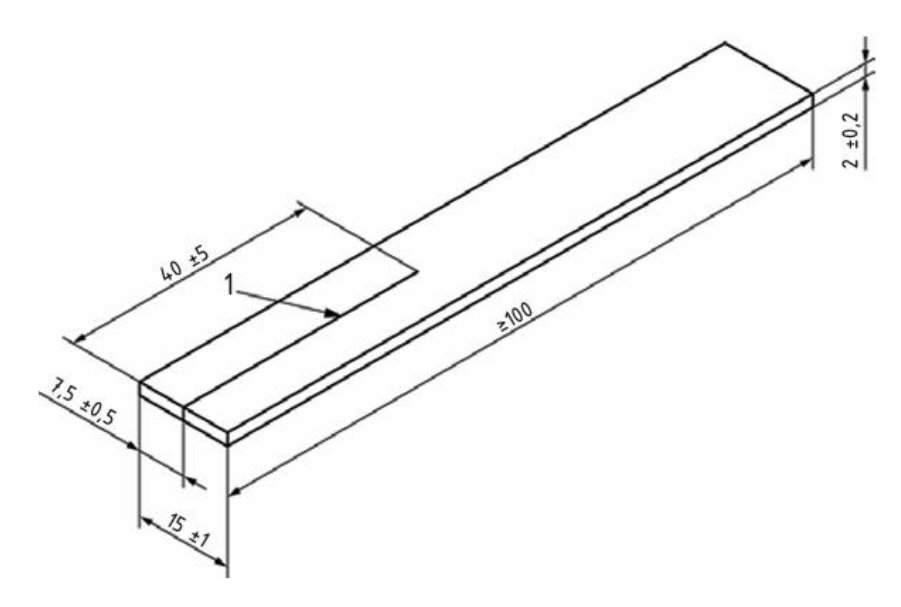


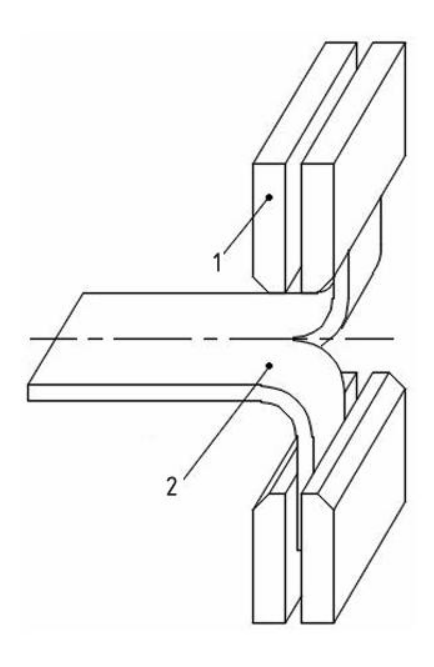
Figure 3.3.1: Trouser test piece die (dimensions are in millimetres)

A sharp razor blade or a sharp knife free from ragged edges shall be used for producing a cut in the test piece. The test piece shall be clamped firmly, especially in the region where the nick is to be introduced. The cutting tool, consisting of a razor blade or similar blade, shall be clamped in a plane perpendicular to the major axis of the test piece, and positioned so as to introduce the nick in the appropriate place. The blade clamping device shall permit no lateral movement and shall be fitted in guides to enable the blade to be moved across the test piece with its edge remaining perpendicular to the plane of the test piece. Alternatively, the blade shall be fixed and the test piece arranged to move in an analogous manner.

A thickness gauge measures the thickness of the test piece.

The testing machine shall be capable of registering the applied forces within 1% during the test while maintaining the specified constant rate of separation of the jaws of 100 mm/min \pm 10 mm. A low-inertia machine having autographic force-recording facilities is essential when using the trouser test piece.

The machine shall be provided with a type of grip which tightens automatically as the tension increases and exerts a uniform pressure across the widened end of the test piece. Each grip shall incorporate a means for positioning so that the test pieces are inserted symmetrically and in axial alignment with the direction of the pull. The depth of insertion shall be such that the test piece is adequately gripped, within the parallel-sides portion, when testing angle and crescent test pieces. Trouser test pieces shall be inserted in the grips in accordance with Figure 3.3.2.



Key

- 1 grip
- 2 test piece

Figure 3.3.2: Positioning of trouser test piece in testing machine

Test pieces shall be cut from rubber sheet of uniform thickness. Preferably, the sheet shall have a thickness of $2.0 \text{ mm} \pm 0.2 \text{ mm}$; however, it is recognized that, when sheets are prepared from finished products, this thickness cannot always be achieved. Sheets may be moulded or prepared from products by cutting or buffing.

The sheets shall be conditioned at standard laboratory temperature for at least 3 h before test pieces are cut from them. Each test piece shall be cut from the sheet by punching with a die, shaped as shown in Figure 3.3.1, using a single stroke of the press. The rubber shall, if necessary, be wetted with water or soap solution and shall be supported on a sheet of slightly yielding material (e.g. leather, rubber belting or cardboard) on a flat rigid surface. The test pieces shall be allowed to dry thoroughly prior to testing.

The tear strength is particularly susceptible to grain effects in the rubber. Each test piece shall, if possible, be taken in such a way that the tear strength can be determined in two directions which are at an angle of 90° to one another i.e. one at right angles to the grain and the other parallel to the grain. The directions in which the test piece is taken shall be indicated so that the effect of anisotropy can be assessed. The direction of tear propagation is parallel to the length of the trouser test piece.

The cut of depth of test piece is $40 \text{ mm} \pm 5 \text{ mm}$ made at the centre of the width of the test piece (Figure 3.3.1). It is important that the last 1 mm (approximately) of the cut is made with a razor blade or a sharp knife. Test pieces shall be cut, measured and then tested, preferably immediately, but if not tested immediately they shall be kept at chosen standard laboratory temperature until tested. The period between cutting of the test piece and testing shall not exceed 24 h. The cut shall be made after any ageing treatment has been carried out. Unless any ageing treatment, the cut shall be made immediately after the preparation of the test pieces.

The test is normally carried out at a standard laboratory temperature. If the test is to be carried out at a temperature other than a standard laboratory temperature, the test piece shall be conditioned for a period sufficient to reach substantial temperature equilibrium at the test temperature, immediately prior to testing. This period shall be kept as short as possible in order to avoid ageing the rubber.

The thickness of the test piece is measured in the region in which tearing is expected to occur. Subsequently, the test piece is mounted in the testing machine. The test piece is extended at a rate of separation of the grips of $100 \text{ mm/min} \pm 10 \text{ mm/min}$ until the test piece breaks. An autographic recording of the force throughout the tearing process is made.

The tear strength T_S , expressed in kN/m of thickness, is calculated using Equation (3.3.1):

$$T_S = \frac{F}{d} \tag{3.3.1}$$

where:

- F is the median force in N;
- *d* is the median thickness in mm. [12]

4 Experimental set up

4.1 Elastomeric compound

The elastomeric compound analysed in this thesis is the EPDM (Ethylene Propylene Diene Monomer), which is based on ethylene, propylene and a third diene monomer that allows cross-linking with sulphur.

Its main characteristics are the follows:

- excellent resistance to atmospheric agents, ozone, and UV rays;
- excellent resistance to water and steam;
- good resistance to high temperatures (up to approximately 130°C, even higher with special formulations);
- poor resistance to oils and fuels;
- excellent elasticity even at low temperatures.

EPDMs are used in automotive door and window seals, cable and pipe sheathing, roofing and waterproofing, and industrial gaskets.

These elastomers are composed of ethylene (-CH₂-CH₂-), which provides flexibility; propylene (-CH₂-CH_{(CH₃)-), which reduces crystallinity and improves weather resistance; and diene, which allows sulphur cross-linking.}

The ratio of ethylene to propylene influences mechanical properties and processability. The diene introduces double bonds into the main chain, which can be exploited for vulcanization (sulphur cross-linking), making the material more elastic and resistant.

EPDM is nonpolar, so it has poor compatibility with oils and polar solvents, but excellent resistance to water and weathering. [13]

Figure 4.1.1 shows the atomic structure of EPDM.

Figure 4.1.1: Atomic structure of EPDM

4.2 Laboratory specimens and oven

The specimens of the elastomers used in this thesis are produced by Bottino Girardi. These specimens are ring-shaped. In Bottino Girardi factory, the elastomeric compound is poured inside a die with pressure to be vulcanised. Vulcanisation is a process to improve the mechanical properties of rubber. The raw rubber is heated with sulphur or other crosslinking agents. The sulphur atoms form crosslinks (bridges) between the long rubber polymer chains to prevent them from sliding. This process increases the elasticity, improves the strength and resistance to wear, makes rubber less sticky and more resistant to heat and chemicals and reduces the plasticity.

To exploit more efficiently the die and to increase the productivity, after about ten minutes, when the elastomeric compound solidifies and assumes the form of a tube, it is extracted from the die and put inside an oven for about four hours, where the post-curing process occurs. In this way, the sulphur atoms continue to

form crosslinks between the rubber polymer chains in the oven and the die is used to vulcanise other compound. After the post-curing, the tube is taken out from the oven and cut in rings.

The die has four cavities, indicated with 1, 2, 3 and 4 numbers, in which the elastomeric compound can be poured. From each cavity, a hollow tube is extracted and cut to obtain seven rings, indicated with A, B, C, D, E, F and G letters. The rings are sent to LBN Ricerca laboratory where they are tested. Figure 4.2.1 shows a tube and the rings obtained from it, while Figure 4.2.2 shows a section of an enduro motorcycle tyre and a ring used for laboratory tests.

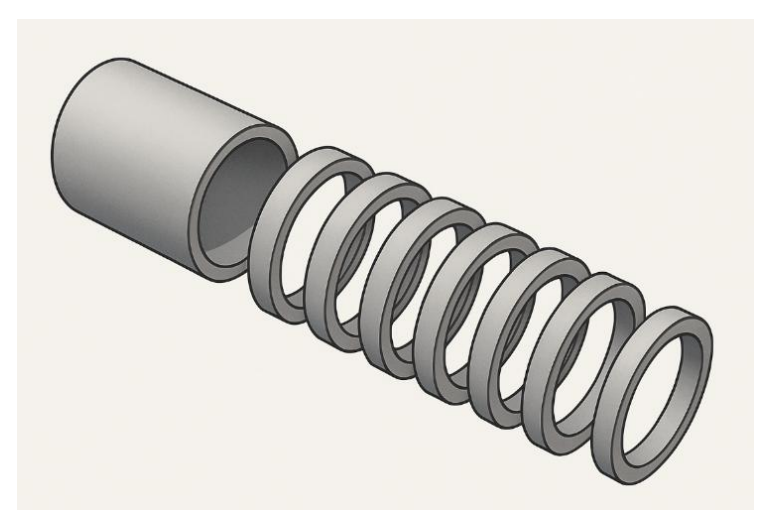


Figure 4.2.1: Rings obtained by a tube



Figure 4.2.2: Section of a motorcycle enduro tyre (top) and ring used for laboratory tests (bottom)

The oven has fifteen positions in which the tubes can be placed. The positions, which can be seen in Figure 4.2.3, are the following:

- FCM: Front Centre Middle;
- FUL: Front Up Left;

- FUR: Front Up Right;
- FDL: Front Down Left;
- FDR: Front Down Right;
- C: Centre;
- MCL: Middle Centre Left;
- MCR: Middle Centre Right;
- CU: Centre Up;
- CD: Centre Down;
- BCM: Back Centre Middle;
- BUL: Back Up Left;
- BUR: Back Up Right;
- BDL: Back Down Left;
- BDR: Back Down Right.

The reference system used to describe the positions is in the centre with the axes oriented according to Figure 4.2.3 and the dimensions of the oven are the following:

- length of 2.5 m;
- width of 1.5 m;
- height of 2 m.

Furthermore, the oven is heated from below and the door is in the front.

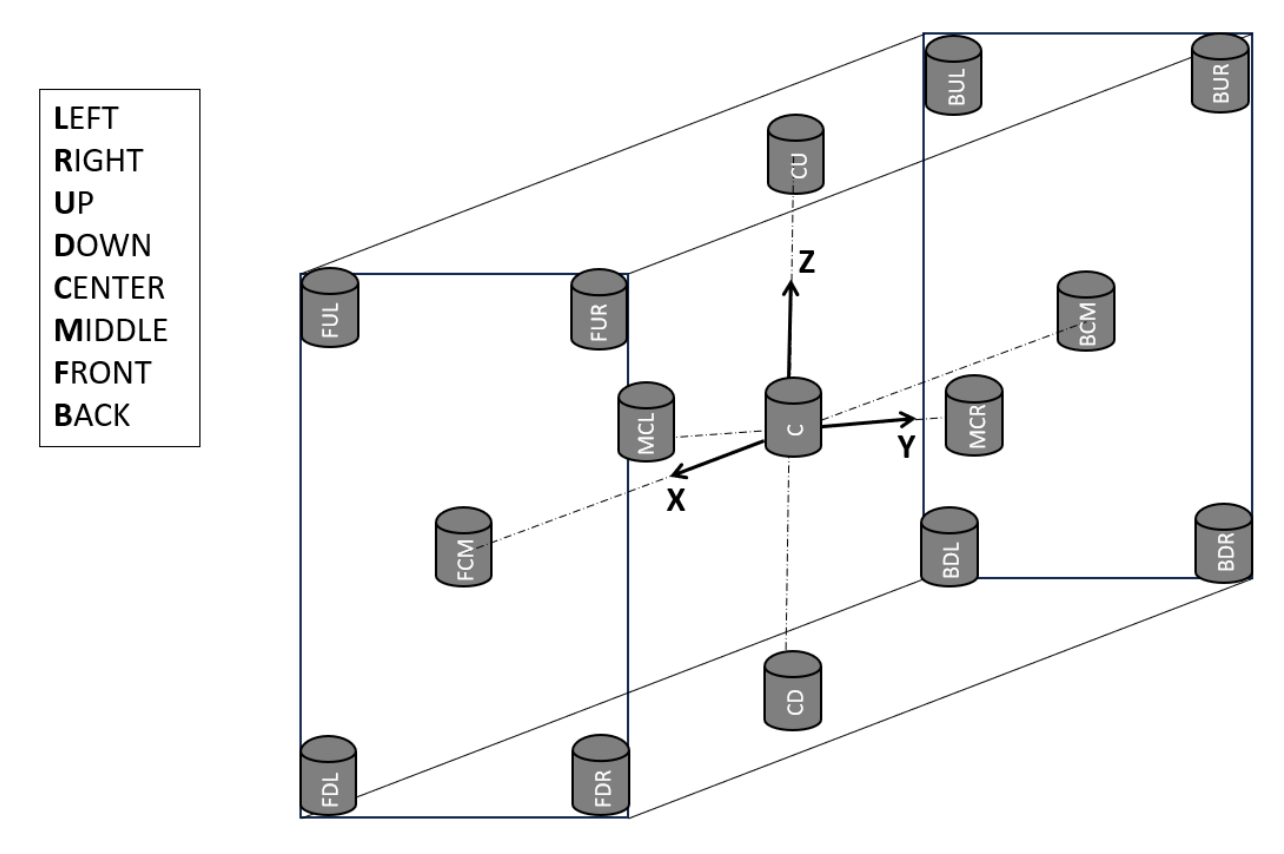


Figure 4.2.3: Sketch of Bottino Girardi oven with the positions of the tubes

In this thesis, only the rings obtained from one of the four cavities available in the die are analysed because a previous investigation showed that the cavity does not affect the mechanical properties of rubber: this means that there are seven rings for each position of the oven. The rings are sent to LBN Ricerca laboratory divided in fifteen groups corresponding to the fifteen positions of the oven.

In this thesis, the tests are carried out on ring specimens to investigate anisotropy induced by the proposed industrial process in order to produce enduro motorcycle tyres.

4.3 Hardness Shore test

Hardness Shore test is carried out as described in Paragraph 3.1.

The durometer, which is showed in Figure 4.3.1, has four legs and a bubble to adjust the position of the instrument in order to make the surface of the support horizontal. Furthermore, there are a lever to bring the specimen to the indentor and a screen to read the value of hardness as well.



Figure 4.3.1: Durometer

For each ring, eight measurement are carried out, four for each side.

4.4 Tensile test

Tensile test is carried out as explained in Paragraph 3.2.

From each ring, a dumb-bell specimen is cut using the instrument of Figure 4.4.1. The instrument has a lever to bring the die to the specimen. The die has the shape of the dumb-bell.



Figure 4.4.1: Instrument to cut the specimens

After obtaining the dumb-bell specimen, the thickness gauge showed in Figure 4.4.2 is used to measure the thickness of the specimen at its centre. The value of thickness is used to calculate the initial cross-sectional area of the specimen. The dumb-bell shall be placed with its concavity upwards. As rubber is a soft material, the tip of the thickness gauge can affect the measured value with its weight: for this reason, this thickness gauge is made especially for rubbers.

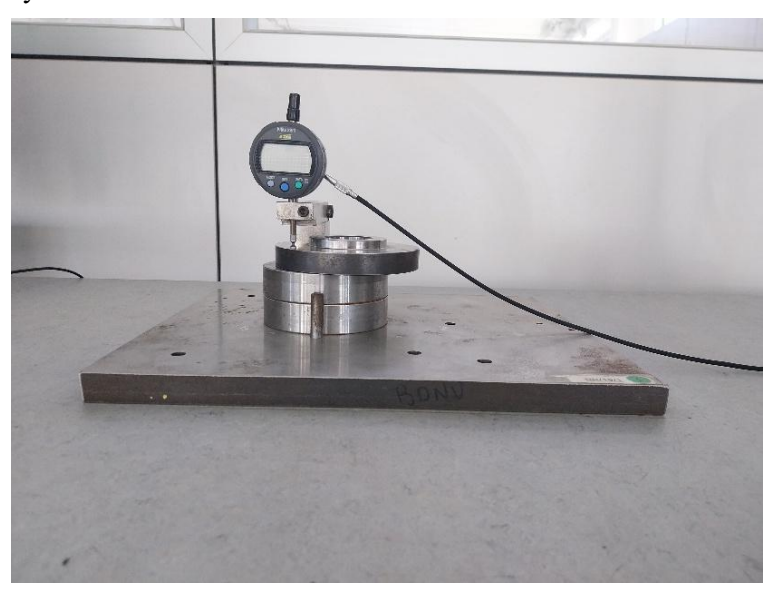


Figure 4.4.2: Thickness gauge

Finally, the testing machine showed in Figure 4.4.3 is used to carry out the tensile test. The dumb-bell is clamped by the two grips, then the extensometer is applied and the test can be started.



Figure 4.4.3: Tensile testing machine

For each dumb-bell, the corresponding stress-strain curves as well as the values of stress and strain at break are obtained.

4.5 Tear test

Tear test is carried out as explained in Paragraph 3.3.

From each ring, a trouser specimen is obtained using the instrument showed in Figure 4.4.1 and a cutter to create the initial cut.

The thickness gauge of Figure 4.4.2 is used to measure the thickness of the trouser at one extremity.

Finally, the testing machine of Figure 4.4.3 is used to carry out the tear test. The grips of the testing machine clamp the trouser by the two extremities of the cut and the test is started.

For each trouser, the corresponding curve of force as a function of displacement of the crosshead of the testing machine as well as the value of force at break are obtained. Then, from the force at break, tear strength is calculated using Equation (3.3.1).

5 Data analysis

5.1 Statistical methodologies

After collecting all the data from laboratory tests, the data are analysed by using Minitab, which is a software to study statistics. The scope of this thesis is to investigate if there is a correlation between the mechanical properties of rubber, the position of the tube inside the oven and the position of the ring inside the tube.

First of all, all the data are visualised using descriptive statistical tools, such as boxplots and dotplots.

Subsequently, the outliers are identified through the Grubbs' test. In fact, when something is measured, there are factors which can lead to accidental errors. These values have to be identified and excluded from the study.

Afterwards, the ANOVA (Analysis Of Variance) is carried out. The ANOVA allows to understand if there are correlations between the mechanical properties of the elastomers, the position of the tube inside the oven and the position of the ring inside the tube.

Finally, the response surface regression is carried out to create a model which predicts the mechanical properties of the rubber as a function of the position of the tube inside the oven and of the position of the ring inside the tube.

5.1.1 Descriptive statistics

Some useful tools of descriptive statistics are boxplots and dotplots.

A boxplot is a method for demonstrating graphically the locality, spread and skewness groups of numerical data through their quartiles. In addition, there can be lines called whiskers extending from the box indicating variability outside the upper and lower quartiles. Outliers that differ significantly from the rest of the dataset may be plotted as individual points beyond the whiskers on the boxplot. The parameters of the boxplot are the following:

- minimum (Q_0 or 0^{th} percentile): the lowest data point in the data set excluding any outliers;
- maximum (Q_4 or 100th percentile): the highest data point in the data set excluding any outliers;
- median (Q_2 or 50^{th} percentile): the middle value in the data set;
- first quartile (Q_I or 25th percentile): also known as the lower quartile, it is the median of the lower half of the dataset;
- third quartile (Q_3 or 75^{th} percentile): also known as the upper quartile, it is the median of the upper half of the dataset.

Another important element that can also be employed to obtain a boxplot is the interquartile range *IQR*, which is calculated using Equation (5.1.1):

$$IQR = Q_3 - Q_1 (5.1.1)$$

The box is drawn from Q_1 to Q_3 with a horizontal line drawn inside it to denote the median. Some boxplots include an additional character to represent the mean of the data.

A popular choice for the boundaries of the whiskers is based on the 1.5 IQR value. From above the upper quartile (Q_3) , a distance of 1.5 times the IQR is measured out and a whisker is drawn up to the largest observed data point from the dataset that falls within this distance. Similarly, a distance of 1.5 times the IQR is measured out below the lower quartile (Q_I) and a whisker is drawn down to the lowest observed data point from the dataset that falls within this distance. Because the whiskers must end at an observed data point, the whisker lengths can look unequal, even though 1.5 IQR is the same for both sides. All other observed data points outside the boundary of the whiskers are plotted as outliers. The outliers can be plotted on the boxplot as a dot, a small circle, a star, etc. [14] [15]

Figure 5.1.1 shows the structure of a boxplot with whiskers and outliers.

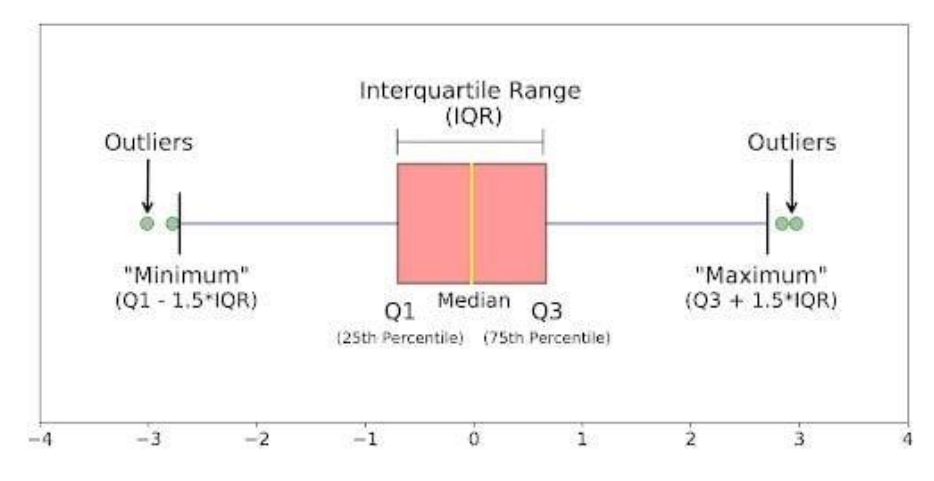


Figure 5.1.1: Boxplot

A dotplot is a statistical chart consisting of data points plotted on a fairly simple scale, typically using filled in circles. It is one of the simplest statistical plots and is suitable for small to moderate sized data sets. It is useful for highlighting clusters and gaps, as well as outliers. Their other advantage is the conservation of numerical information. When dealing with larger data sets (around 20-30 or more data points) the boxplot may be more efficient, as dotplots may become too cluttered after this point. [14] [15]

Figure 5.1.2 shows an example of a dotplot made by Minitab in which there is a scale with values of torque and on each value there are some points representing how many times that value has been obtained.

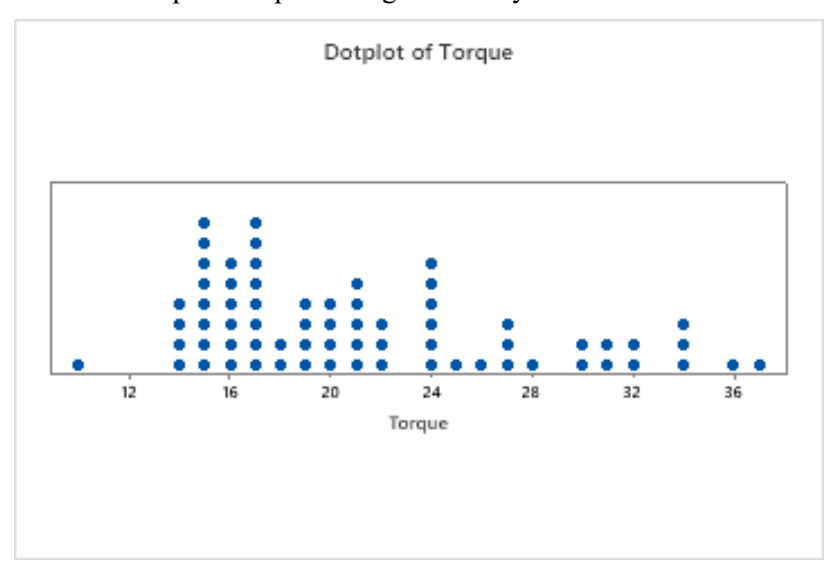


Figure 5.1.2: Dotplot

5.1.2 Outlier identification

To identify outliers on Minitab software, the Grubbs' test can be used.

Grubbs' test is based on the assumption of normality. This means that one should first verify that the data can be reasonably approximated by a normal distribution before applying the Grubbs test. Grubbs' test detects one outlier at a time. This outlier is expunged from the dataset and the test is iterated until no outliers are detected.

The Grubbs' test statistic G is calculated using Equation (5.1.2):

$$G = \frac{\max_{i=1,\dots,N} |X_i - \bar{X}|}{s} \tag{5.1.2}$$

where:

- *N* is the number of samples
- X_i is the sample i;
- \bar{X} is the sample mean;
- *s* is the standard deviation. [16]

Afterwards, Grubbs' critical value G_{crit} is calculated. The critical value depends on the number of samples N and on the significance level α . Table 5.1.1 shows Grubbs' critical values for different number of samples N and significance level α .

In this thesis, the significance level α is set to 0.05.

Table 5.1.1: Grubbs' critical values for different number of samples N and significance values α

			Alpha		
N	0.1	0.075	0.05	0.025	0.01
3	1.15	1.15	1.15	1.15	1.15
4	1.42	1.44	1.46	1.48	1.49
5	1.6	1.64	1.67	1.71	1.75
6	1.73	1.77	1.82	1.89	1.94
7	1.83	1.88	1.94	2.02	2.1
8	1.91	1.96	2.03	2.13	2.22
9	1.98	2.04	2.11	2.21	2.32
10	2.03	2.1	2.18	2.29	2.41
11	2.09	2.14	2.23	2.36	2.48
12	2.13	2.2	2.29	2.41	2.55
13	2.17	2.24	2.33	2.46	2.61
14	2.21	2.28	2.37	2.51	2.66
15	2.25	2.32	2.41	2.55	2.71
16	2.28	2.35	2.44	2.59	2.75
17	2.31	2.38	2.47	2.62	2.79

Finally, Grubbs' test statistic is compared to Grubb's critical value:

- if $G < G_{crit}$: the sample is not an outlier and is kept in the study;
- if $G > G_{crit}$: the sample is an outlier and is excluded from the study. [17]

5.1.3 ANOVA

The ANOVA (Analysis Of Variance) is a family of statistical methods used to compare the means of two or more groups by analysing variance. Specifically, the ANOVA compares the amount of variation between the group means to the amount of variation within each group. If the between-group variation is substantially larger than the within-group variation, it suggests that the group means are likely different. This comparison is done using an F-test. The underlying principle of the ANOVA is based on the law of total variance, which states that the total variance in a dataset can be broken down into components attributable to different sources. In the case of the ANOVA, these sources are the variation between groups and the variation within groups.

The ANOVA uses traditional standardized terminology. Sample variance s^2 is calculated using Equation (5.1.3):

$$s^{2} = \frac{1}{N-1} \sum_{i=1}^{N} (X_{i} - \bar{X})^{2}$$
(5.1.3)

where the divisor is called the degrees of freedom (DF), the summation is called the sum of squares (SS), the result is called the mean square (MS) and the squared terms are deviations from the sample mean.

The fundamental technique is a partitioning of the total sum of squares SS_{total} into components related to the effects used in the model using Equation (5.1.4):

$$SS_{total} = SS_{error} + SS_{aroups} (5.1.4)$$

where:

- SS_{error} represents the variation within each group;
- SS_{groups} represents the variation between groups means.

The number of total degrees of freedom DF_{total} can be partitioned in a similar way using Equation (5.1.5):

$$DF_{total} = DF_{error} + DF_{groups} (5.1.5)$$

where:

- DF_{error} represents the degrees of freedom within each group;
- DF_{groups} represents the degrees of freedom between groups means.

The *F*-test is used for comparing the factors of the total deviation. For example, in one-way, or single-factor ANOVA, statistical significance is tested by comparing the *F* test statistic using Equation (5.1.6):

$$F = \frac{variance\ between\ groups}{variance\ within\ groups} \tag{5.1.6}$$

If all the groups are similar, the group means will be close, and the F-value will be small. If at least one group is very different, the variation between groups will be large, and the F-value will be large. So the larger the F-statistic, the more evidence there is that at least one group is different from the others.

Let us assume to have k groups, each with n_i observations with $i = 1 \dots k$.

Let us assume that:

- \bar{X}_i is the mean of group *i*;
- \bar{X} is the overall (grand) mean;
- X_{ij} is the j^{th} value in group i.

The total sum of squares SS_{total} is calculated using Equation (5.1.7):

$$SS_{total} = \sum_{i=1}^{k} \sum_{j=1}^{n_i} (X_{ij} - \bar{X})^2$$
 (5.1.7)

The number of total degrees of freedom DF_{total} is calculated using Equation (5.1.8):

$$DF_{total} = N - 1 \tag{5.1.8}$$

The sum of squares between groups SS_{groups} is calculated using Equation (5.1.9):

$$SS_{groups} = \sum_{i=1}^{k} n_i (\bar{X}_i - \bar{X})$$
(5.1.9)

The number of degrees of freedom between groups DF_{groups} is calculated using Equation (5.1.10):

$$DF_{aroups} = k - 1 \tag{5.1.10}$$

The mean square between groups MS_{groups} is calculated using Equation (5.1.11):

$$MS_{groups} = \frac{SS_{groups}}{DF_{groups}} \tag{5.1.11}$$

The sum of squares within groups SS_{error} is calculated using Equation (5.1.12):

$$SS_{error} = \sum_{i=1}^{k} \sum_{j=1}^{n_i} (X_{ij} - \bar{X}_i)^2$$
 (5.1.12)

The number of degrees of freedom within groups DF_{error} is calculated using Equation (5.1.13):

$$DF_{error} = N - k (5.1.13)$$

The mean square within groups MS_{error} is calculated using Equation (5.1.14):

$$MS_{error} = \frac{SS_{error}}{DF_{error}} \tag{5.1.14}$$

Finally, the F-value is calculated using Equation (5.1.15):

$$F = \frac{MS_{groups}}{MS_{error}} \tag{5.1.15}$$

Furthermore, from the F-statistic and the number of groups and samples, the p-value is calculated. The p-value represents how likely it is to get an F-statistic as big as the one calculated just by random chance, if all the group means were actually equal: this is called "null hypothesis". The p-value is compared to the significance level α :

- if $p < \alpha$: the null hypothesis is rejected, the differences between groups are unlikely due to chance and they are statistically significant.;
- if $p \ge \alpha$: the null hypothesis is not rejected, the differences between groups may be due to random variation and they are not statistically significant. [14] [15]

Figure 5.1.3 shows an example of residual plots obtained by Minitab when the ANOVA is performed. Residuals are the differences between values measured in laboratory and values predicted by the model. The normal probability plot (top left) shows the standardised residuals versus the theoretical quartiles of the normal distribution and allows to understand if residuals follow a normal distribution: if points follow a straight line, normality is respected. The versus fits plot (top right) shows the residuals versus the values predicted by the model and allows to understand if the residuals variance is constant: if points are randomly distributed around zero, residuals variance is constant. The histogram plot (bottom left) shows the frequency versus the residuals

and allows to understand if residuals follow a normal distribution: if the histogram has a bell shape, normality is respected. The versus order plot (bottom right) shows the residuals versus the observation order and allows to understand if residuals are independent from time: if points are randomly distributed around zero, time independence is respected.

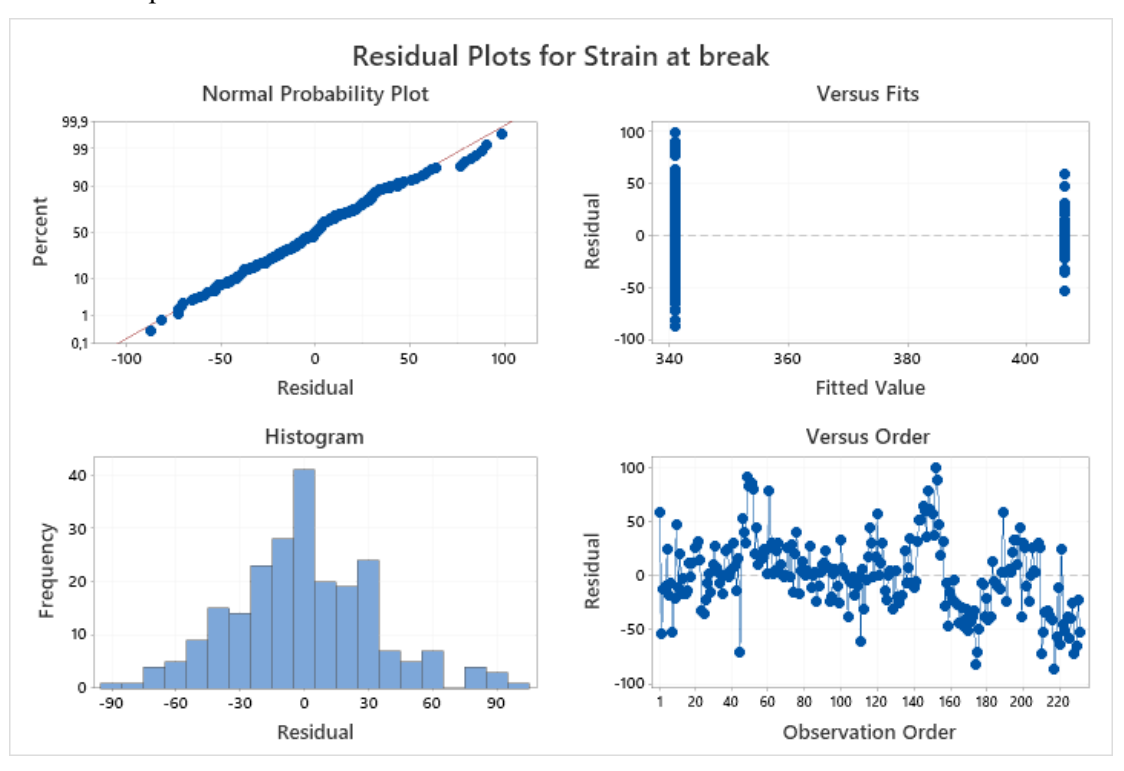


Figure 5.1.3: Residual plots

5.1.4 Response surface regression

The regression equation is used to describe the relationship between the response and the terms in the model. In this thesis, the responses are the mechanical properties analysed, while the terms are the coordinates of the oven *X*, *Y*, *Z*, which are continuous factors, and the ring, which is a categorical factor.

Equation (5.1.16) is the first-order regression equation with more than one term:

$$y = b_0 + b_1 x_1 + b_2 x_2 + \dots + b_k x_k \tag{5.1.16}$$

where:

- *y* is the response variable;
- b_0 is the constant;
- $b_1, b_2, ..., b_k$ are the coefficients;
- $x_1, x_2, ..., x_k$ are the values of the continuous factors.

If the response surface contains curvature, then a polynomial model of higher degree is used. Equation (5.1.17) is the second-order regression equation:

$$y = b_0 + \sum_{i=1}^k b_i x_i + \sum_{i=1}^k b_{ii} x_i^2 + \sum_{i \le i} b_{ij} x_i x_j + \varepsilon$$
 (5.1.17)

where ε is the error term. [18]

5.2 Hardness Shore test

5.2.1 Descriptive statistics

All the hardness values have been normalised dividing for a constant number to ensure industrial confidentiality without changing the variance: therefore, the values in this analysis are normalized but the behaviour is the same.

Figure 5.2.1 shows the boxplot of hardness values measured in laboratory grouped by the position of the tube inside the oven. As it can be observed, the boxplot of FDL position is completely misaligned from the others: this suggests that there may be a correlation between the hardness and the position of the tube inside the oven.

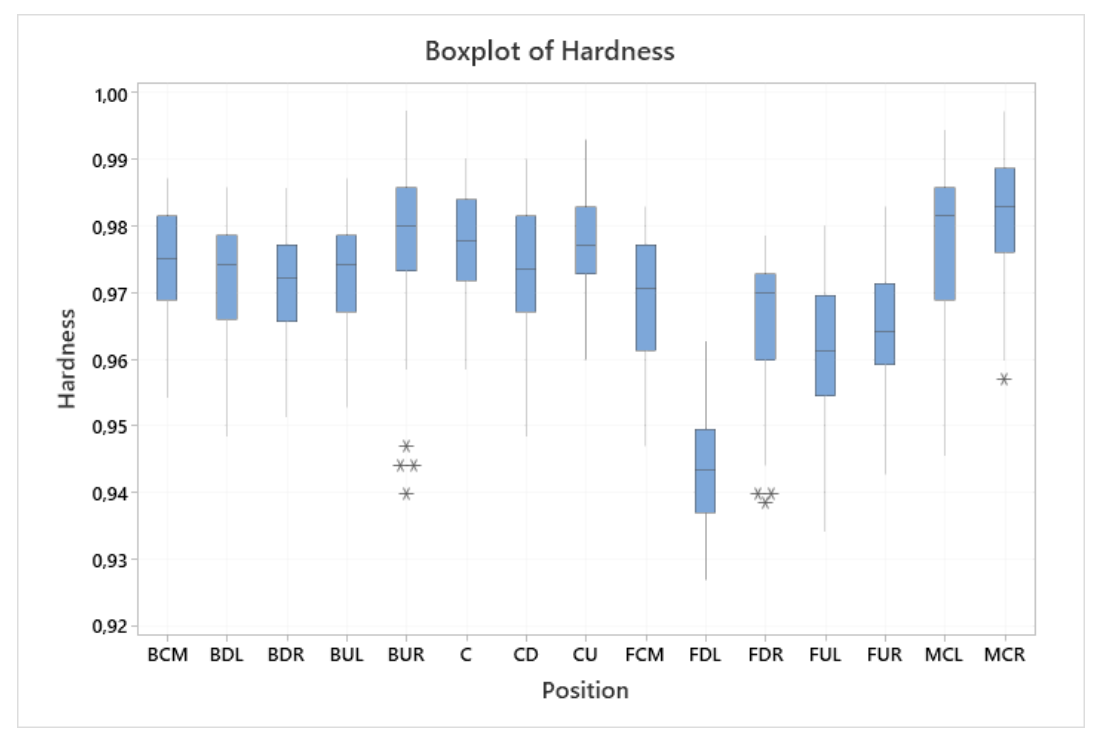


Figure 5.2.1: Boxplot of hardness values grouped by the position of the tube inside the oven

Figure 5.2.2 shows the boxplot of hardness values measured in laboratory grouped by the position of the ring inside the tube.

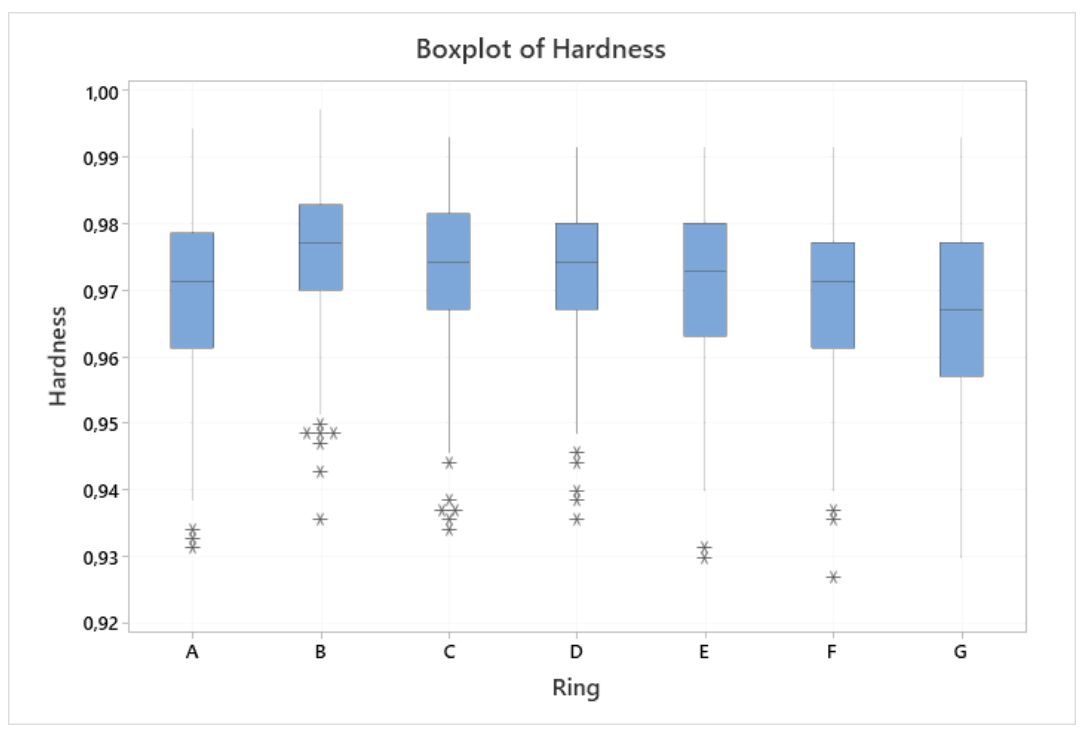


Figure 5.2.2: Boxplot of hardness values grouped by the position of the ring inside the tube

Figure 5.2.3 shows the dotplot of hardness values measured in laboratory grouped by the position of the tube inside the oven.

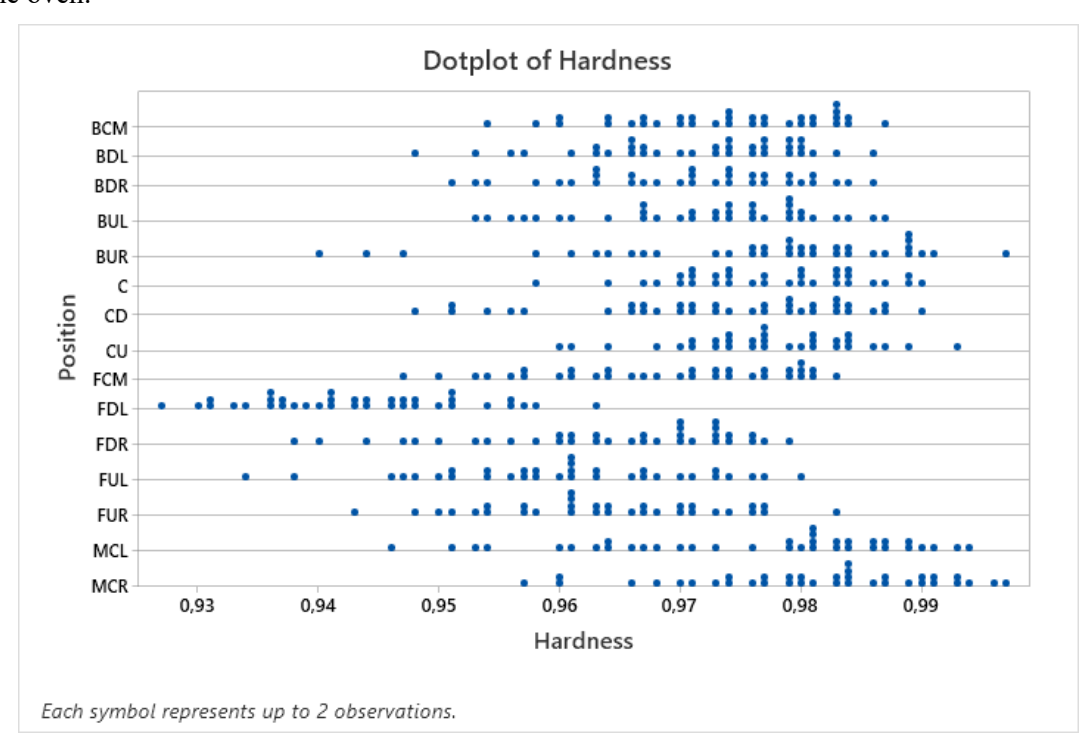


Figure 5.2.3: Dotplot of hardness values grouped by the position of the tube inside the oven

Figure 5.2.4 shows the dotplot of hardness values measured in laboratory grouped by the position of the ring inside the tube.

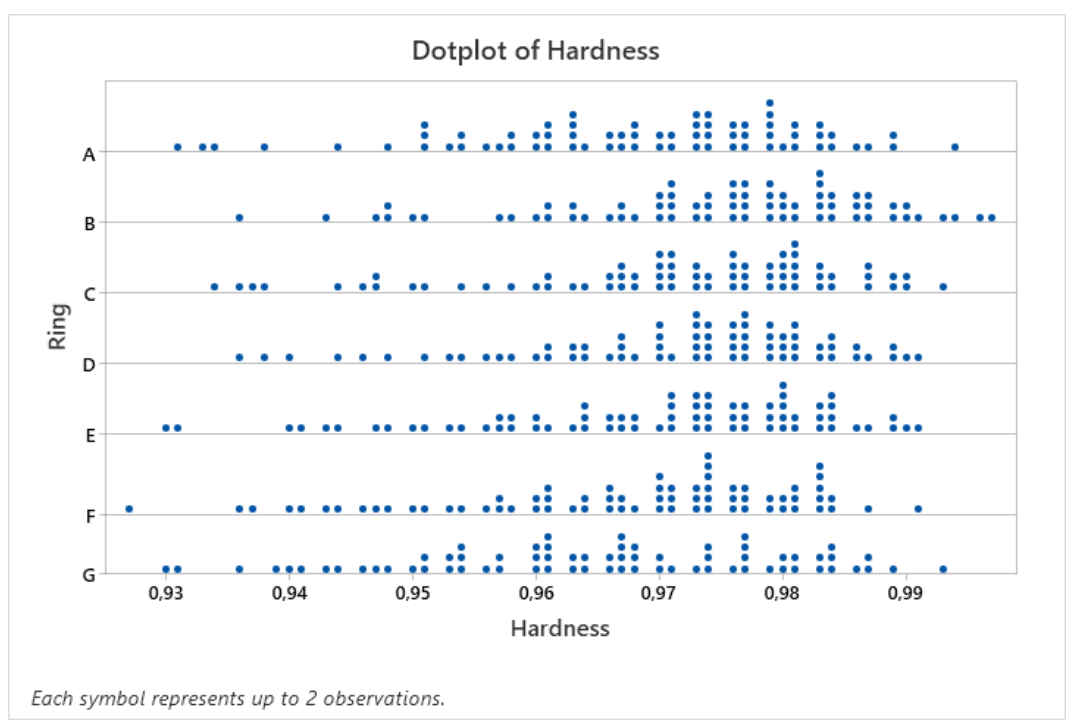


Figure 5.2.4: Dotplot of hardness values grouped by the position of the ring inside the tube

5.2.2 Outlier identification

The Grubbs' test to identify outliers is carried out before proceeding with ANOVA. Figure 5.2.5 shows the outlier plot of hardness values grouped by the position of the tube inside the oven: as it can be seen, no outlier is found by the test.

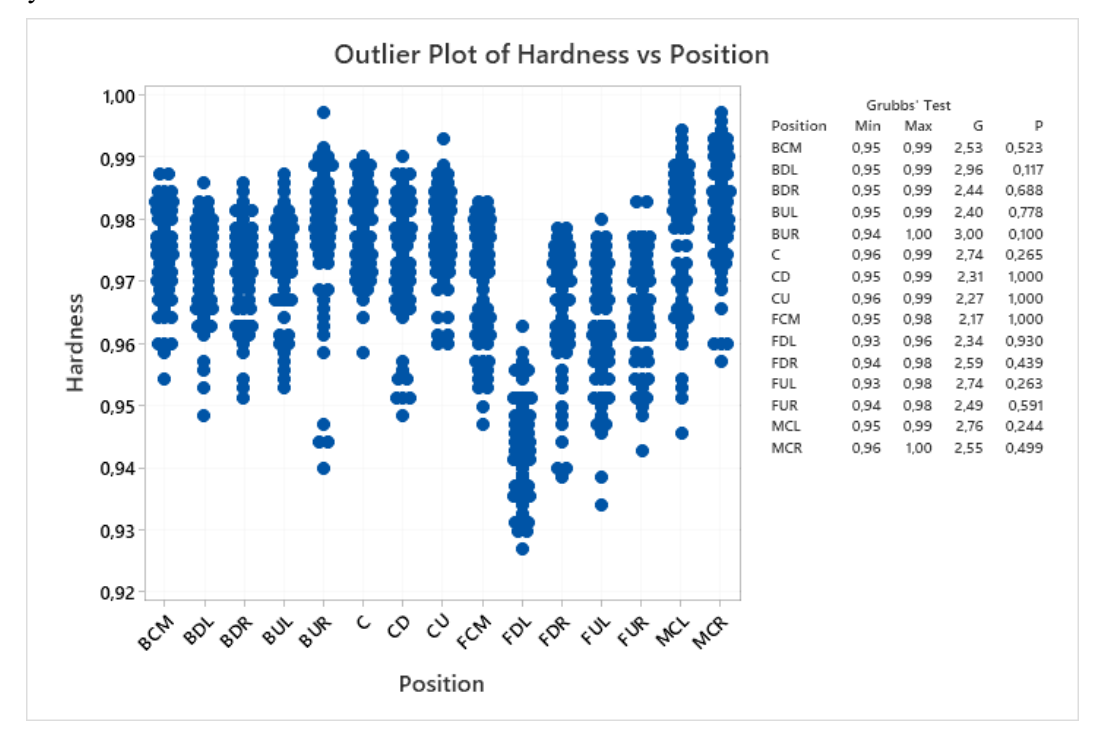


Figure 5.2.5: Outlier plot of hardness values grouped by the position of the tube inside the oven

5.2.3 ANOVA

The ANOVA is carried out to investigate if there are correlations between the hardness, the position of the tube inside the oven and the position of the ring in the tube.

Table 5.2.1 shows the results of the ANOVA. As it can be observed, the F-values of both the position and the ring are very high, while the p-values are much lower than 0.05. This indicates that the hardness is affected by both the position of the tube inside the oven and the position of the ring inside the tube.

Table 5.2.1: Results of the ANOVA of the hardness

Analysis of Variance

Source	DF	Adj SS	Adj MS	F-Value	P-Value
Position	14	0,066895	0,004778	60,16	0,000
Ring	6	0,006764	0,001127	14,19	0,000
Error	819	0,065046	0,000079		
Lack-of-Fit	84	0,008184	0,000097	1,26	0,067
Pure Error	735	0,056863	0,000077		
Total	839	0,138705			

Table 5.2.2 shows the model summary of the ANOVA. The coefficient of determination R^2 is 53.10%, indicating that the model represents half of the data variability. This could be due to the presence of the supplier factor and of the vulcanisation cycles, which are not considered in this analysis.

Table 5.2.2: Model summary of the ANOVA of the hardness

Model Summary

S R-sq R-sq(adj) R-sq(pred) 0,0089119 53,10% 51,96% 50,67%

Figure 5.2.6 shows the residual plots for the hardness. As it can be seen, in the normal probability plot (top left) the points follow a straight line and the histogram plot (bottom left) has a bell shape: this means that normality is respected. In the versus fits plot (top right) the points are randomly distributed around zero: this means that residuals variance is constant. Finally, in the versus order plot (bottom right) the points are randomly distributed around zero: this means that time independence is respected.

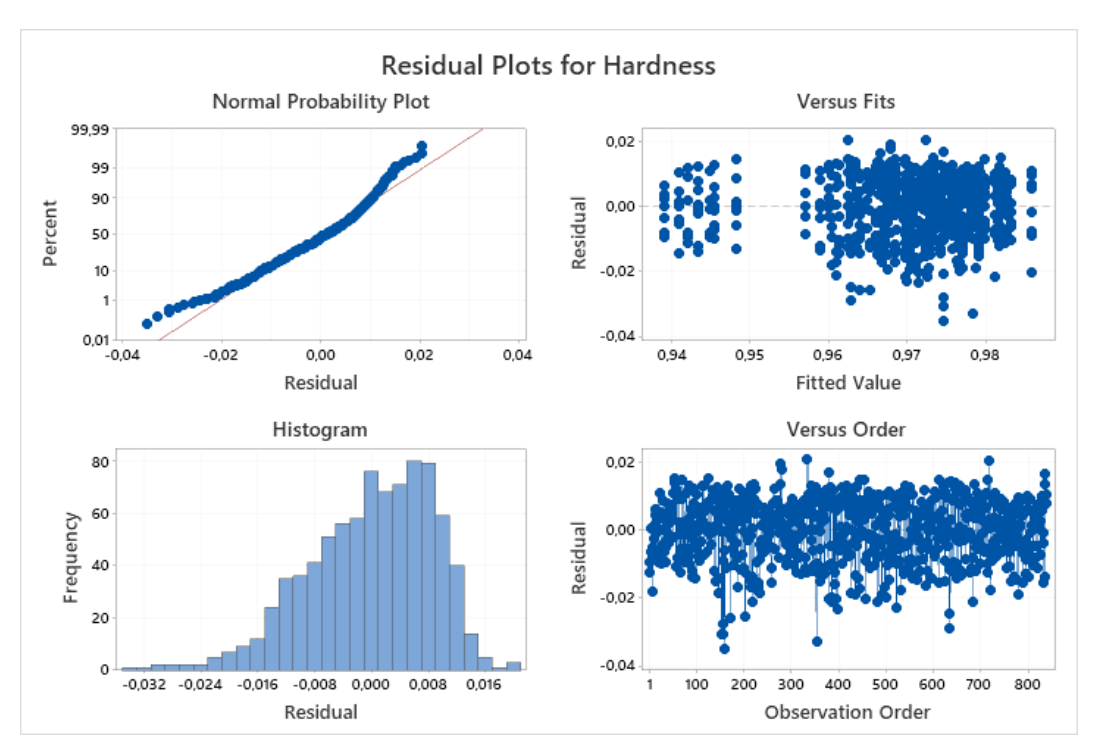


Figure 5.2.6: Residual plots for the hardness

5.2.4 Response surface regression

As the ANOVA highlights a correlation between the hardness, the position of the tube inside the oven and the position of the tube inside the ring, the response surface regression is carried out using as terms the coordinates of the oven X, Y, Z and the ring. In the response surface regressions of this thesis, the significance level α is set to 0.15, so only the terms with a p-value lower than 0.15 are considered significant.

Table 5.2.3 shows the model summary of the response surface regression. The coefficient of determination R^2 is 48.64%, indicating that the model represents half of the data variability. Also in this case, this could be due to the presence of the supplier factor and of the vulcanisation cycles, which are not considered in this analysis.

Table 5.2.3: Model summary of the response surface regression of the hardness

Model Summary S R-sq R-sq(adj) R-sq(pred) 0,0092926 48,64% 47,77% 46,73%

Table 5.2.4 shows the ANOVA for each significant term with a level of confidence of 0.15 of the response surface regression. By looking at the columns of *F*-values and *p*-values, it is possible to understand which terms affect more the model of the hardness.

Table 5.2.4: ANOVA for each significant term of the response surface regression of the hardness

Analysis of Variance

Source	DF	Adj SS	Adj MS	F-Value	P-Value
Model	14	0,067464	0,004819	55,80	0,000
Linear	9	0,039705	0,004412	51,09	0,000
Χ	1	0,022345	0,022345	258,76	0,000
Υ	1	0,006233	0,006233	72,19	0,000
Z	1	0,004363	0,004363	50,53	0,000
Ring	6	0,006764	0,001127	13,05	0,000
Square	2	0,022520	0,011260	130,40	0,000
X*X	1	0,010481	0,010481	121,38	0,000
Z*Z	1	0,003553	0,003553	41,15	0,000
2-Way Interaction	3	0,005238	0,001746	20,22	0,000
X*Y	1	0,003249	0,003249	37,62	0,000
X*Z	1	0,000875	0,000875	10,14	0,002
Y*Z	1	0,001114	0,001114	12,90	0,000
Error	825	0,071241	0,000086		
Lack-of-Fit	90	0,014378	0,000160	2,06	0,000
Pure Error	735	0,056863	0,000077		
Total	839	0,138705			

Figure 5.2.7 shows the Pareto chart of the standardised effects. The standardised effect indicates how influent each term is and, in this case, all the terms with a standardised effect higher than 1.44 are considered significant.

By looking at Table 5.2.4 and at Figure 5.2.7 it can be stated that the significant terms with a level of confidence of 0.15 in descending order are X, X^2 , Y, Z, Ring, Z^2 , X*Y, Y*Z and X*Z.

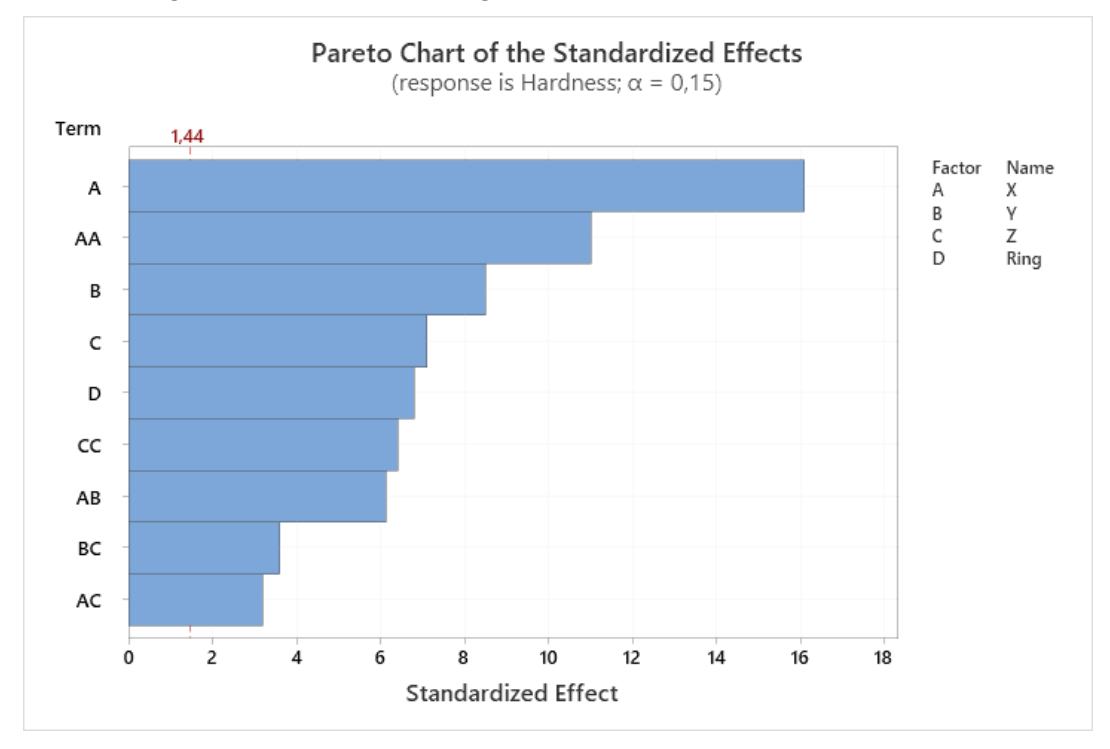


Figure 5.2.7: Pareto Chart of the standardised effects of the response surface regression of the hardness

Table 5.2.5 shows the regression equations of the hardness as a function of the coordinates of the oven. There are seven equations: one for each ring.

Table 5.2.5: Regression equations of the hardness as a function of the coordinates of the oven

Regression Equation in Uncoded Units

Ring	
А	Hardness = 0,97774 - 0,005053 X + 0,004448 Y + 0,002791 Z - 0,005233 X*X - 0,004761 Z*Z + 0,002872 X*Y + 0,001118 X*Z - 0,002103 Y*Z
В	$ \begin{tabular}{lll} \mbox{Hardness} &= 0.98384 - 0.005053 \mbox{ X} + 0.004448 \mbox{ Y} + 0.002791 \mbox{ Z} - 0.005233 \mbox{ X*X} - 0.004761 \mbox{ Z*Z} \\ &+ 0.002872 \mbox{ X*Y} + 0.001118 \mbox{ X*Z} - 0.002103 \mbox{ Y*Z} \end{tabular} $
С	$ \begin{tabular}{lll} \mbox{Hardness} &= 0.98044 - 0.005053 \mbox{ X} + 0.004448 \mbox{ Y} + 0.002791 \mbox{ Z} - 0.005233 \mbox{ X*X} - 0.004761 \mbox{ Z*Z} \\ &+ 0.002872 \mbox{ X*Y} + 0.001118 \mbox{ X*Z} - 0.002103 \mbox{ Y*Z} \end{tabular} $
D	$\begin{aligned} \text{Hardness} &= 0.98107 - 0.005053 \ X + 0.004448 \ Y + 0.002791 \ Z - 0.005233 \ X*X - 0.004761 \ Z*Z \\ &+ 0.002872 \ X*Y + 0.001118 \ X*Z - 0.002103 \ Y*Z \end{aligned}$
Е	Hardness = 0,97905 - 0,005053 X + 0,004448 Y + 0,002791 Z - 0,005233 X*X - 0,004761 Z*Z + 0,002872 X*Y + 0,001118 X*Z - 0,002103 Y*Z
F	$\begin{aligned} \text{Hardness} &= 0,97659 - 0,005053 \ X + 0,004448 \ Y + 0,002791 \ Z - 0,005233 \ X*X - 0,004761 \ Z*Z \\ &+ 0,002872 \ X*Y + 0,001118 \ X*Z - 0,002103 \ Y*Z \end{aligned}$
G	$Hardness = 0.97462 - 0.005053 \ X + 0.004448 \ Y + 0.002791 \ Z - 0.005233 \ X*X - 0.004761 \ Z*Z \\ + 0.002872 \ X*Y + 0.001118 \ X*Z - 0.002103 \ Y*Z$

Figure 5.2.8 shows the surface plots of hardness as a function of the coordinates of the oven for ring A. In each plot, the axes represent the hardness and two coordinates, while the third coordinate is kept constant with value equal to 0.

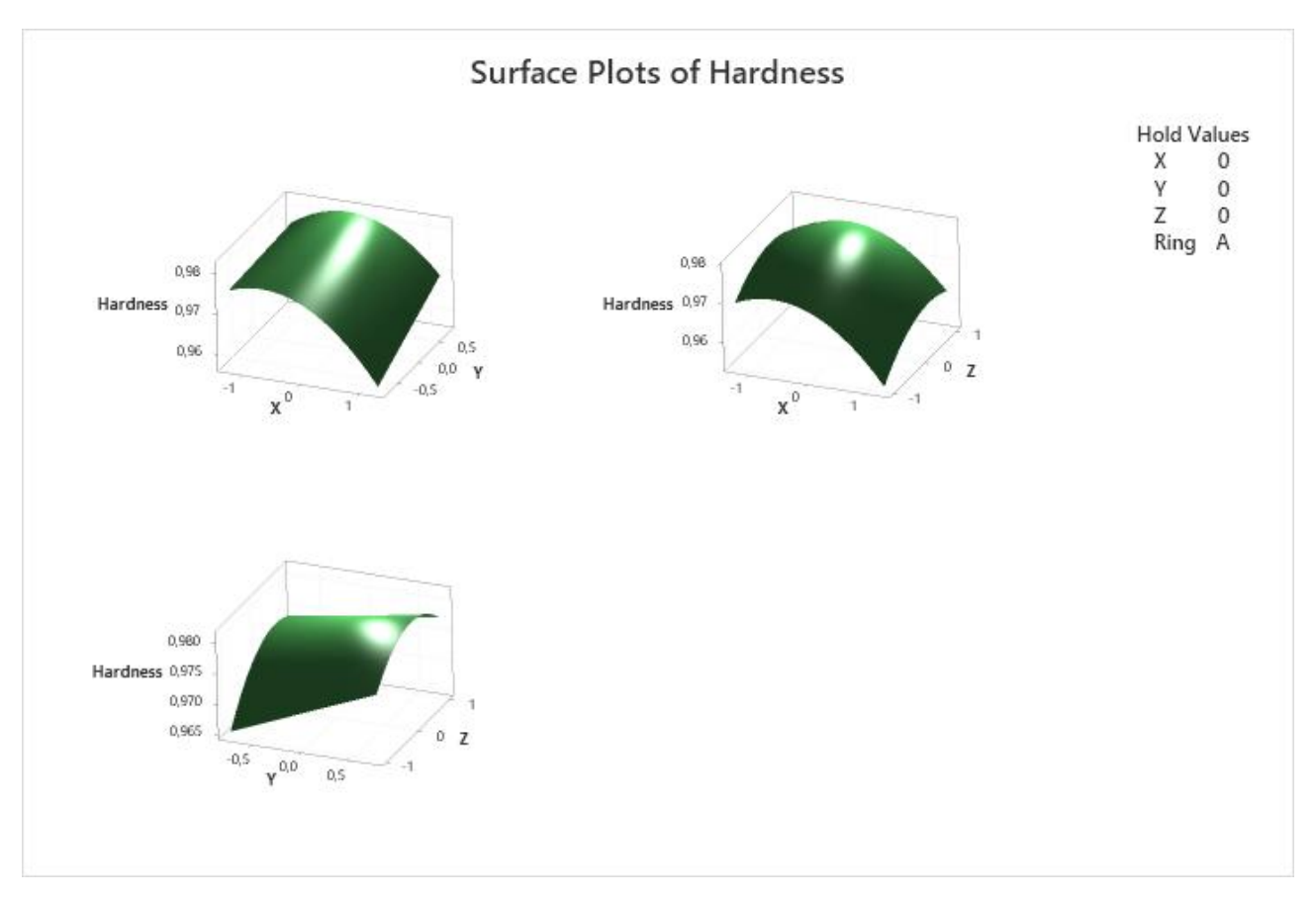


Figure 5.2.8: Surface plots of hardness as a function of the coordinates of the oven for ring A

Finally, the multiple response prediction for both the maximum and the minimum value of hardness is found.

Table 5.2.6 shows the maximum value of hardness predicted by the response surface regression as well as its coordinates, its ring and its 95% CI (Confidence Interval). The maximum value is 0.988 Shore with a 95% CI between 0.986 and 0.990 and it is expected to be near MCR position in ring B.

Table 5.2.6: Multiple response prediction for the maximum value of hardness

Multiple Response Prediction

Variable Setting X -0,265152 Y 0,75 Z 0,0909091 Ring B Response Fit SE Fit 95% CI 95% PI Hardness 0,98762 0,00108 (0,98550; 0,98974) (0,96926; 1,00598)

Table 5.2.7 shows the minimum value of hardness predicted by the response surface regression as well as its coordinates, its ring and its 95% CI (Confidence Interval). The minimum value is 0.944 Shore with a 95% CI between 0.941 and 0.946 and it is expected to be in FDL position in ring G.

Table 5.2.7: Multiple response prediction for the minimum value of hardness

Multiple Response Prediction

Variable S	Setting			
Χ	1,25			
Υ	-0,75			
Z	-1			
Ring	G			
Response	Fit	SE Fit	95% CI	95% PI
Hardness	0,94357	0,00135	(0,94091; 0,94622)	(0,92513; 0,96200)

Figure 5.2.9 shows the sketch of the oven with the means of the measured hardness values for each position (number inside the rectangles) and the predicted maximum and minimum values (numbers inside the circles). The scale of colours is set to assign the green to the lowest values and the red to the highest ones. As it can be observed, the values in the front are the lowest, while the values on the back and in the centre are the highest. This highlights that hardness depends on the post-curing temperature: the higher the temperature is, the higher the hardness is. This can be explained by the fact that increasing the temperature, the sulphur atoms form more crosslinks between the long rubber polymer chains and so they become more compact: the result is that the elastomer becomes harder. Therefore, in the front the hardness values are lower because there is the oven door and so the temperature is lower, while on the back and in the centre the hardness values are higher because they are far from the door and so the temperature is higher. Furthermore, the predicted maximum and minimum values are near the measured maximum and minimum values: this highlights that the model obtained by the response surface regression is reliable.

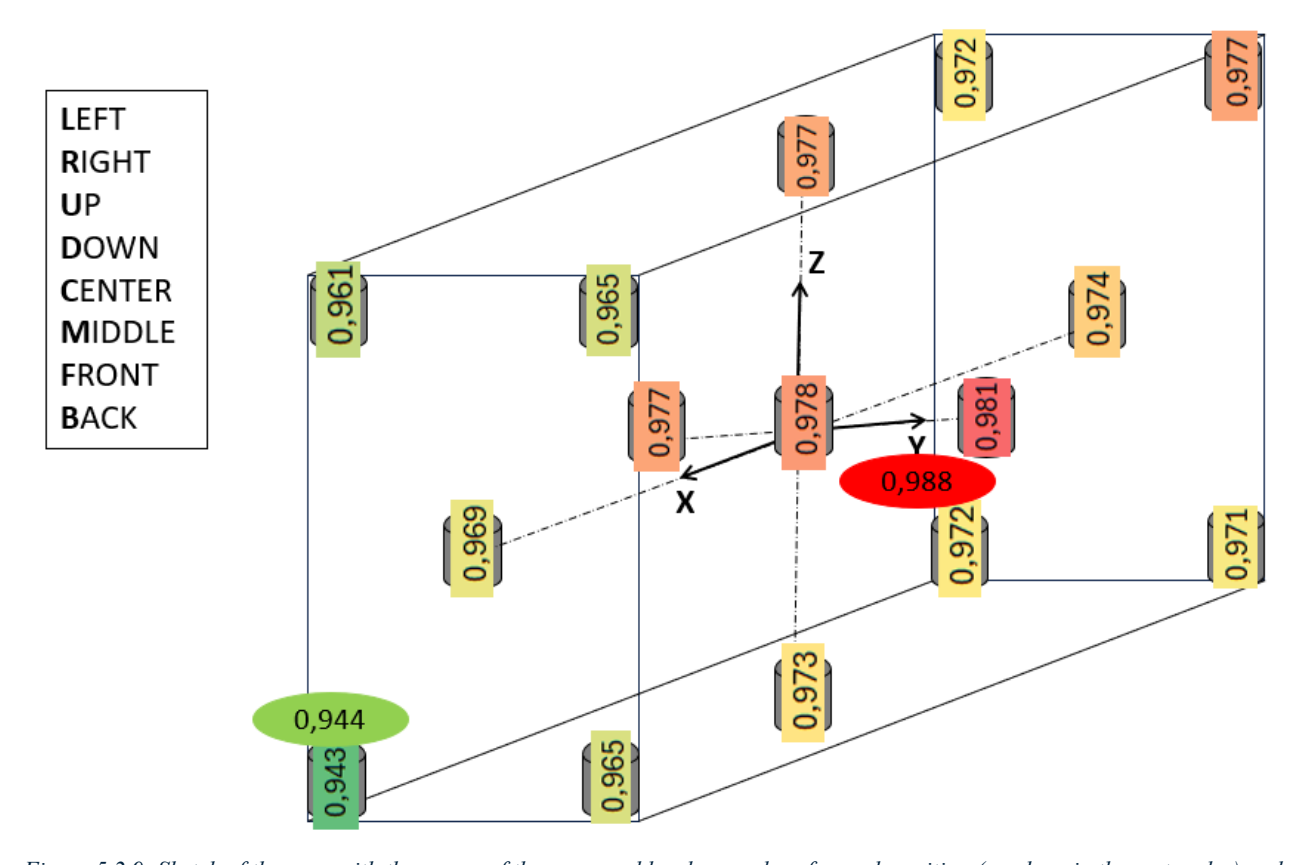


Figure 5.2.9: Sketch of the oven with the means of the measured hardness values for each position (numbers in the rectangles) and the predicted maximum and minimum values (numbers in the circles)

5.3 Tensile test: stress at break

5.3.1 Descriptive statistics

All the stress at break values have been normalised multiplying for a constant number to ensure industrial confidentiality without changing the variance: therefore, the same considerations done for hardness are valid.

Figure 5.3.1 shows the boxplot of stress at break values measured in laboratory grouped by the position of the tube inside the oven.

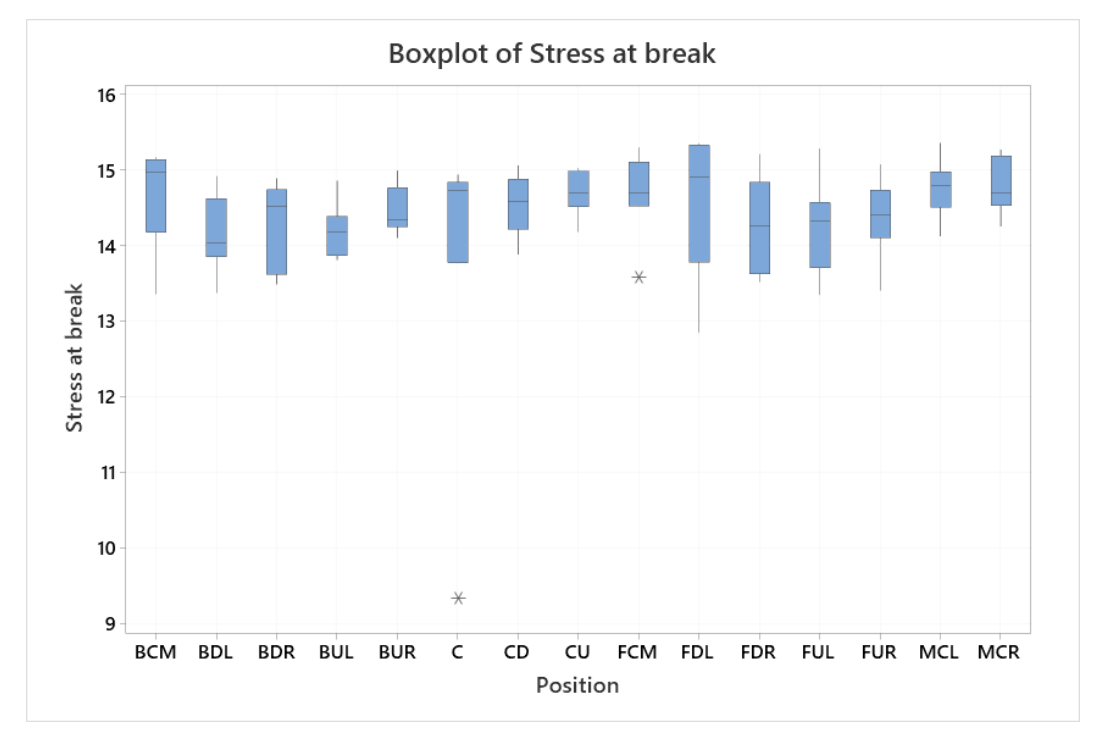


Figure 5.3.1: Boxplot of stress at break values grouped by the position of the tube inside the oven

Figure 5.3.2 shows the boxplot of stress at break values measured in laboratory grouped by the position of the ring inside the tube.

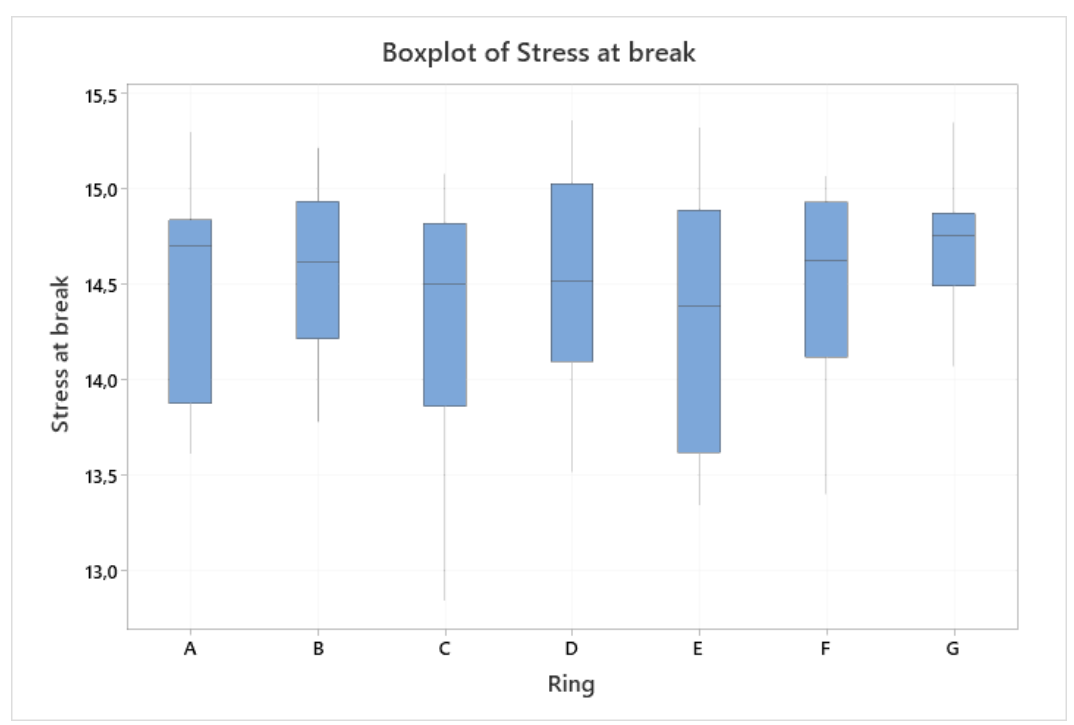


Figure 5.3.2: Boxplot of stress at break values grouped by the position of the ring inside the tube

Figure 5.3.3 shows the dotplot of stress at break values measured in laboratory grouped by the position of the tube inside the oven.

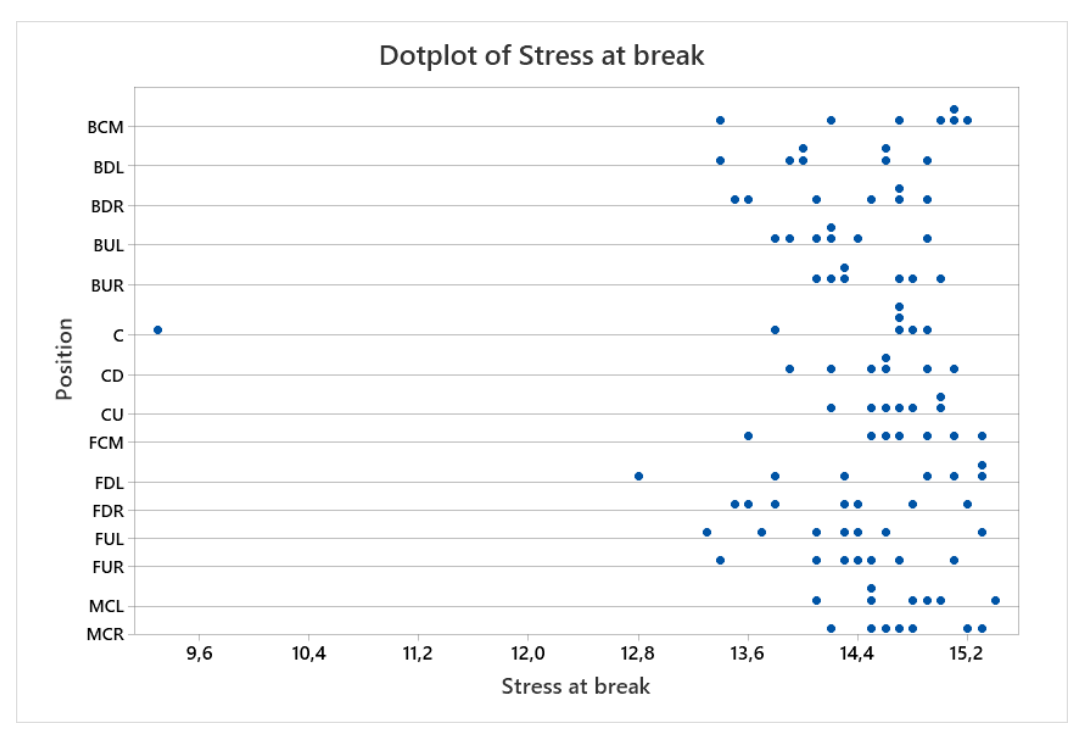


Figure 5.3.3: Dotplot of stress at break values grouped by the position of the tube inside the oven

Figure 5.3.4 shows the dotplot of stress at break values measured in laboratory grouped by the position of the ring inside the tube.

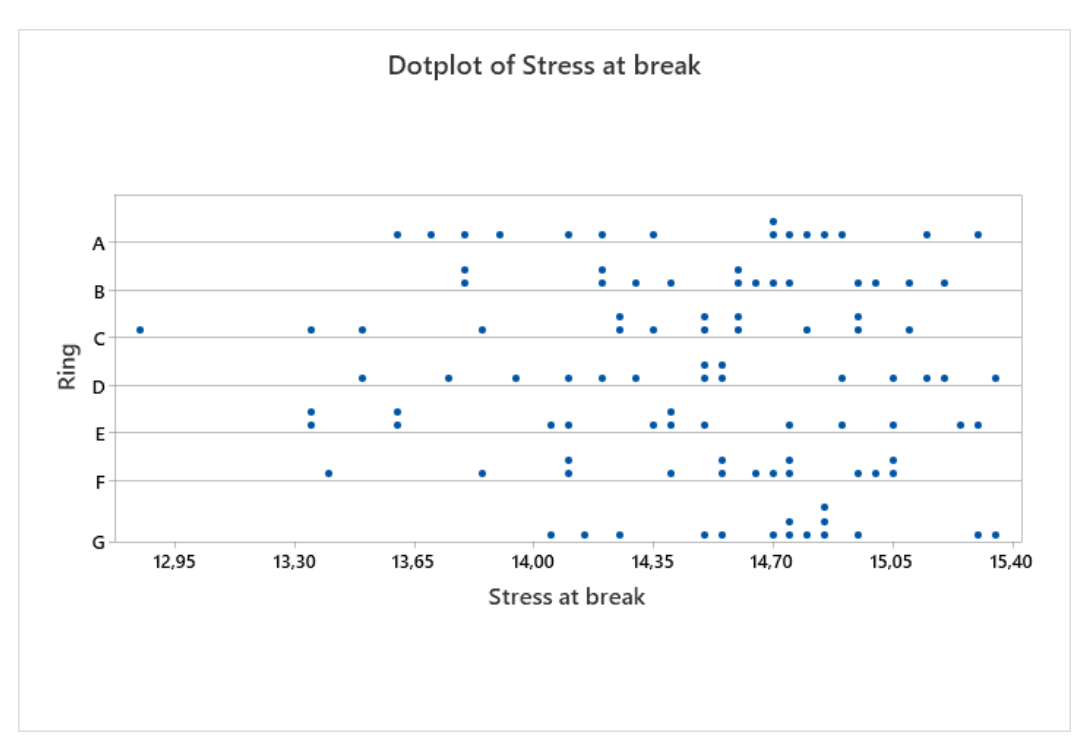


Figure 5.3.4: Dotplot of stress at break values grouped by the position of the ring inside the tube

5.3.2 Outlier identification

The Grubbs' test to identify outliers is carried out before proceeding with ANOVA. Figure 5.3.5 shows the outlier plot of stress at break values grouped by the position of the tube inside the oven: as it can be seen, only one outlier is found by the test in C position. Before proceeding with the ANOVA, the outlier is replaced by the median of the other values in C position.

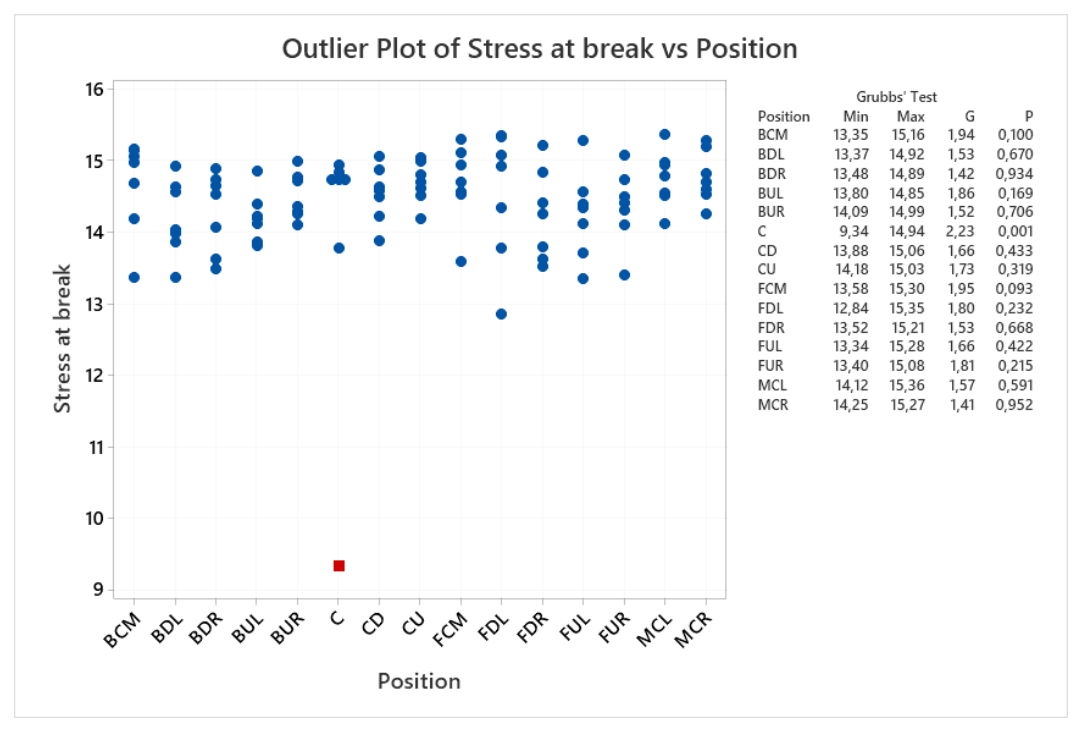


Figure 5.3.5: Outlier plot of stress at break values grouped by the position of the tube inside the oven

5.3.3 ANOVA

The ANOVA is carried out to investigate if there are correlations between the stress at break, the position of the tube inside the oven and the position of the ring in the tube.

Table 5.3.1 shows the results of the ANOVA. As it can be observed, the *F*-values of both the position and the ring are low, while the *p*-values are higher than 0.05. This indicates that the stress at break is affected by neither the position of the tube inside the oven nor the position of the ring inside the tube.

Table 5.3.1: Results of the ANOVA of the stress at break

Analysis of Variance

Source	DF	Adj SS	Adj MS	F-Value	P-Value
Position	14	4,317	0,3084	1,10	0,366
Ring	6	1,782	0,2970	1,06	0,391
Error	84	23,461	0,2793		
Total	104	29,559			

Table 5.3.2 shows the model summary of the ANOVA. The coefficient of determination R^2 is 20.63%, indicating that the model represents only a small portion of the data variability. This could be due to the fact that the ANOVA doesn't highlights a correlation between the stress at break, the position of the tube inside the oven and the position of the ring inside the tube.

Table 5.3.2: Model summary of the ANOVA of the stress at break

Model Summary

S R-sq R-sq(adj) R-sq(pred) 0,528481 20,63% 1,74% 0,00%

Figure 5.3.6 shows the residual plots for the stress at break. As it can be seen, in the normal probability plot (top left) the points follow a straight line and the histogram plot (bottom left) has a bell shape: this means that normality is respected. In the versus fits plot (top right) the points are randomly distributed around zero: this means that residuals variance is constant. Finally, in the versus order plot (bottom right) the points are randomly distributed around zero: this means that time independence is respected.

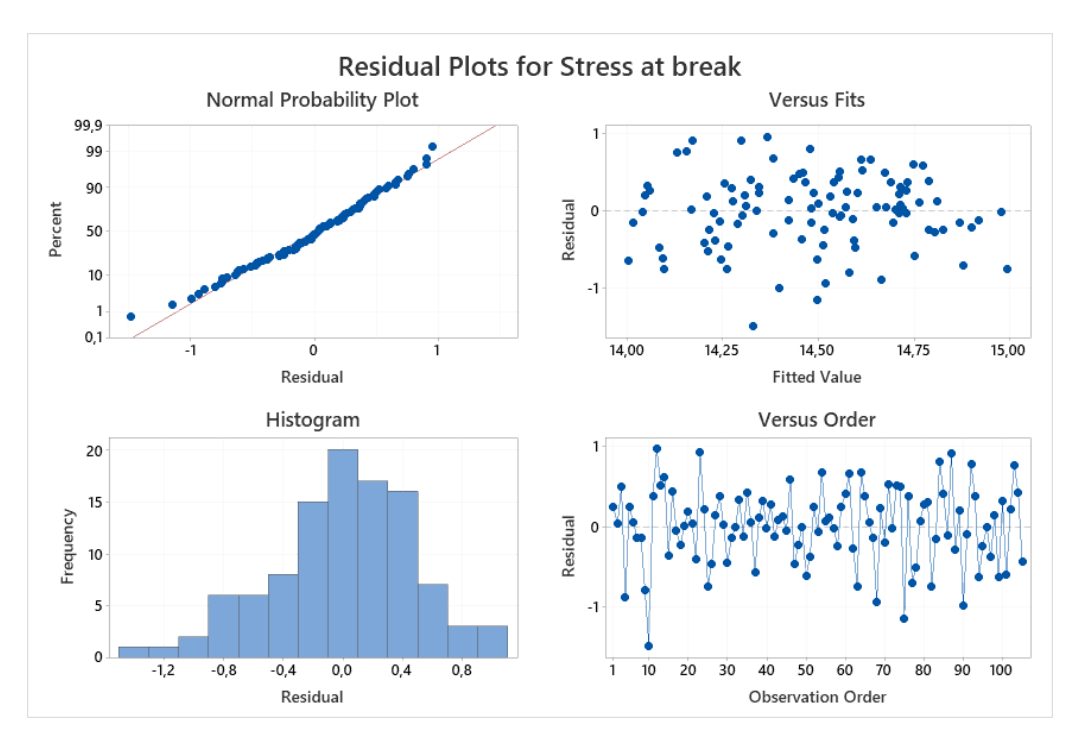


Figure 5.3.6: Residual plots for the stress at break

As the ANOVA does not highlight a correlation between the stress at break, the position of the tube inside the oven or the position of the ring in the tube, there is no need to proceed with the response surface regression because the model wouldn't be significative.

5.4 Tensile test: strain at break

5.4.1 Descriptive statistics

All the strain at break values have been normalised multiplying for a constant number to ensure industrial confidentiality without changing the variance: therefore, the same considerations done for hardness are valid.

Figure 5.4.1 shows the boxplot of strain at break values measured in laboratory grouped by the position of the tube inside the oven. As it can be observed, the boxplot of FDL position is completely misaligned from the others: this suggests that there may be a correlation between the strain at break and the position of the tube inside the oven.

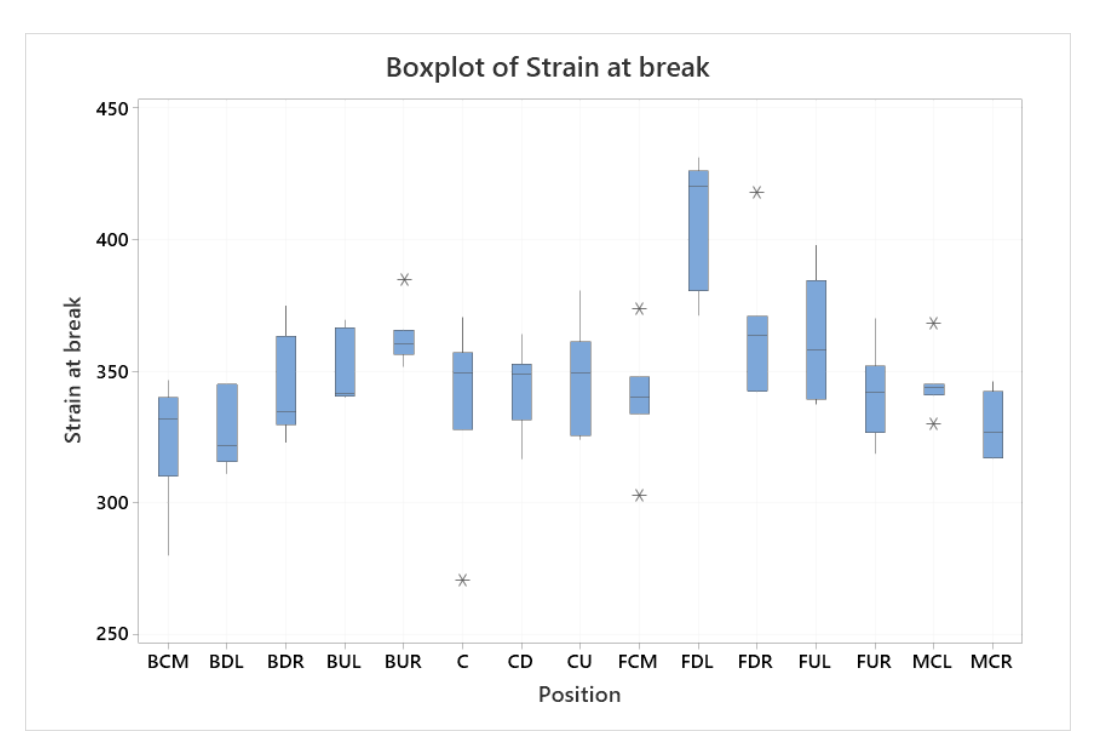


Figure 5.4.1: Boxplot of strain at break values grouped by the position of the tube inside the oven

Figure 5.4.2 shows the boxplot of strain at break values measured in laboratory grouped by the position of the ring inside the tube.

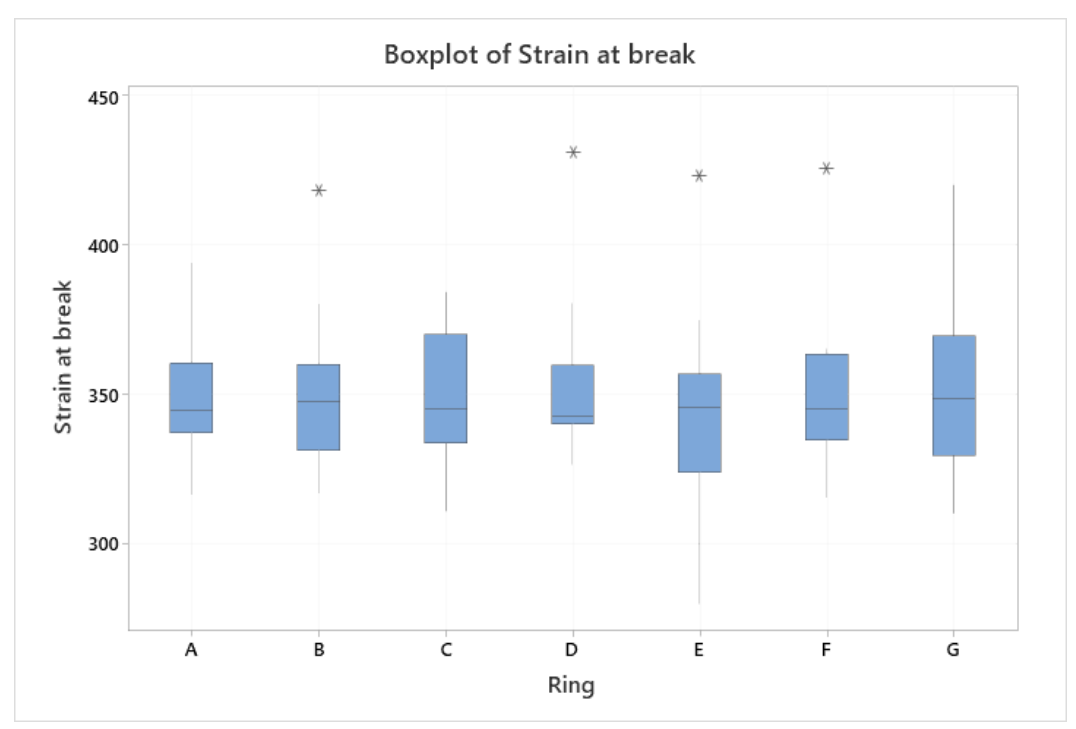


Figure 5.4.2: Boxplot of strain at break values grouped by the position of the ring inside the tube

Figure 5.4.3 shows the dotplot of strain at break values measured in laboratory grouped by the position of the tube inside the oven.

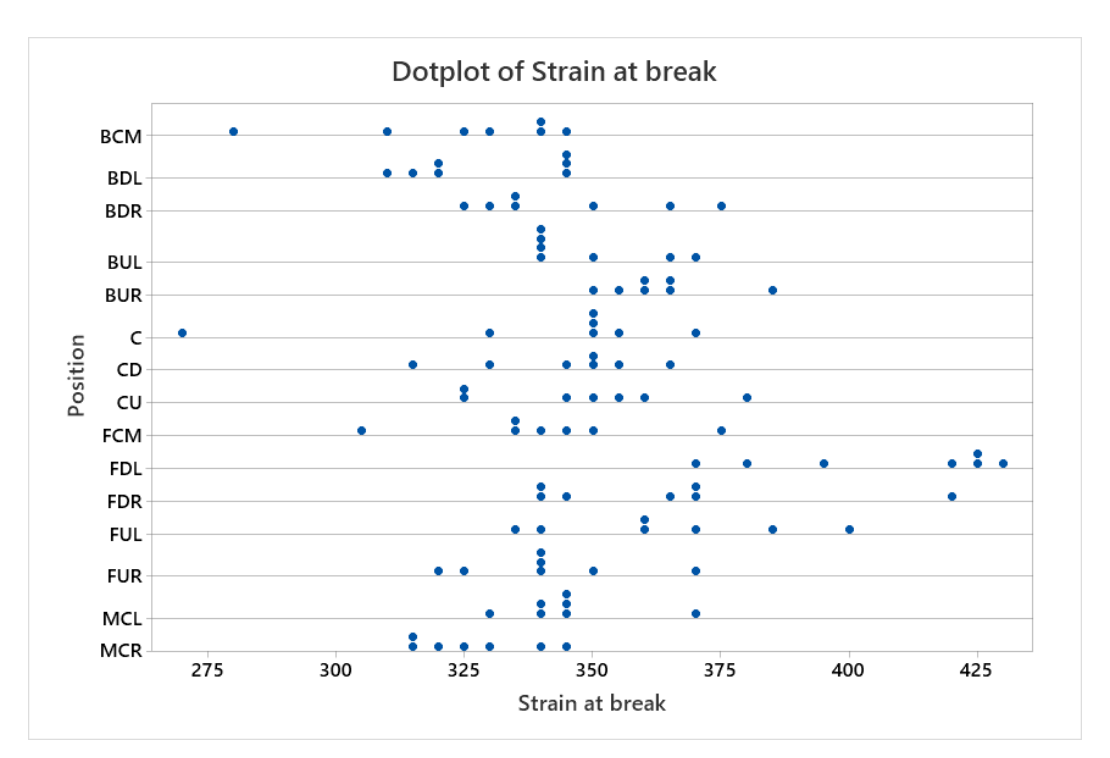


Figure 5.4.3: Dotplot of strain at break values grouped by the position of the tube inside the oven

Figure 5.4.4 shows the dotplot of strain at break values measured in laboratory grouped by the position of the ring inside the tube.

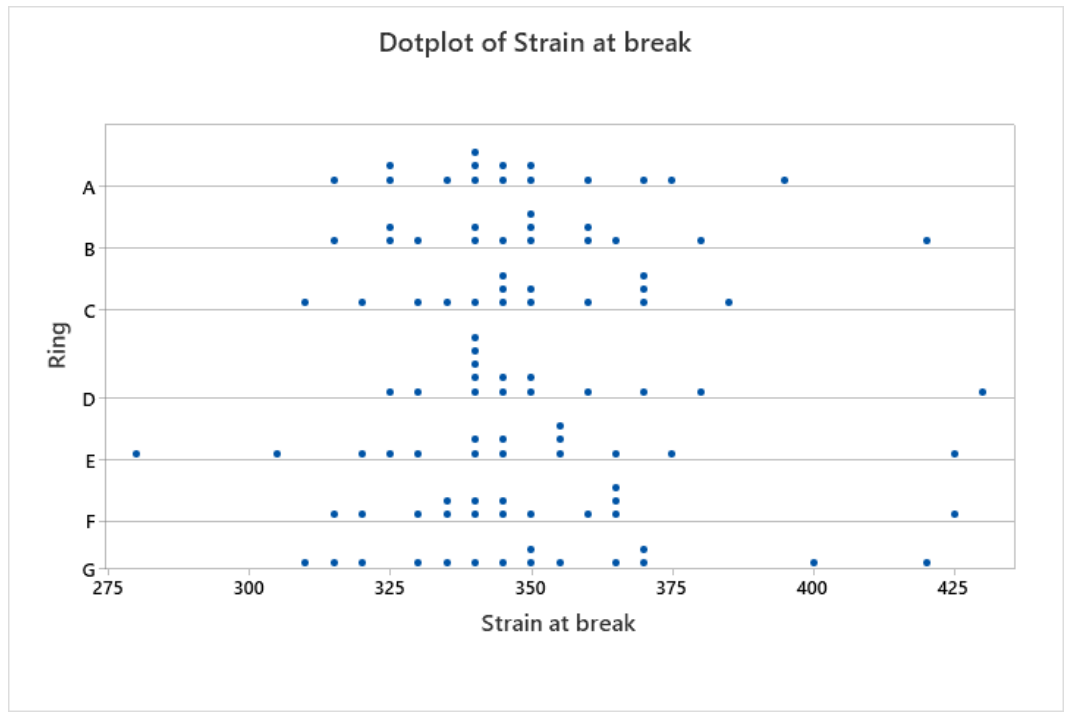


Figure 5.4.4: Dotplot of strain at break values grouped by the position of the ring inside the tube

5.4.2 Outlier identification

The Grubbs' test to identify outliers is carried out before proceeding with ANOVA. Figure 5.4.5 shows the outlier plot of strain at break values grouped by the position of the tube inside the oven: as it can be seen, three

outliers are found by the test in BUR, C and MCL positions. Before proceeding with the ANOVA, each outlier is replaced by the median of the other values in the same position.

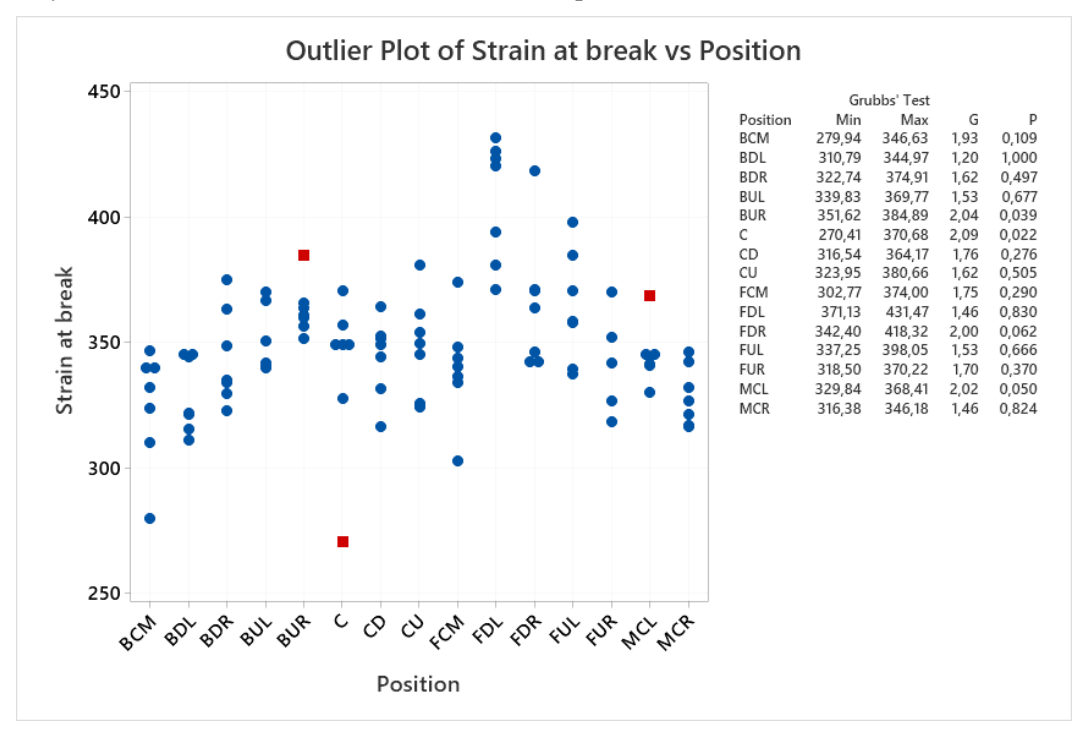


Figure 5.4.5: Outlier plot of strain at break values grouped by the position of the tube inside the oven

5.4.3 ANOVA

The ANOVA is carried out to investigate if there are correlations between the strain at break, the position of the tube inside the oven and the position of the ring in the tube.

Table 5.4.1 shows the results of the ANOVA. As it can be observed, the position has an high F-value and a p-value lower than 0.05, while the ring has a low F-value and a p-value higher than 0.05. This indicates that the strain at break is affected by the position of the tube inside the oven, but not by the position of the ring inside the tube.

Table 5.4.1: Results of the ANOVA of the strain at break

Analysis of Variance

Source	DF	Adj SS	Adj MS	F-Value	P-Value
Position	14	38936,6	2781,2	8,25	0,000
Ring	6	692,0	115,3	0,34	0,913
Error	84	28320,0	337,1		
Total	104	67948,6			

Table 5.4.2 shows the model summary of the ANOVA. The coefficient of determination R^2 is 58.32%, indicating that the model represents more than half of the data variability. The same considerations done for the hardness are valid.

Model Summary

S R-sq R-sq(adj) R-sq(pred) 18,3614 58,32% 48,40% 34,88%

Figure 5.4.6 shows the residual plots for the strain at break. As it can be seen, in the normal probability plot (top left) the points follow a straight line and the histogram plot (bottom left) has a bell shape: this means that normality is respected. In the versus fits plot (top right) the points are randomly distributed around zero: this means that residuals variance is constant. Finally, in the versus order plot (bottom right) the points are randomly distributed around zero: this means that time independence is respected.

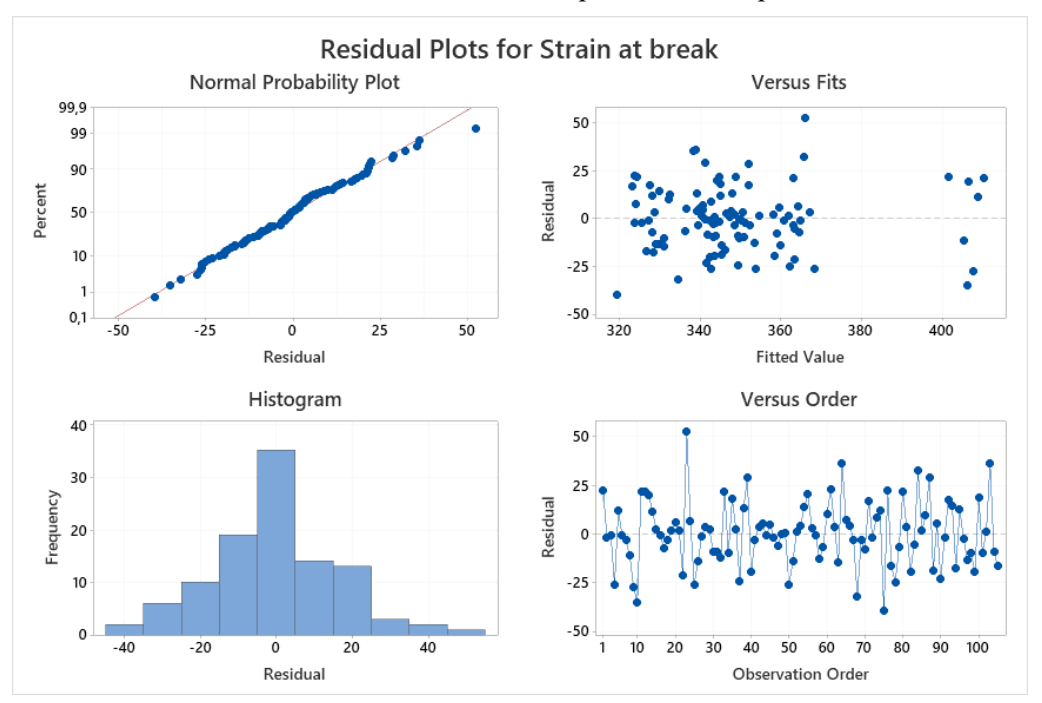


Figure 5.4.6: Residual plots for the strain at break

5.4.4 Response surface regression

As the ANOVA highlights a correlation only between the strain at break and the position of the tube inside the oven, the response surface regression is carried out using as terms only the coordinates of the oven X, Y, and Z.

Table 5.4.3 shows the model summary. The coefficient of determination R^2 is 50.27%, indicating that the model represents half of the data variability. The same considerations done for the hardness are valid.

Table 5.4.3: Model summary of the response surface regression of the strain at break

Model Summary

S R-sq R-sq(adj) R-sq(pred) 18,4752 50,27% 47,76% 43,85%

Table 5.4.4 shows the ANOVA for each significant term with a level of confidence of 0.15 of the regression equation. By looking at the columns of *F*-values and *p*-values, it is possible to understand which terms affect more the model of the strain at break.

Table 5.4.4: ANOVA for each significant term of the response surface regression of the strain at break

Analysis of Variance

Source	DF	Adj SS	Adj MS	F-Value	P-Value
Model	5	34157	6831,4	20,01	0,000
Linear	2	10290	5144,8	15,07	0,000
Χ	1	8419	8419,2	24,67	0,000
Υ	1	1870	1870,4	5,48	0,021
Square	1	7794	7794,4	22,84	0,000
Z*Z	1	7794	7794,4	22,84	0,000
2-Way Interaction	2	16073	8036,4	23,54	0,000
X*Y	1	6815	6815,2	19,97	0,000
X*Z	1	9258	9257,5	27,12	0,000
Error	99	33792	341,3		
Lack-of-Fit	9	4780	531,1	1,65	0,114
Pure Error	90	29012	322,4		
Total	104	67949			

Figure 5.4.7 shows the Pareto chart of the standardised effects. In this case, all the terms with a standardised effect higher than 1.451 are considered significant.

By looking at Table 5.4.4 and at Figure 5.4.7 it can be stated that the significant terms with a level of confidence of 0.15 in descending order are X*Z, X, Z^2 , X*Y and Y.

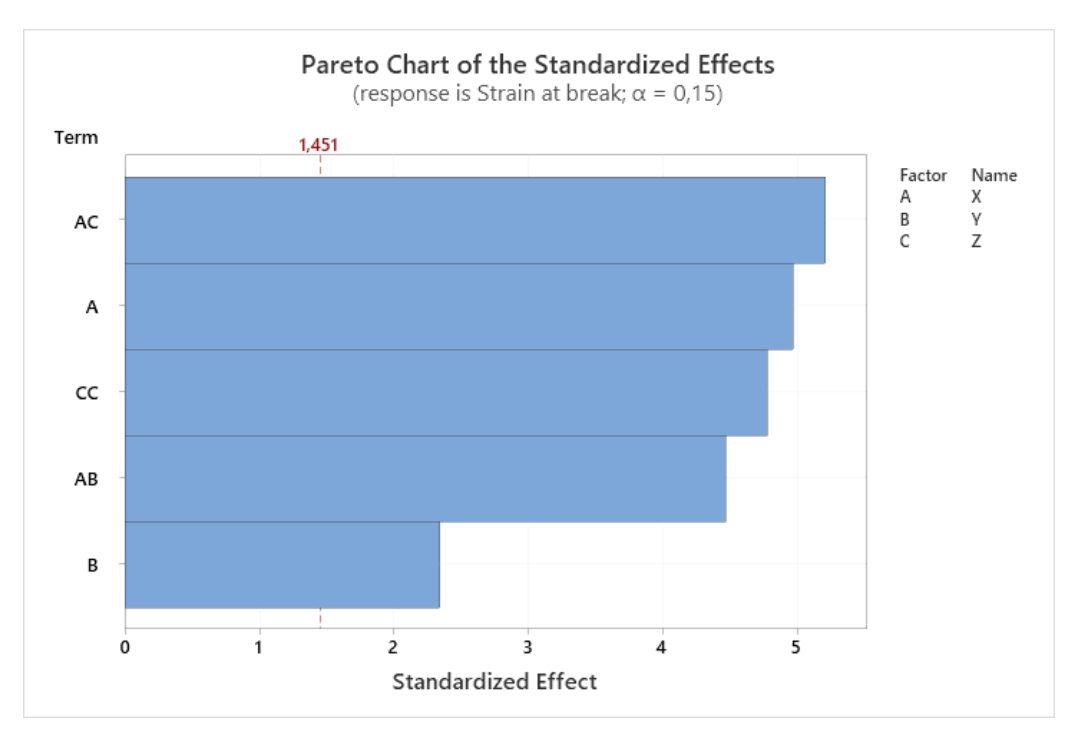


Figure 5.4.7: Pareto Chart of the standardised effects of the response surface regression of the strain at break

Table 5.4.5 shows the regression equation of the strain at break as a function of the coordinates of the oven. In this case, there is only one equation because the strain at break does not depend on the position of the ring inside the tube.

Table 5.4.5: Regression equation of the strain at break as a function of the coordinates of the oven

Regression Equation in Coded Units

Strain at break = 336,94 + 10,97 X - 5,17 Y + 18,28 Z*Z - 11,03 X*Y - 12,86 X*Z

Uncoded coefficients are not available with non-hierarchical model.

Figure 5.4.8 shows the surface plots of strain at break as a function of the coordinates of the oven. In each plot, the axes represent the strain at break and two coordinates, while the third coordinate is kept constant with value equal to 0.

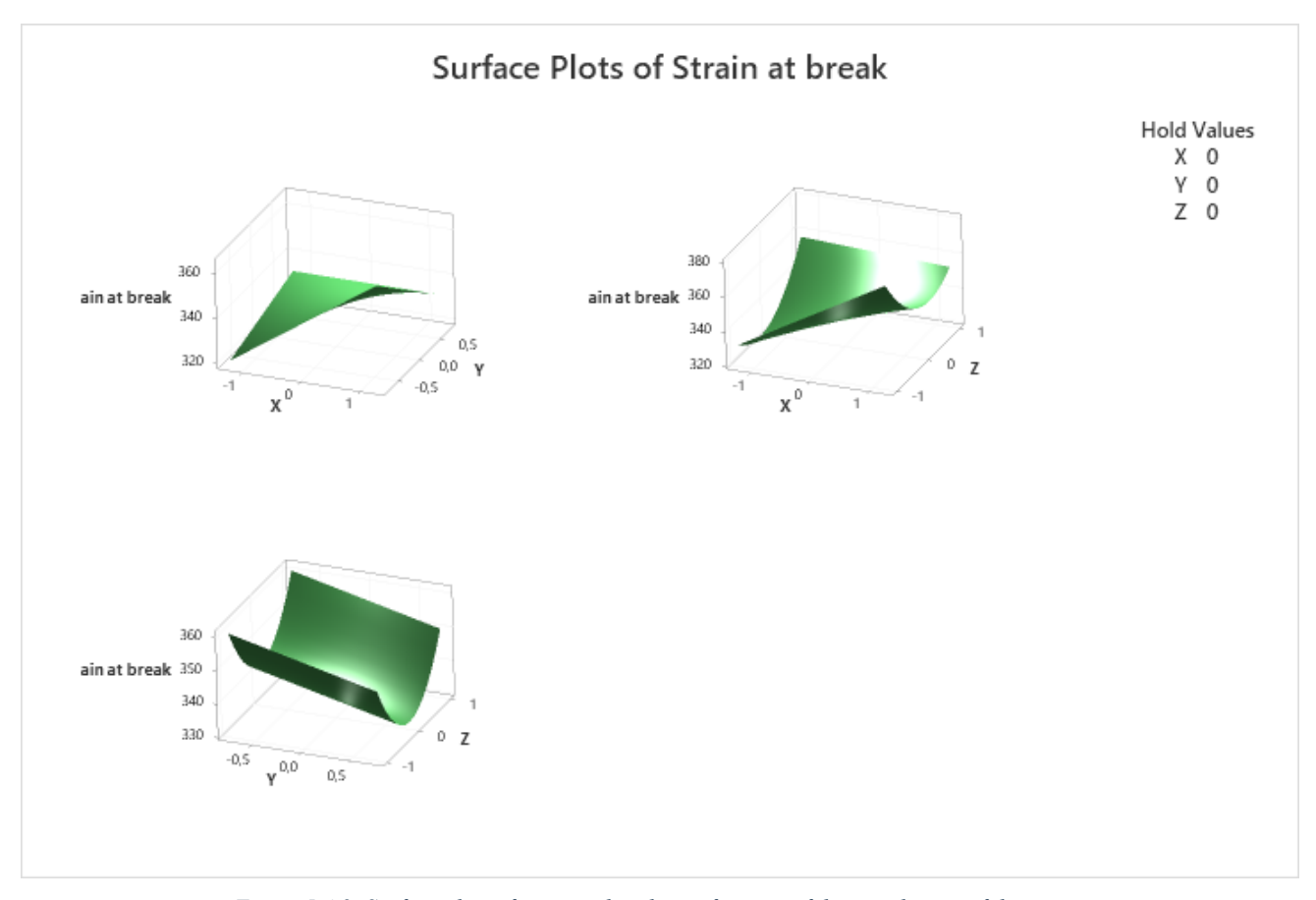


Figure 5.4.8: Surface plots of strain at break as a function of the coordinates of the oven

Finally, the multiple response prediction for both the maximum and the minimum value of strain at break is found.

Table 5.4.6 shows the maximum value of strain at break predicted by the response surface regression as well as its coordinates, its ring and its 95% CI (Confidence Interval). The maximum value is 395% with a 95% CI between 385% and 406% and it is expected to be in FDL position.

Table 5.4.6: Multiple response prediction for the maximum value of strain at break

Multiple Response Prediction

Strain at break 395,24

Variable Setting X 1,25 Y -0,75 Z -1 Response Fit SE Fit 95% CI 95% PI

5,18 (384,97; 405,52) (357,17; 433,31)

Table 5.4.7 shows the minimum value of strain at break predicted by the response surface regression as well as its coordinates, its ring and its 95% CI (Confidence Interval). The minimum value is 318% Shore with a 95% CI between 308 and 328 and it is expected to be near BCM position.

Table 5.4.7: Multiple response prediction for the minimum value of strain at break

Multiple Response Prediction

Variable	Setting			
Χ	-1,25			
Υ	-0,75			
Ζ .	-0,353535			
Response	Fit	SE Fit	95% CI	95% PI
Strain at b	reak 317,85	4,91	(308,10; 327,60)	(279,92; 355,78)

Figure 5.4.9 shows the sketch of the oven with the means of the measured strain at break values for each position (number in the rectangles) and the predicted maximum and minimum values (number in the circles). The scale of colours is set to assign the green to the lowest values and the red to the highest ones. As it can be observed, the values in the front are the highest, while the values on the back and in the centre are the lowest. This highlights that strain depends on the post-curing temperature: the higher the temperature is, the lower the strain is. This can be explained by the fact that increasing the temperature, the sulphur atoms form more crosslinks between the long rubber polymer chains and so their movement is limited. The elongation depends on the mobility of polymeric chains: if there are too many crosslinks, chains can no longer move and they break earlier. Therefore, in the front the strain at break values are higher because there is the oven door and so the temperature is lower, while on the back and in the centre the strain at break values are lower because they are far from the door and so the temperature is higher. Furthermore, the predicted maximum and minimum values are near the measured maximum and minimum values: this highlights that the model obtained by the response surface regression is reliable.

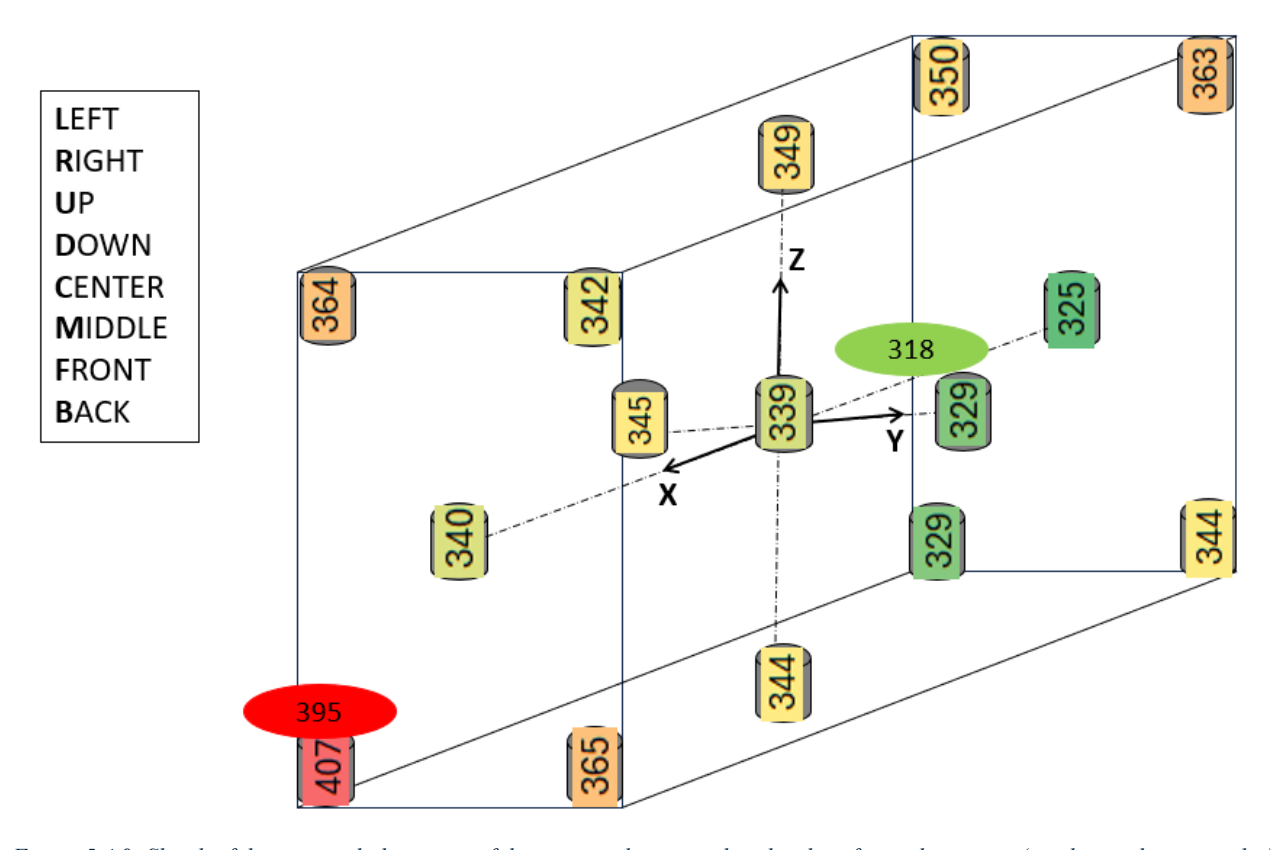


Figure 5.4.9: Sketch of the oven with the means of the measured strain at break values for each position (number in the rectangles) and the predicted maximum and minimum values (numbers in the circles)

5.5 Tear test: tear strength at break

5.5.1 Descriptive statistics

All the tear strength at break values have been normalised multiplying for a constant number to ensure industrial confidentiality without changing the variance: therefore, the same considerations done for hardness are valid.

Figure 5.5.1 shows the boxplot of tear strength at break values measured in laboratory grouped by the position of the tube inside the oven. As it can be observed, some boxplots are completely misaligned from the others: this suggests that there may be a correlation between the tensile strength at break and the position of the tube inside the oven.

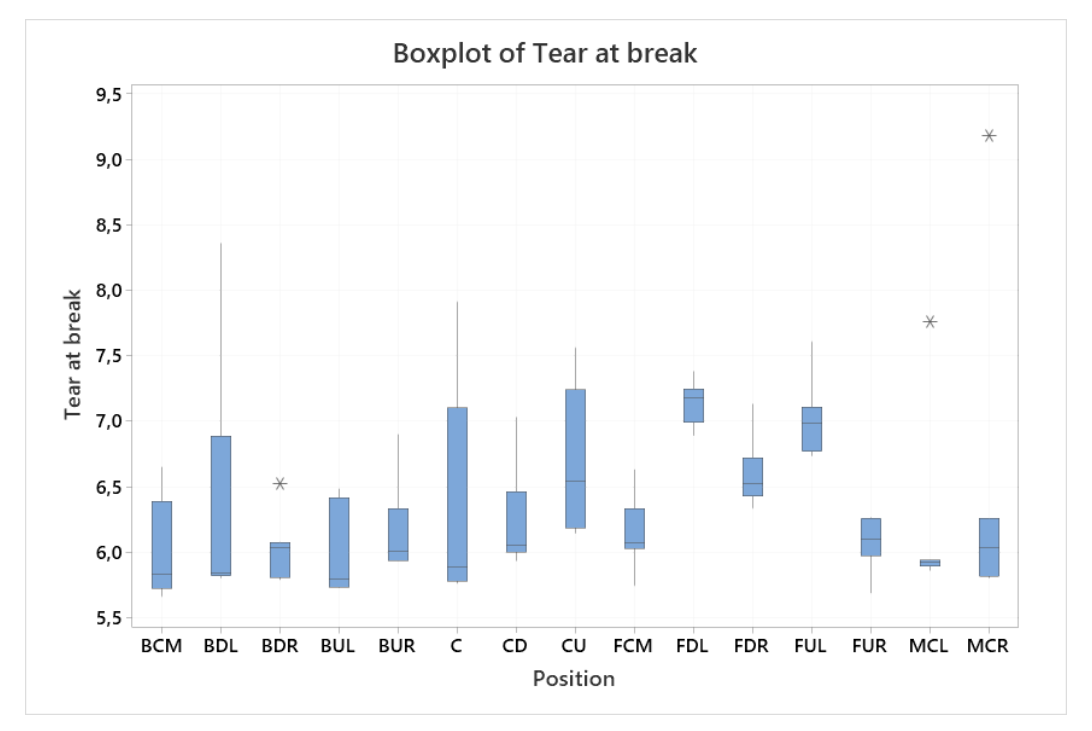


Figure 5.5.1: Boxplot of tear strength at break values grouped by the position of the tube inside the oven

Figure 5.5.2 shows the boxplot of tear strength at break values measured in laboratory grouped by the position of the ring inside the tube.

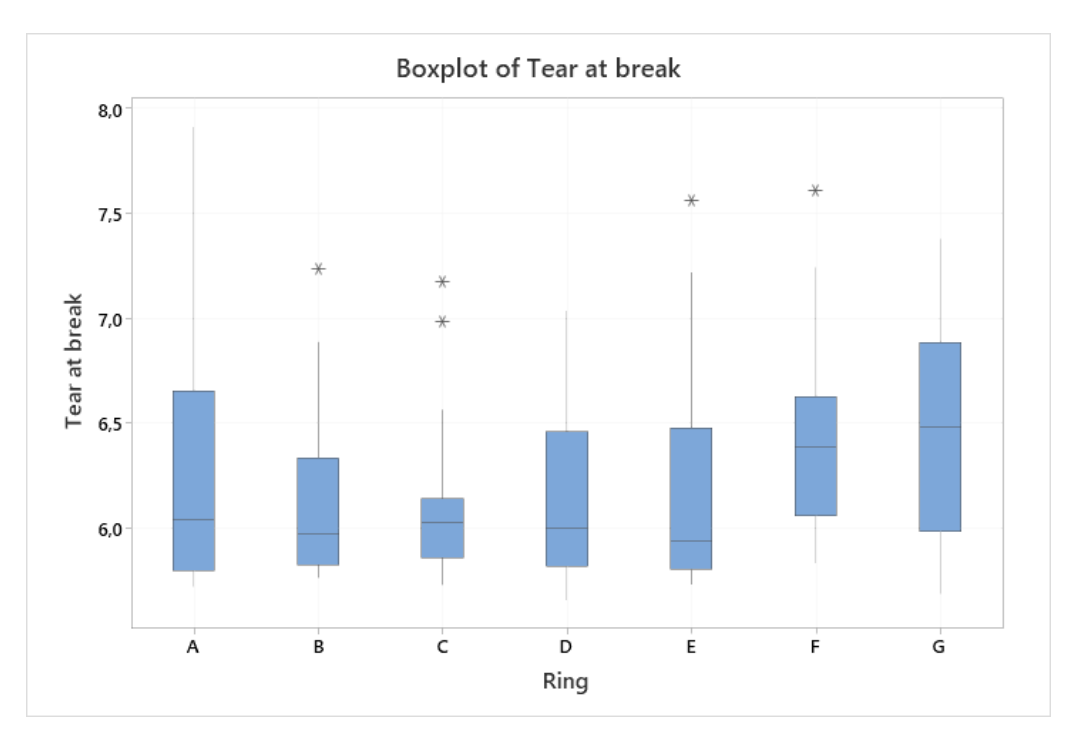


Figure 5.5.2: Boxplot of tear strength at break values grouped by the position of the ring inside the tube

Figure 5.5.3 shows the dotplot of tear strength at break values measured in laboratory grouped by the position of the tube inside the oven.

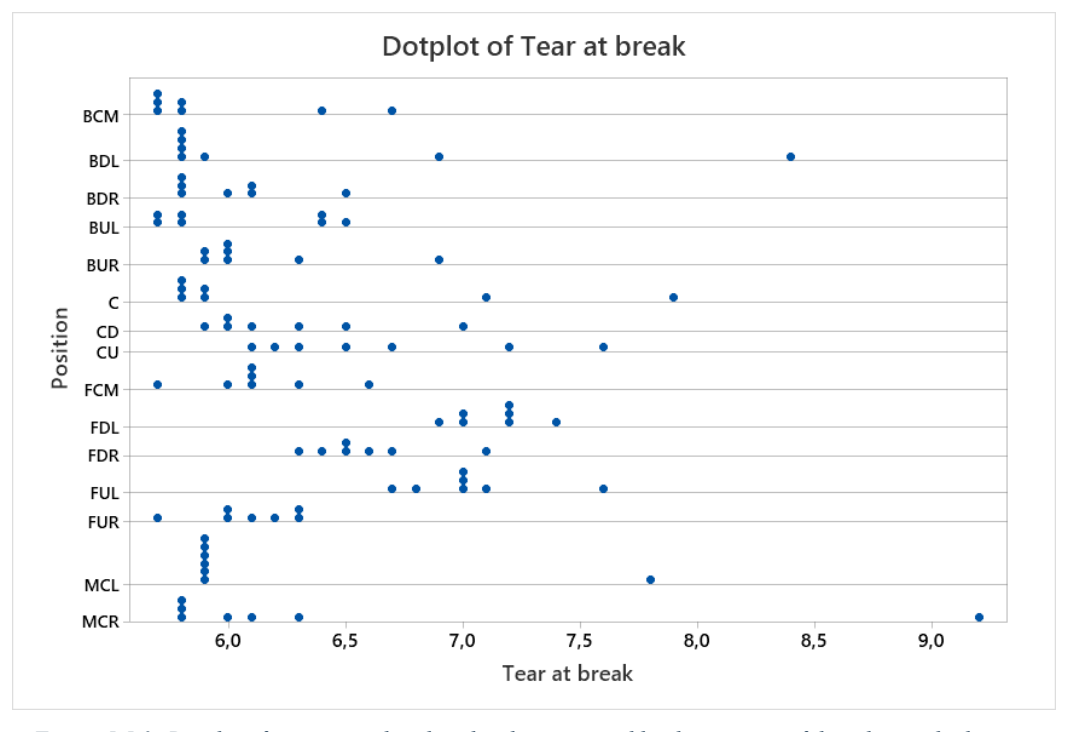


Figure 5.5.3: Dotplot of tear strength at break values grouped by the position of the tube inside the oven

Figure 5.5.4 shows the dotplot of tear strength at break values measured in laboratory grouped by the position of the ring inside the tube.

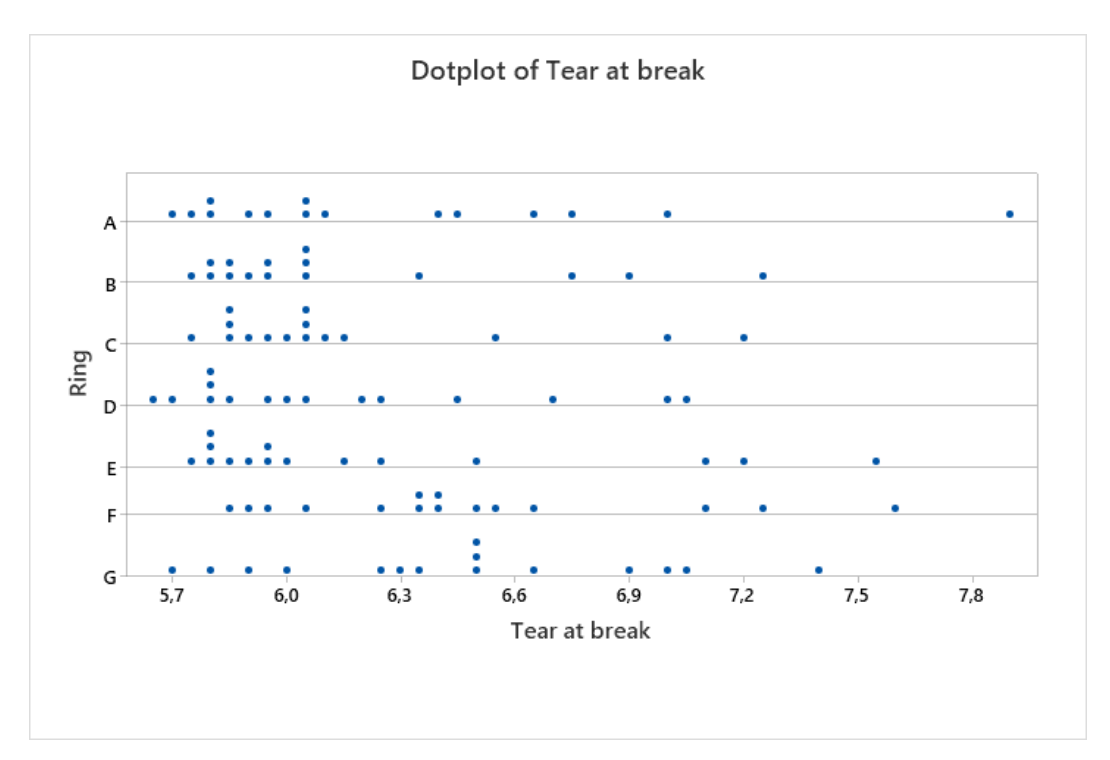


Figure 5.5.4: Dotplot of tear strength at break values grouped by the position of the ring inside the tube

5.5.2 Outlier identification

The Grubbs' test to identify outliers is carried out before proceeding with ANOVA. Figure 5.5.5 shows the outlier plot of tear strength at break values grouped by the position of the tube inside the oven: as it can be seen, five outliers are found by the test in BDL, BUR, FDR, MCL and MCR positions. Before proceeding with the ANOVA, each outlier is replaced by the median of the other values in the same position.

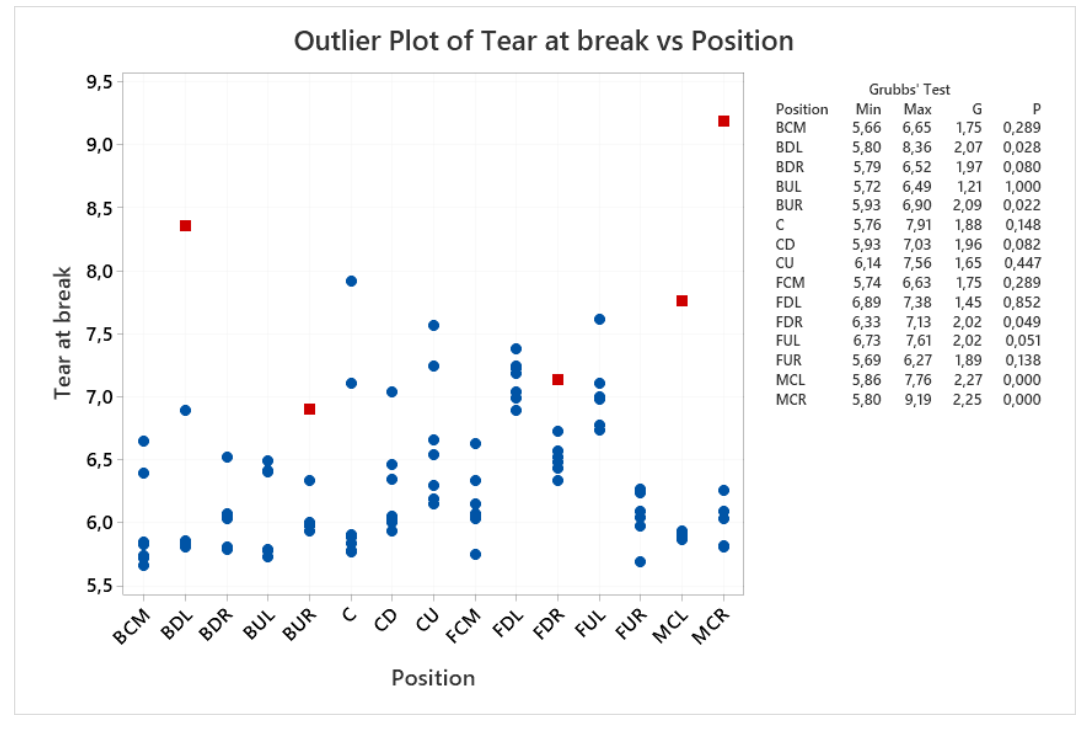


Figure 5.5.5: Outlier plot of tear strength at break values grouped by the position of the tube inside the oven

5.5.3 ANOVA

The ANOVA is carried out to investigate if there are correlations between the tear strength at break, the position of the tube inside the oven and the position of the ring in the tube.

Table 5.5.1 shows the results of the ANOVA. As it can be observed, the position has an *F*-value quite high and a *p*-value much lower than 0.05, while the ring has a quite low *F*-value and a *p*-value slightly lower than 0.05. This indicates the influence of the position of the tube inside the oven on the tear strength is quite strong, while the influence of the position of the ring inside the tube is quite weak.

Table 5.5.1: Results of the ANOVA of the tear strength at break

Analysis of Variance

Source	DF	Adj SS	Adj MS	F-Value	P-Value
Position	14	15,043	1,0745	8,94	0,000
Ring	6	1,755	0,2925	2,43	0,032
Error	84	10,099	0,1202		
Total	104	26,897			

Table 5.5.2 shows the model summary of the ANOVA. The coefficient of determination R^2 is 62.45%, indicating that the model represents more than half of the data variability. The same considerations done for the hardness are valid.

Table 5.5.2: Model summary of the ANOVA of the tear strength at break

Model Summary

S	R-sq	R-sq(adj)	R-sq(pred)
0,346741	62,45%	53,51%	41,33%

Figure 5.5.6 shows the residual plots for the tear strength at break. As it can be seen, in the normal probability plot (top left) the points follow a straight line and the histogram plot (bottom left) has a bell shape: this means that normality is respected. In the versus fits plot (top right) the points are randomly distributed around zero: this means that residuals variance is constant. Finally, in the versus order plot (bottom right) the points are randomly distributed around zero: this means that time independence is respected.

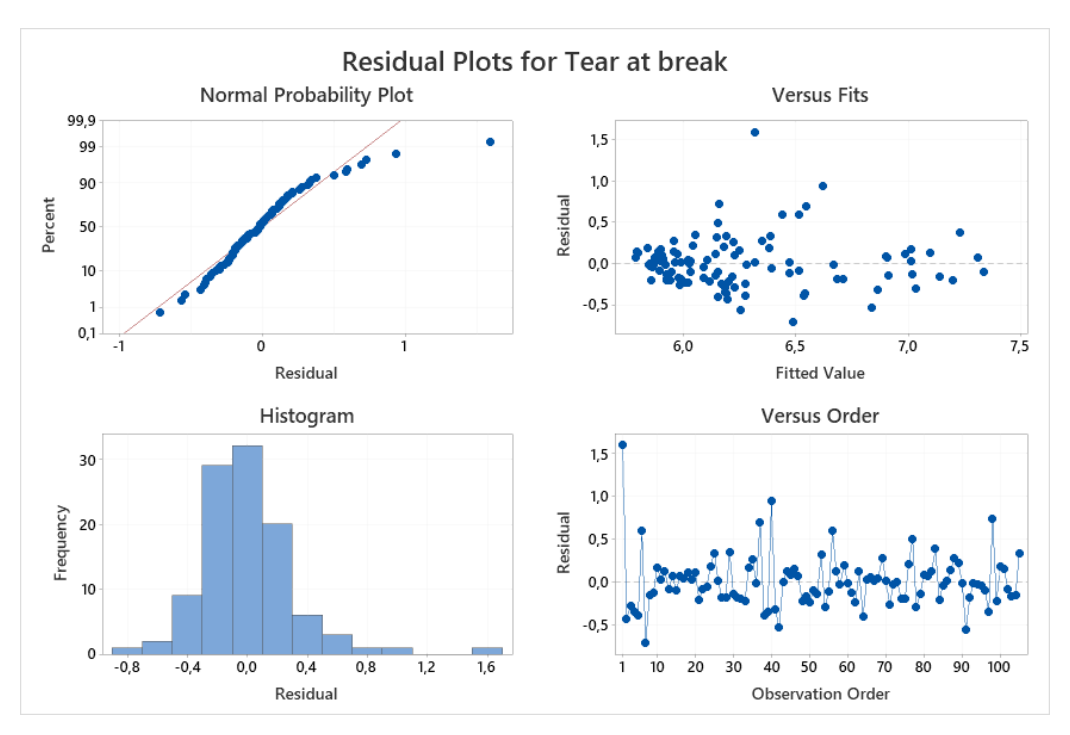


Figure 5.5.6: Residual plots for the tear strength at break

5.5.4 Response surface regression

As the ANOVA highlights a correlation between the tear strength at break, the position of the tube inside the oven and the position of the tube inside the ring, the response surface regression is carried out using as terms the coordinates of the oven X, Y, Z and the ring.

Table 5.5.3 shows the model summary. The coefficient of determination R^2 is 58.11%, indicating that the model represents more than half of the data variability. The same considerations done for the hardness are valid.

Table 5.5.3: Model summary of the surface regression of the tear strength at break

Model Summary S R-sq R-sq(adj) R-sq(pred) 0,361977 58,11% 49,34% 41,48%

Table 5.5.4 shows the ANOVA for each significant term with a level of confidence of 0.15 of the regression equation. By looking at the columns of *F*-values and *p*-values, it is possible to understand which terms affect more the model of the strain at break.

Analysis of Variance

Source	DF	Adj SS	Adj MS	F-Value	P-Value
Model	18	15,6289	0,8683	6,63	0,000
Linear	8	9,0368	1,1296	8,62	0,000
X	1	5,6826	5,6826	43,37	0,000
Υ	1	1,5994	1,5994	12,21	0,001
Ring	6	1,7548	0,2925	2,23	0,048
Square	2	2,7357	1,3679	10,44	0,000
Y*Y	1	0,4552	0,4552	3,47	0,066
Z*Z	1	2,7355	2,7355	20,88	0,000
2-Way Interaction	8	3,8564	0,4820	3,68	0,001
X*Y	1	2,1902	2,1902	16,72	0,000
X*Z	1	0,3282	0,3282	2,50	0,117
Z*Ring	6	1,3380	0,2230	1,70	0,130
Error	86	11,2684	0,1310		
Total	104	26.8972			

Figure 5.5.7 shows the Pareto chart of the standardised effects. In this case, all the terms with a standardised effect higher than 1.453 are considered significant.

By looking at Table 5.5.4 and at Figure 5.5.7 it can be stated that the significant terms with a level of confidence of 0.15 in descending order are X, Z^2 , X*Y, Y, Ring, Y^2 , X*Z and Z*Ring.

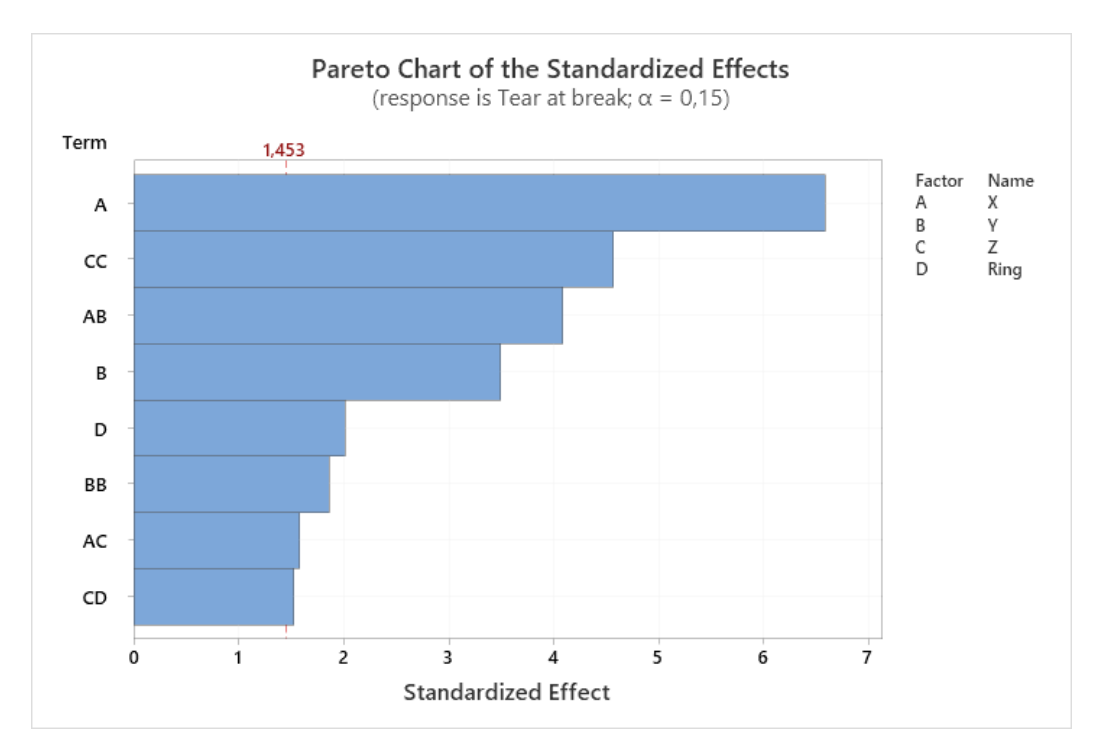


Figure 5.5.7: Pareto Chart of the standardised effects of the response surface regression of the tear strength at break

Table 5.5.5 shows the regression equations of the tear strength at break as a function of the coordinates of the oven. There are seven equations: one for each ring.

Regression Equation in Coded Units

Ring Tear at break = 6,130 + 0,2849 X - 0,1512 Y - 0,1524 Y*Y + 0,3736 Z*Z - 0,1978 X*Y - 0,0766 X*Z + 0,078 Z Tear at break = 6,008 + 0,2849 X - 0,1512 Y - 0,1524 Y*Y + 0,3736 Z*Z - 0,1978 X*Y В - 0,0766 X*Z + 0,061 Z C Tear at break = $5,999 + 0,2849 \times -0,1512 \times -0,1524 \times +0,3736 \times -0,1978 \times \times$ - 0,0766 X*Z - 0,065 Z Tear at break = 6,002 + 0,2849 X - 0,1512 Y - 0,1524 Y*Y + 0,3736 Z*Z - 0,1978 X*Y D - 0,0766 X*Z - 0,066 Z Ε Tear at break = 6,085 + 0,2849 X - 0,1512 Y - 0,1524 Y*Y + 0,3736 Z*Z - 0,1978 X*Y - 0,0766 X*Z + 0,149 Z F Tear at break = $6,326 + 0,2849 \times -0,1512 \times -0,1524 \times +0,3736 \times -0,1978 \times \times$ - 0,0766 X*Z + 0,122 Z Tear at break = 6,299 + 0,2849 X - 0,1512 Y - 0,1524 Y*Y + 0,3736 Z*Z - 0,1978 X*Y G - 0,0766 X*Z - 0,280 Z

Uncoded coefficients are not available with non-hierarchical model.

Figure 5.5.8 shows the surface plots of tear strength at break as a function of the coordinates of the oven for ring A. In each plot, the axes represent the tear strength and two coordinates, while the third coordinate is kept constant with value equal to 0.

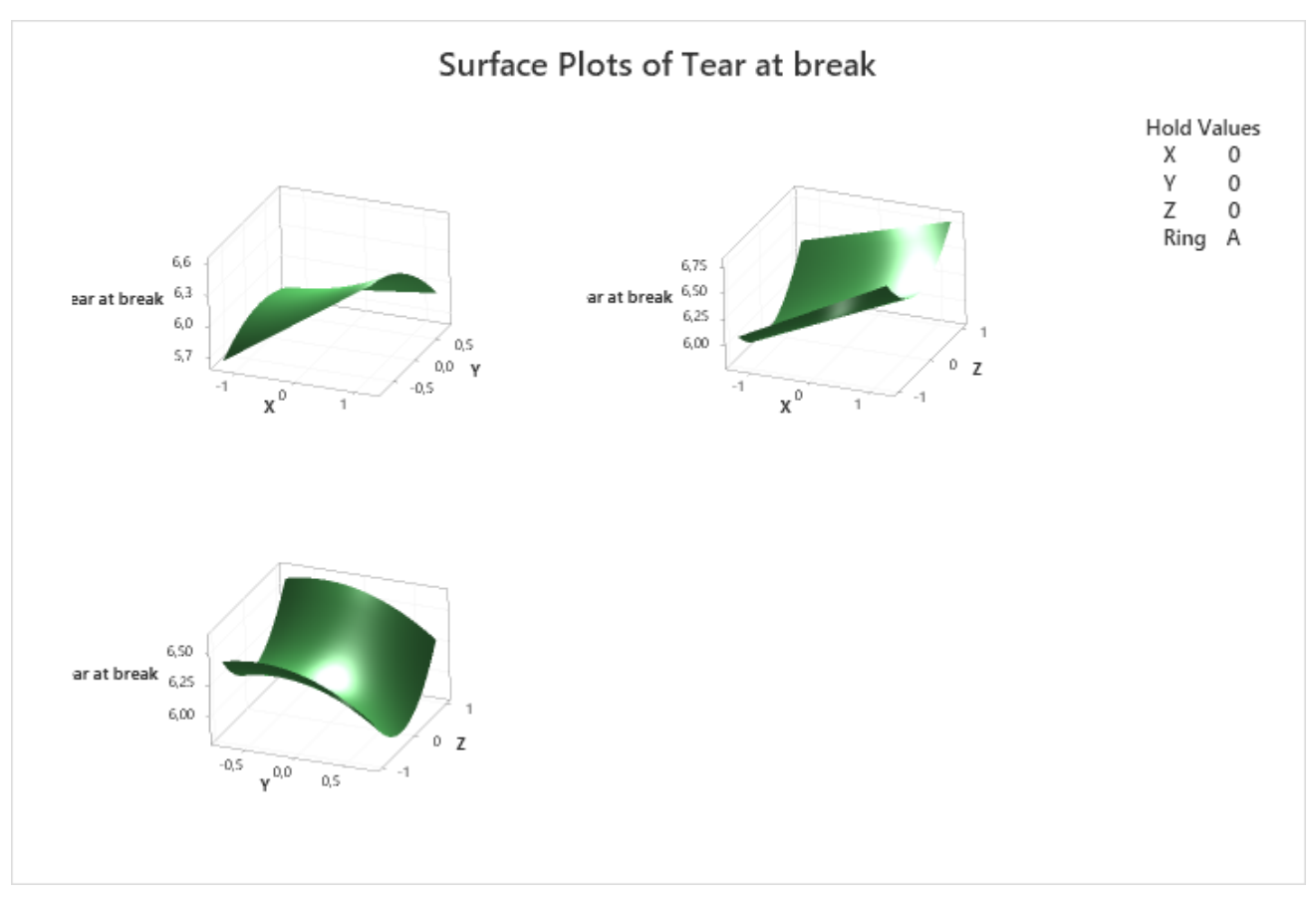


Figure 5.5.8: Surface plots of tear strength at break as a function of the coordinates of the oven

Finally, the multiple response prediction for both the maximum and the minimum value of tear strength is found.

Table 5.5.6 shows the maximum value of tear strength at break predicted by the response surface regression as well as its coordinates, its ring and its 95% CI (Confidence Interval). The maximum value is 7.5 N/mm with a 95% CI between 7.2 N/mm and 7.9 N/mm and it is expected to be in FDL position in ring G.

Table 5.5.6: Multiple response prediction for the maximum value of tear strength at break

Multiple Response Prediction Variable Setting X 1,25 Y -0,75 Z Z -1 Ring G Response Fit SE Fit 95% CI 95% PI Tear at break 7.510 0.171 (7.170; 7.850) (6.714; 8.306)

Table 5.5.7 shows the minimum value of tear strength at break predicted by the response surface regression as well as its coordinates, its ring and its 95% CI (Confidence Interval). The minimum value is 5.5 N/mm with a 95% CI between 5.2 N/mm and 5.8 N/mm and it is expected to be near BCM position in ring B.

Table 5.5.7: Multiple response prediction for the minimum value of tear strength at break

Multiple Response Prediction

Variable	Setting	1		
Χ	-1,25)		
Υ	-0,75)		
Z	-0,191919)		
Ring	Е	}		
Respons	e Fit	SE Fit	95% CI	95% PI
Tear at hr	eak 5 511	0 141	(5 231- 5 701)	(4 739: 6 283)

Figure 5.5.9 shows the sketch of the oven with the means of the measured tear strength at break values for each position (number in the rectangles) and the predicted maximum and minimum values (numbers in the circles). The scale of colours is set to assign the green to the lowest values and the red to the highest ones. As it can be observed, the values in the front are the highest, while the values on the back and in the centre are the lowest. This highlights that tear strength depends on the post-curing temperature: the higher the temperature is, the lower the tear strength is. This can be explained by the fact that increasing the temperature, the sulphur atoms form more crosslinks between the long rubber polymer chains and so their movement is limited. If there are too many crosslinks, chains can no longer move, the initial cut can propagate more easily and chains break earlier. Therefore, in the front the tear strength at break values are higher because there is the oven door and so the temperature is lower, while on the back and in the centre the tear strength at break values are lower because they are far from the door and so the temperature is higher. Furthermore, the predicted maximum and minimum values are near the measured maximum and minimum values: this highlights that the model obtained by the response surface regression is reliable.

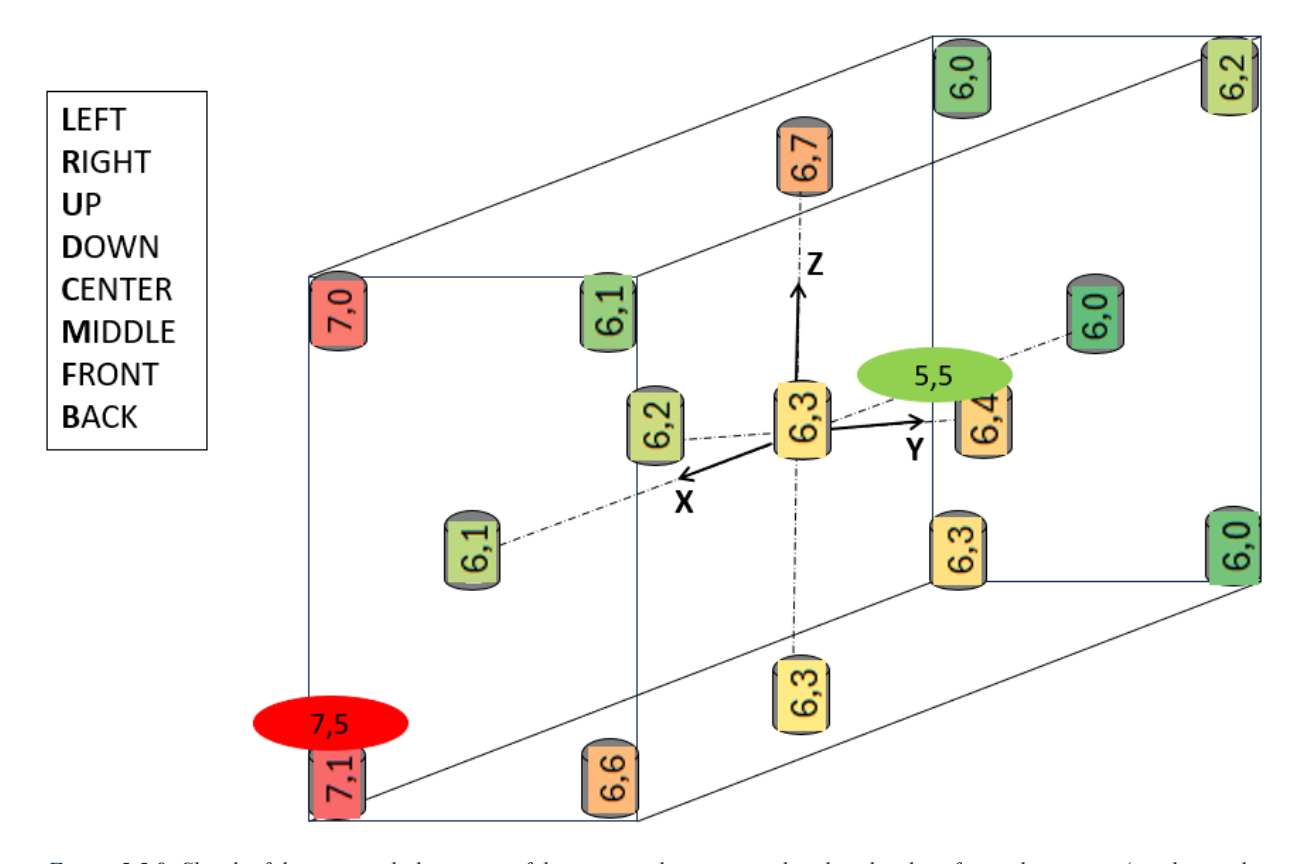


Figure 5.5.9: Sketch of the oven with the means of the measured tear strength at break values for each position (number in the rectangles) and the predicted maximum and minimum values (number in the circles)

6 Post-curing effect analysis

After analysing the correlation between the mechanical properties, the position of the tube inside the oven and the position of the ring inside the tube, the post-curing effect is analysed as well.

The hardness Shore test, the tensile test and the tear test are carried out on the same specimens both before and after post-curing: in this way, it is possible to obtain a comparison between the post-cured and the non-post-cured elastomers.

As in Paragraph 5, Minitab software is used to visualise the data through boxplots and dotplots, to identify the outliers through Grubbs' test and to carry out the ANOVA.

The data in this analysis have been normalised as explained in Paragraph 5.

6.1 Hardness Shore test

6.1.1 Descriptive statistics

Figure 6.1.1 shows the boxplot of hardness values measured in laboratory before and after post-curing. As it can be seen, after the post-curing, the elastomers are harder.

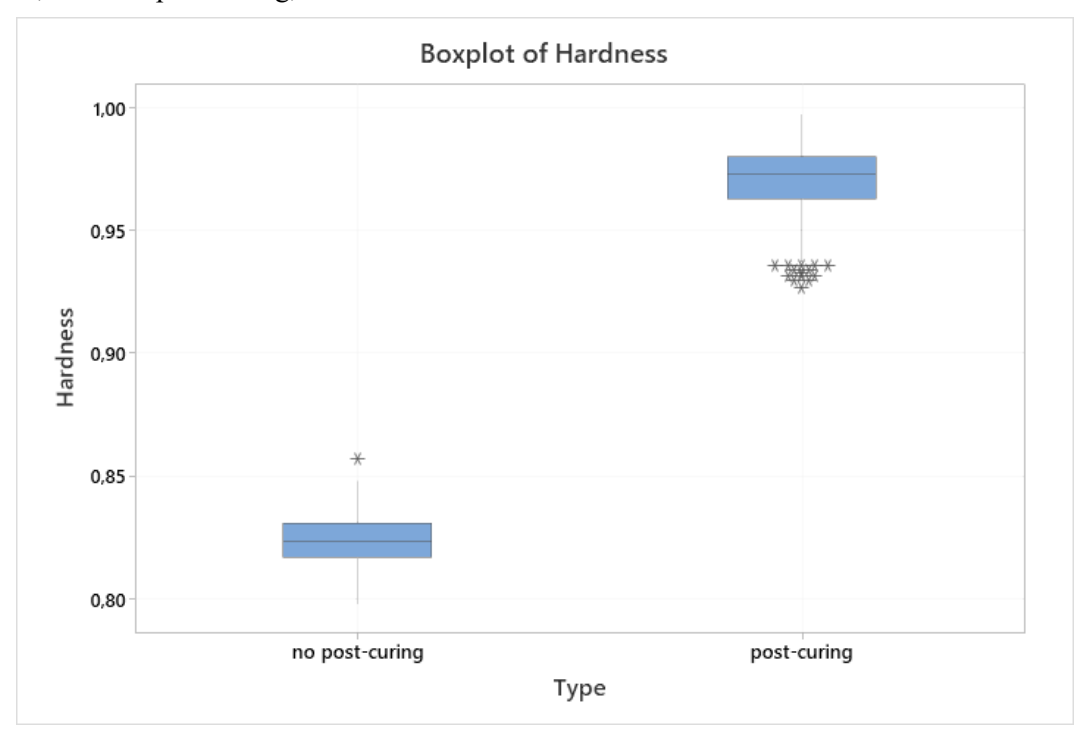


Figure 6.1.1: Boxplot of hardness values before and after post-curing

Figure 6.1.2 shows the dotplot of hardness values before and after post-curing.

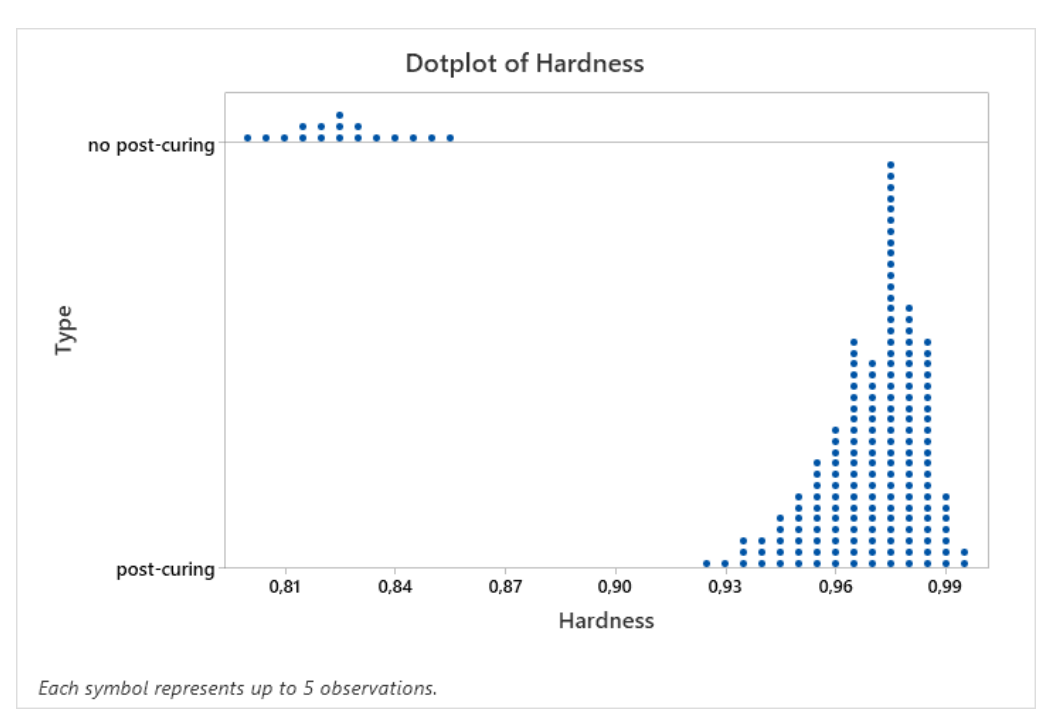


Figure 6.1.2: Dotplot of hardness values before and after post-curing

6.1.2 Outlier identification

The Grubbs' test to identify outliers is carried out before proceeding with ANOVA. Figure 6.1.3 shows the outlier plot of hardness values before and after post-curing: as it can be seen, no outlier is found by the test.

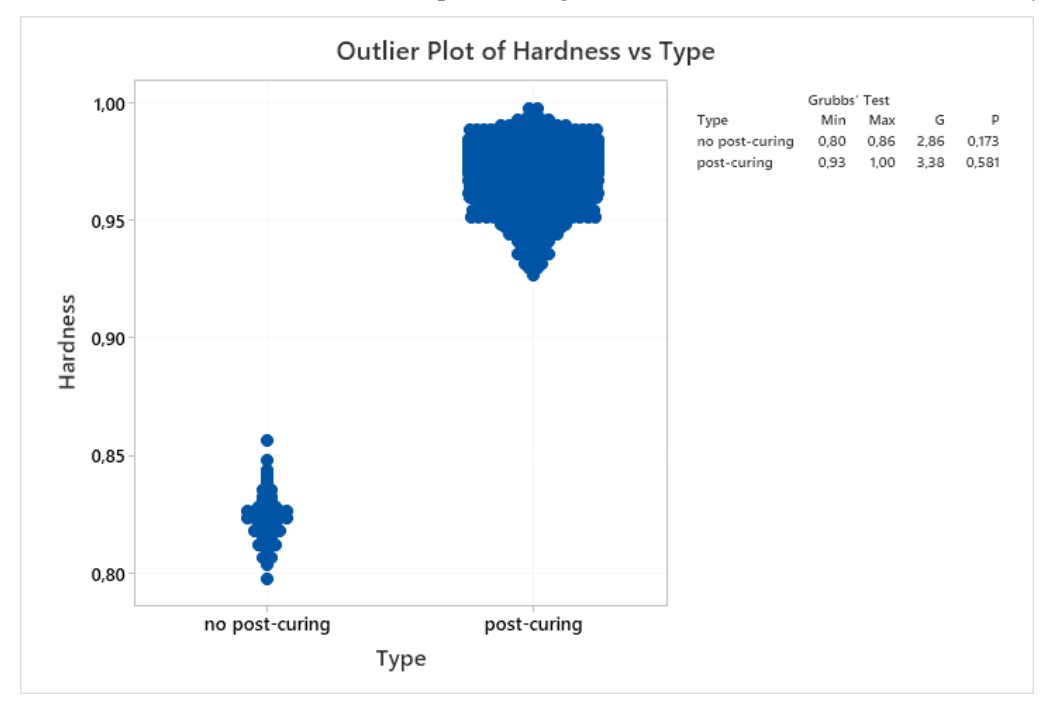


Figure 6.1.3: Outlier plot of hardness values before and after post-curing

6.1.3 ANOVA

The ANOVA is carried out to investigate if the post-cured and the non-post-cured elastomers are different.

Table 6.1.1 shows the results of the ANOVA. As it can be observed, the F-value is very high, while the p-value is much lower than 0.05. This means that the two groups, the post-cured and the non-post cured elastomers, are different.

Table 6.1.1: Results of the ANOVA of the hardness

Analysis of Variance

Source DF Adj SS Adj MS F-Value P-Value Type 1 1,1179 1,11794 6859,03 0,000 Error 894 0,1457 0,00016 Total 895 1,2637

Table 6.1.2 shows the model summary of the ANOVA. The coefficient of determination R^2 is 88.47%, indicating that the model represents most of the data variability.

Table 6.1.2: Model summary of the ANOVA of the hardness

Model Summary

S	R-sq	R-sq(adj)	R-sq(pred)
0,0127667	88,47%	88,46%	88,42%

Figure 6.1.4 shows the residual plots for the hardness. As it can be seen, in the normal probability plot (top left) the points follow a straight line and the histogram plot (bottom left) has a bell shape: this means that normality is respected. In the versus fits plot (top right) the points are randomly distributed around zero: this means that residuals variance is constant. Finally, in the versus order plot (bottom right) the points are randomly distributed around zero: this means that time independence is respected.

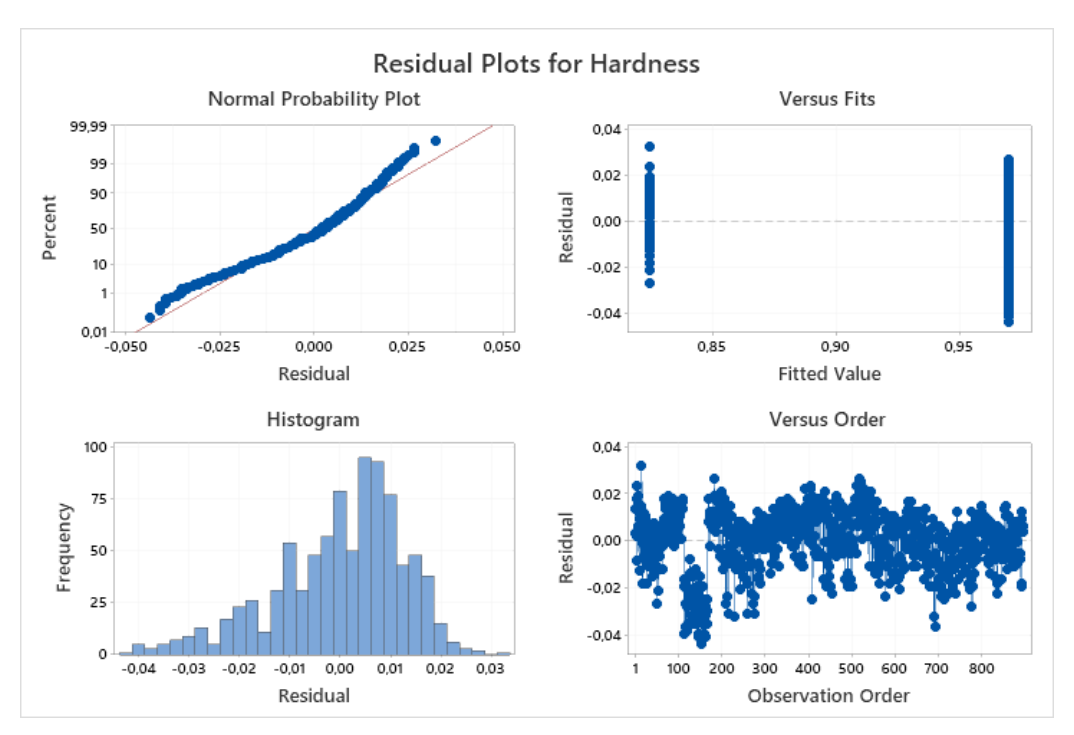


Figure 6.1.4: Residual plot for the hardness

6.2 Tensile test: stress at break

6.2.1 Descriptive statistics

Figure 6.2.1 shows the boxplot of stress at break values measured in laboratory before and after post-curing. As it can be seen, after the post-curing, the stress at break values are higher.

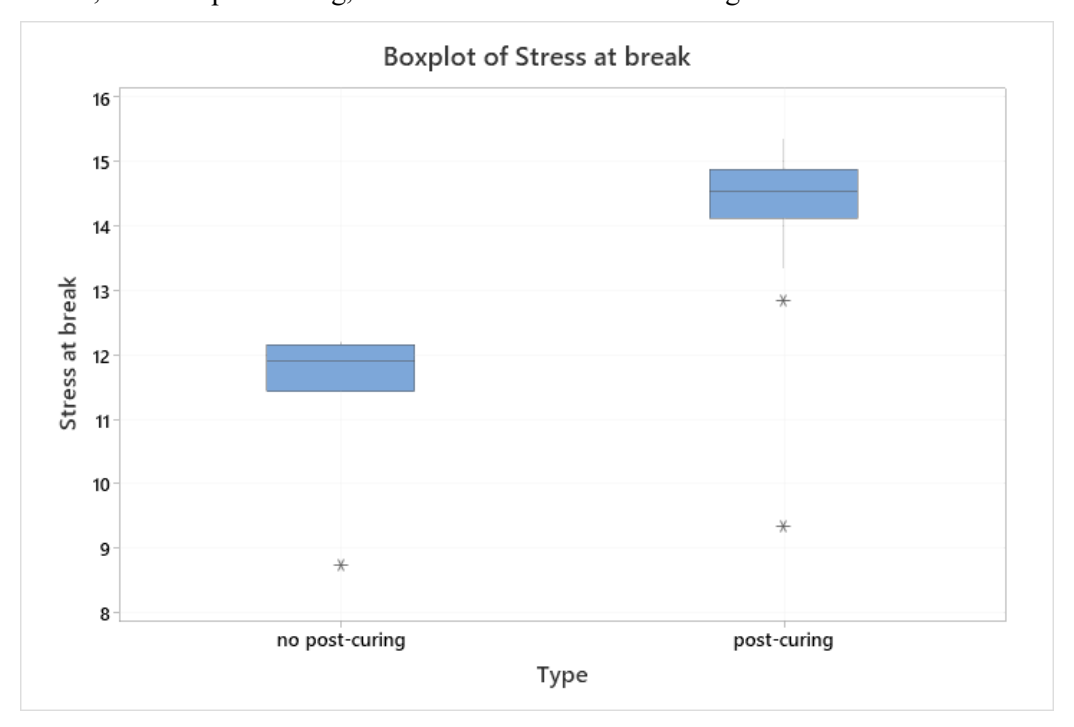


Figure 6.2.1: Boxplot of stress at break values before and after post-curing

Figure 6.2.2 shows the dotplot of stress at break values before and after post-curing.

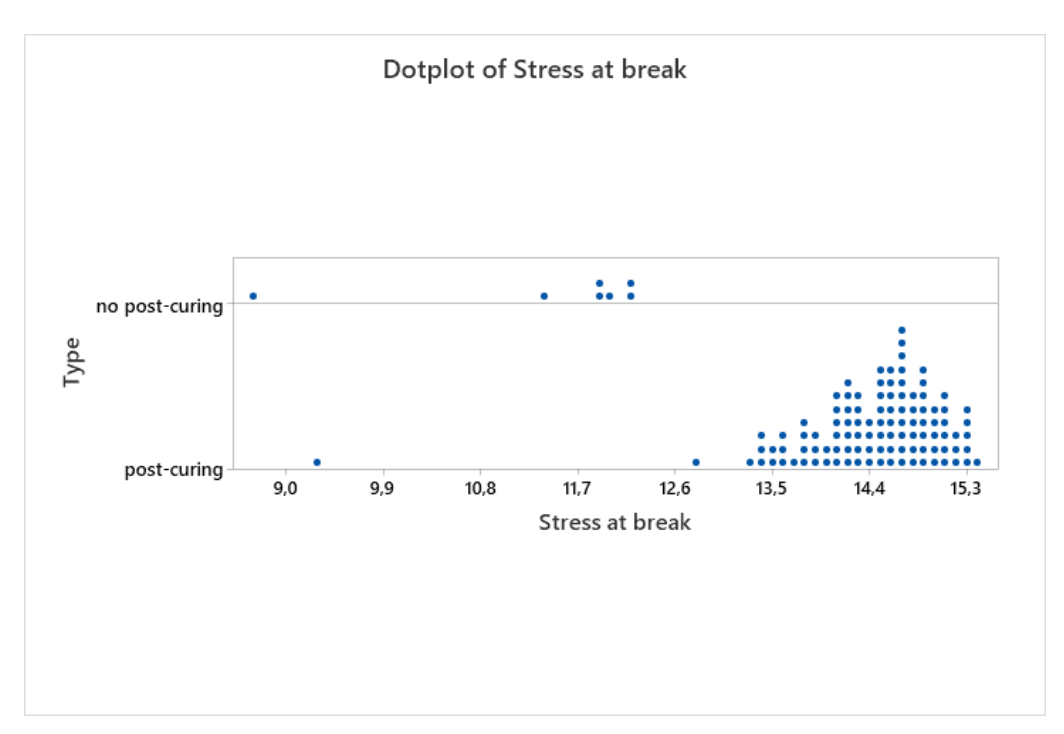


Figure 6.2.2: Dotplot of stress at break values before and after post-curing

6.2.2 Outlier identification

The Grubbs' test to identify outliers is carried out before proceeding with ANOVA. Figure 6.2.3 shows the outlier plot of stress at break values before and after post-curing: as it can be seen, one outlier for each group is found by the test. Before proceeding with the ANOVA, the outliers are replaced by the median of the other values in the same group.

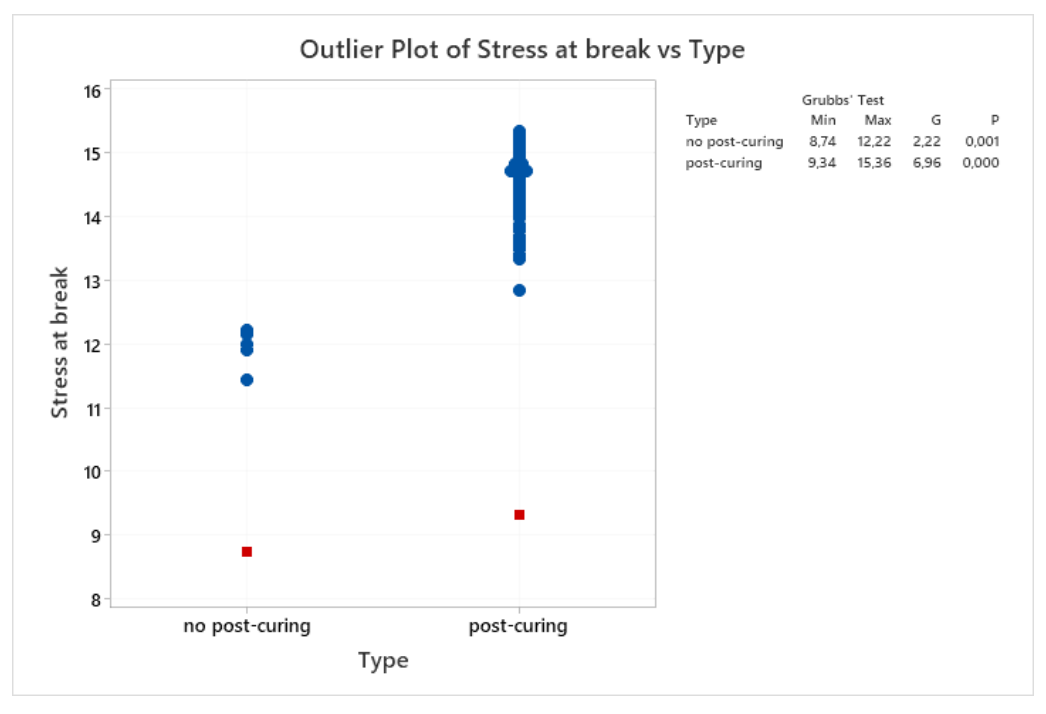


Figure 6.2.3: Outlier plot of stress at break values before and after post-curing

6.2.3 ANOVA

Table 6.2.1 shows the results of the ANOVA. As it can be observed, the *F*-value is very high, while the *p*-value is much lower than 0.05. This means that the two groups, the post-cured and the non-post cured elastomers, are different.

Table 6.2.1: Results of the ANOVA of the stress at break

Analysis of Variance

Source	DF	Adj SS	Adj MS	F-Value	P-Value
Туре	1	42,21	42,2109	155,37	0,000
Error	110	29,88	0,2717		
Total	111	72,09			

Table 6.2.2 shows the model summary of the ANOVA. The coefficient of determination R^2 is 58.55%, indicating that the model represents more than half of the data variability. This could be due to the presence of the supplier factor and of the vulcanisation cycles, which are not considered in this analysis.

Table 6.2.2: Model summary of the ANOVA of the stress at break

Model Summary

S	R-sq	R-sq(adj)	R-sq(pred)
0,521222	58,55%	58,17%	57,57%

Figure 6.2.4 shows the residual plots for the stress at break. As it can be seen, in the normal probability plot (top left) the points follow a straight line and the histogram plot (bottom left) has a bell shape: this means that normality is respected. In the versus fits plot (top right) the points are randomly distributed around zero: this means that residuals variance is constant. Finally, in the versus order plot (bottom right) the points are randomly distributed around zero: this means that time independence is respected.

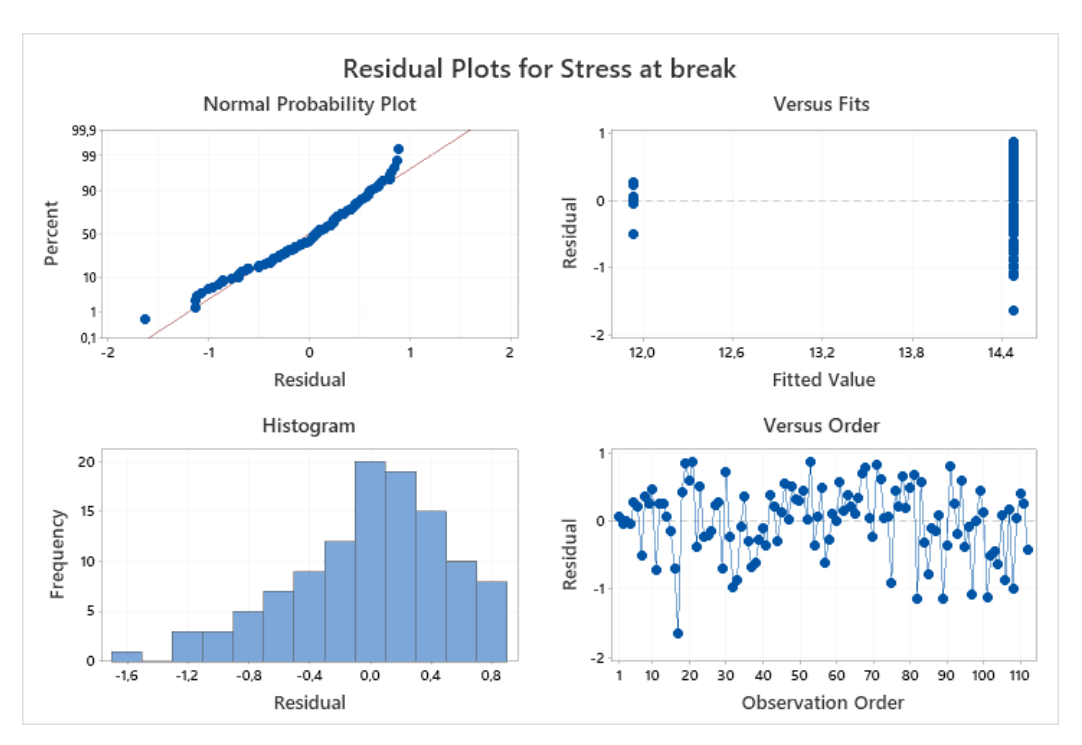


Figure 6.2.4: Residual plot for the stress at break

6.3 Tensile test: strain at break

6.3.1 Descriptive statistics

Figure 6.3.1 shows the boxplot of strain at break values measured in laboratory before and after post-curing. As it can be seen, after the post-curing, the strain at break values are lower.

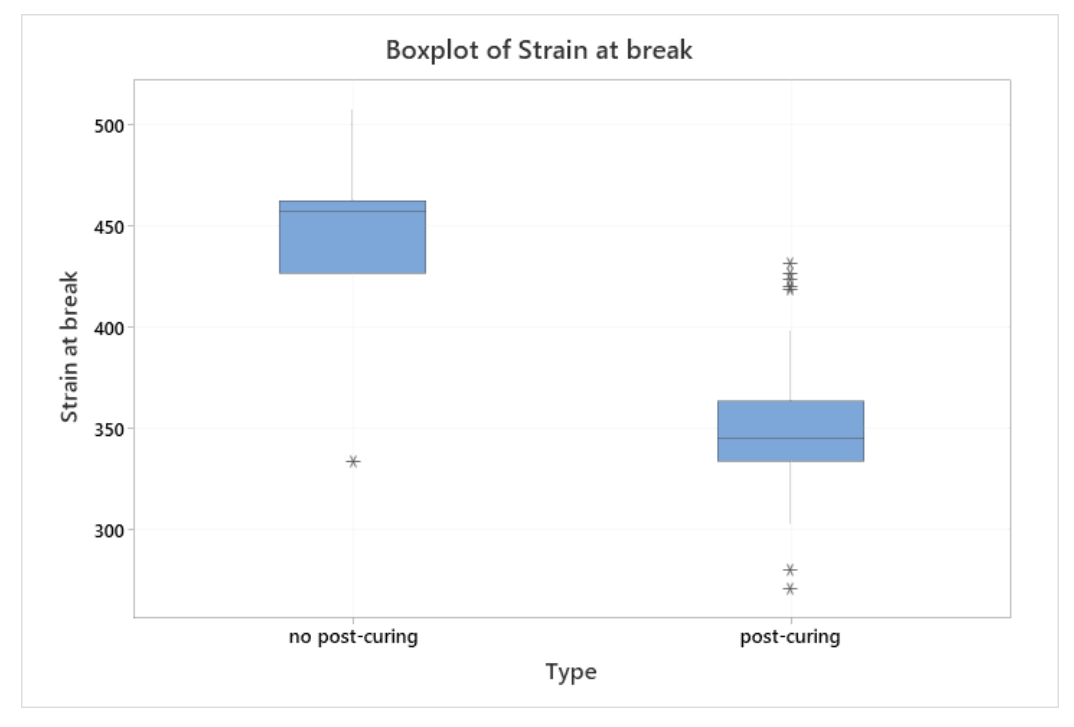


Figure 6.3.1: Boxplot of strain at break values before and after post-curing

Figure 6.3.2 shows the dotplot of strain at break values before and after post-curing.

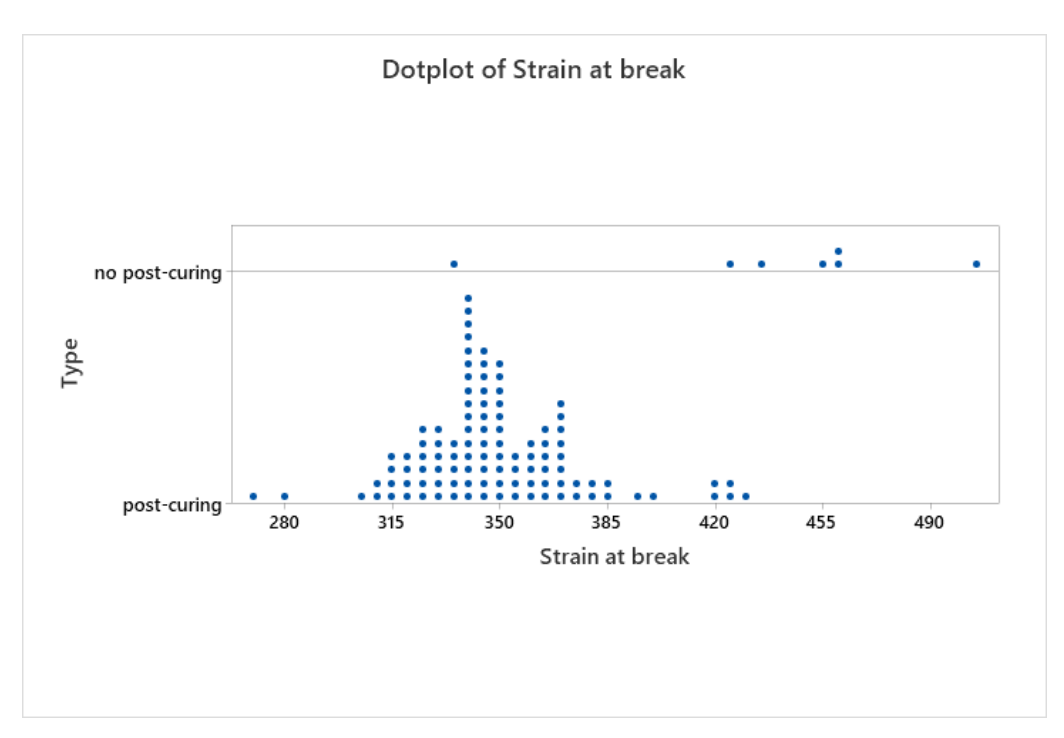


Figure 6.3.2: Dotplot of strain at break values before and after post-curing

6.3.2 Outlier identification

The Grubbs' test to identify outliers is carried out before proceeding with ANOVA. Figure 6.3.3 shows the outlier plot of strain at break values before and after post-curing: as it can be seen, no outlier is found by the test.

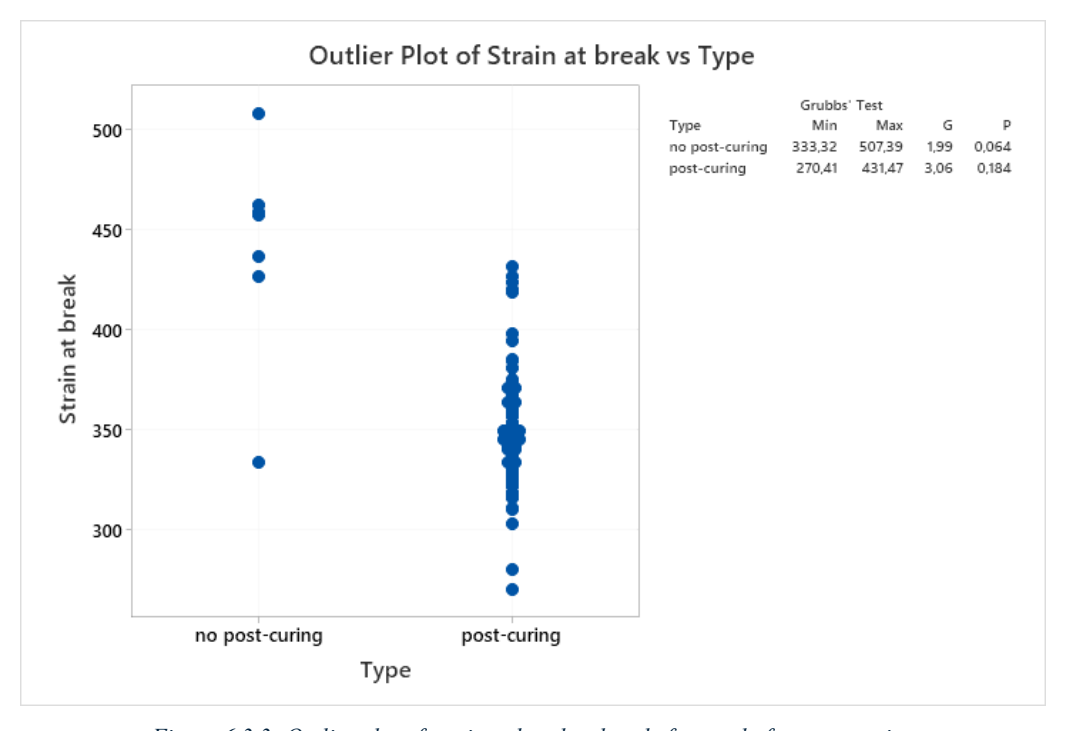


Figure 6.3.3: Outlier plot of strain at break values before and after post-curing

6.3.3 ANOVA

Table 6.3.1 shows the results of the ANOVA. As it can be observed, the *F*-value is very high, while the *p*-value is much lower than 0.05. This means that the two groups, the post-cured and the non-post cured elastomers, are different.

Table 6.3.1: Results of the ANOVA of the strain at break

Analysis of Variance

Source	DF	Adj SS	Adj MS	F-Value	P-Value
Туре	1	54760	54759,9	64,85	0,000
Error	110	92887	844,4		
Total	111	147647			

Table 6.3.2 shows the model summary of the ANOVA. The coefficient of determination R^2 is 37.09%, indicating that the model represents only a small portion of the data variability. The same considerations done for the stress at break are valid.

Table 6.3.2: Model summary of the ANOVA of the strain at break

Model Summary

S	R-sq	R-sq(adj)	R-sq(pred)
29,0590	37.09%	36,52%	31.88%

Figure 6.3.4 shows the residual plots for the stress at break. As it can be seen, in the normal probability plot (top left) the points follow a straight line and the histogram plot (bottom left) has a bell shape: this means that normality is respected. In the versus fits plot (top right) the points are randomly distributed around zero: this means that residuals variance is constant. Finally, in the versus order plot (bottom right) the points are randomly distributed around zero: this means that time independence is respected.

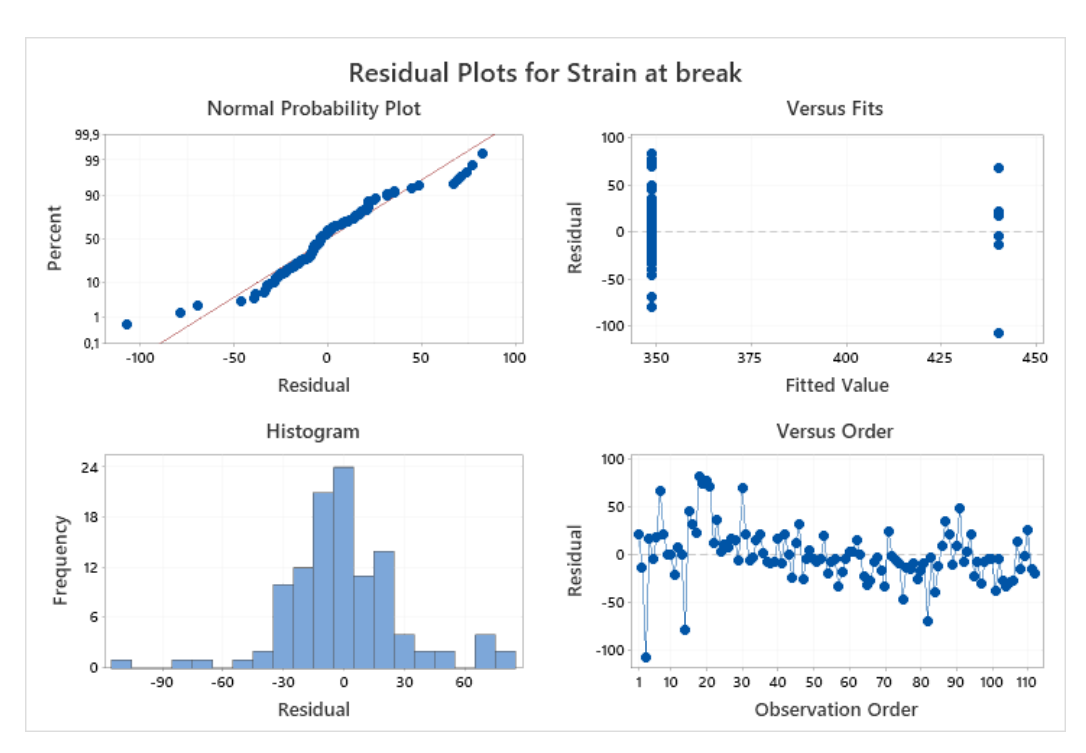


Figure 6.3.4: Residual plot for the strain at break

6.4 Tear test: tear strength at break

6.4.1 Descriptive statistics

Figure 6.4.1 shows the boxplot of tear strength at break values measured in laboratory before and after post-curing. As it can be seen, after the post-curing, the tear strength at break values are lower.

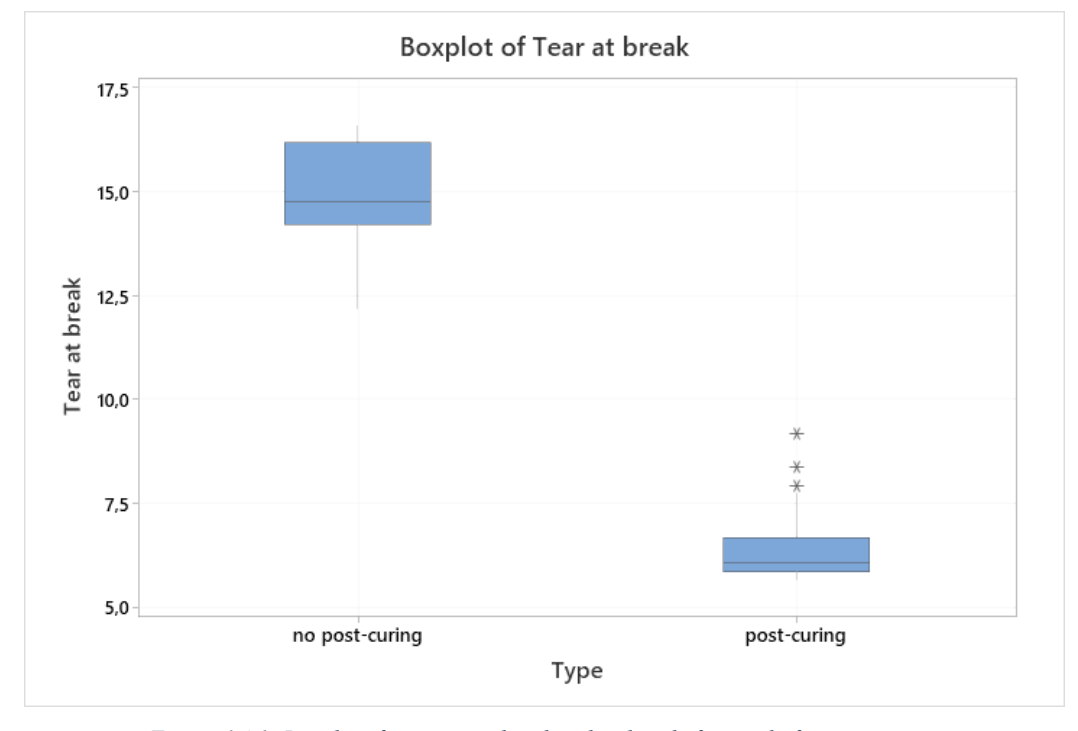


Figure 6.4.1: Boxplot of tear strength at break values before and after post-curing

Figure 6.4.2 shows the dotplot of tear strength at break values measured in laboratory before and after post-curing.

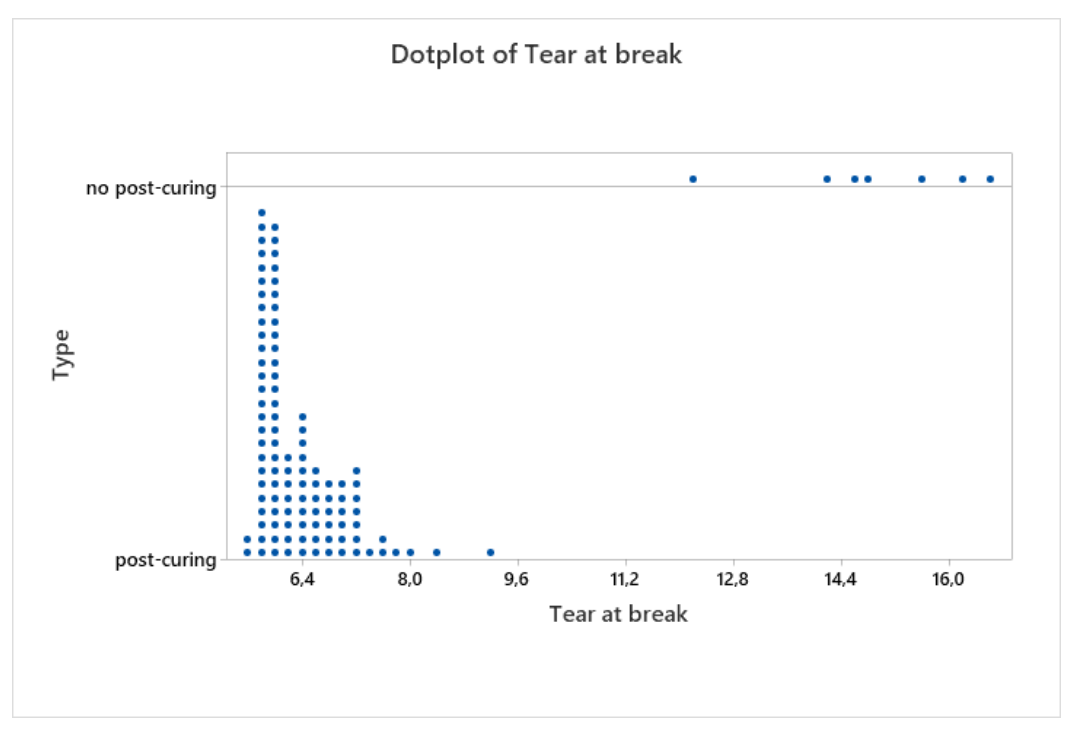


Figure 6.4.2: Dotplot of tear strength at break values before and after post-curing

6.4.2 Outlier identification

The Grubbs' test to identify outliers is carried out before proceeding with ANOVA. Figure 6.4.3 shows the outlier plot of tear strength at break values before and after post-curing: as it can be seen, only one outlier is found by the test in the post-cured group. Before proceeding with the ANOVA, the outlier is replaced by the median of the other values in the same group.

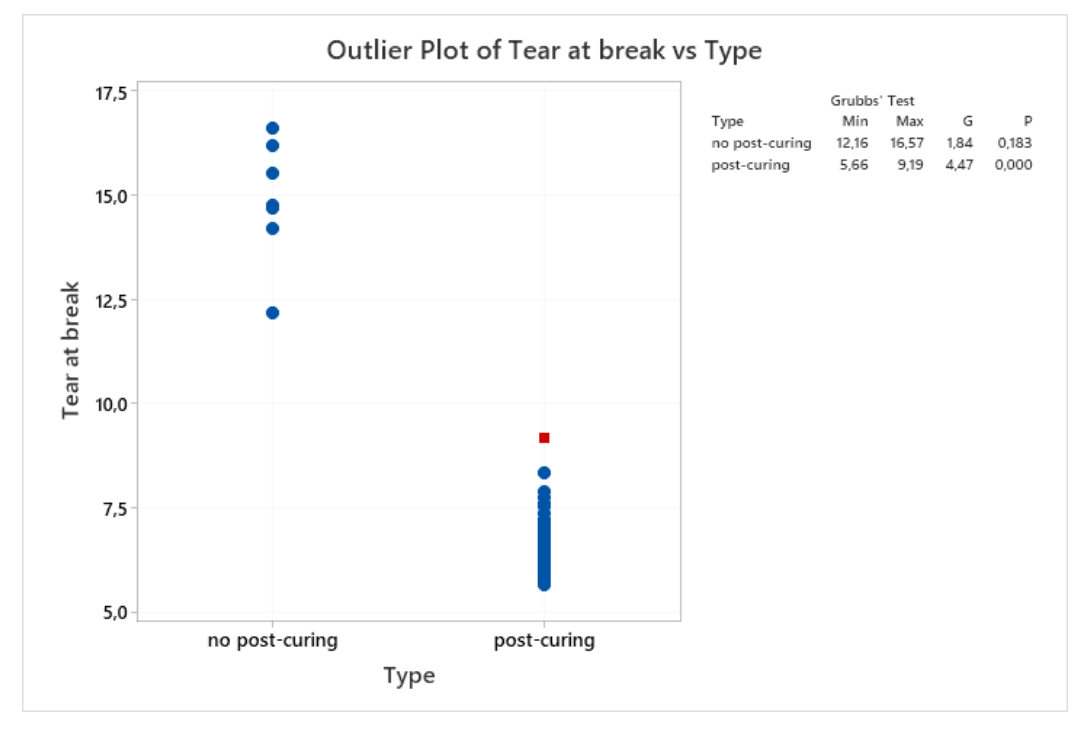


Figure 6.4.3: Outlier plot of tear strength at break values before and after post-curing

6.4.3 ANOVA

Table 6.4.1 shows the results of the ANOVA. As it can be observed, the *F*-value is very high, while the *p*-value is much lower than 0.05. This means that the two groups, the post-cured and the non-post cured elastomers, are different.

Table 6.4.1: Results of the ANOVA of the tear strength at break

Analysis of Variance

Source	DF	Adj SS	Adj MS	F-Value	P-Value
Туре	1	478,06	478,062	1129,19	0,000
Error	110	46,57	0,423		
Total	111	524,63			

Table 6.4.2 shows the model summary of the ANOVA. The coefficient of determination R^2 is 91.12%, indicating that the model represents most of the data variability.

Table 6.4.2: Model summary of the ANOVA of the tear strength at break

Model Summary

S	R-sq	R-sq(adj)	R-sq(pred)
0,650668	91,12%	91,04%	90,12%

Figure 6.4.4 shows the residual plots for the strain at break. As it can be seen, in the normal probability plot (top left) the points follow a straight line and the histogram plot (bottom left) has a bell shape: this means that normality is respected. In the versus fits plot (top right) the points are randomly distributed around zero: this means that residuals variance is constant. Finally, in the versus order plot (bottom right) the points are randomly distributed around zero: this means that time independence is respected.

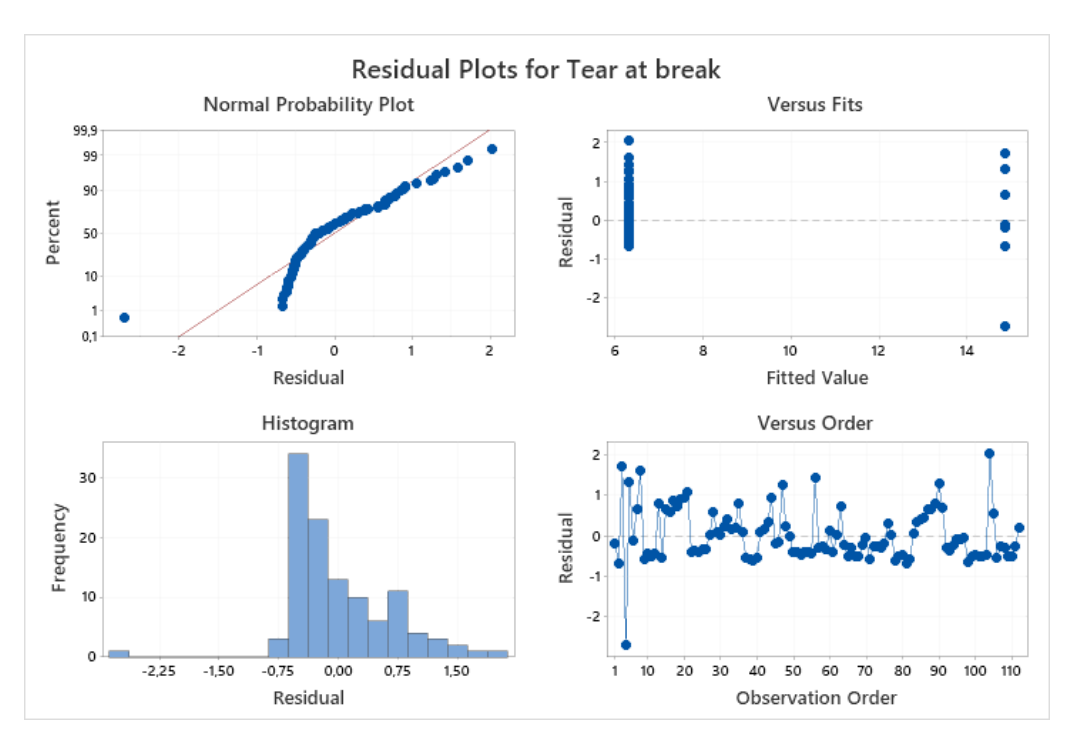


Figure 6.4.4: Residual plot for the tear strength at break

7 Conclusions

AGLA Power Transmission is working on a project to produce advanced tyres for motorcycle sector, in particular for enduro races, without an inner tube, with an anti-puncture system and able to guarantee a long life with a view to the circular economy.

The aim of this thesis was to characterise the mechanical properties of an elastomeric compound which could be used to produce the tyre.

The mechanical properties of the elastomers have been measured in laboratory through hardness Shore test, tensile test and tear test and they have been analysed performing the analysis of variance to investigate if they are affected by the position of the tube inside the oven and by the position of the ring inside the tube.

The laboratory tests allowed to measure the mechanical properties only in specific positions, but it would be useful to know how the mechanical properties behave in each point of the oven for each ring. To solve this problem, the response surface regressions have been carried out: in this way, the equations which correlate the mechanical properties to the position and to the ring have been retrieved and it is possible to know which are the position and the ring which maximise or minimise a mechanical property or allow to reach a target value.

The results of the analysis of variance show that the hardness is affected by both the position of the tube inside the oven and the position of the ring inside the tube. According to the response surface regression, the maximum value of hardness is expected to be near the middle centre right position in the second ring, while the minimum value is expected to be in the front down left position in the seventh ring.

The tensile stress at break is affected by neither the position of the tube inside the oven and the position of the ring inside the tube.

The tensile strain at break is affected by the position of the tube inside the oven, but not by the position of the ring inside the tube. The maximum value of strain at break is expected to be in the front down left position, while the minimum value is expected to be near back centre middle position.

The tear strength at break is affected by both the position of the tube inside the oven and the position of the ring inside the tube. The maximum value of tear strength at break is expected to be in the front down left position in ring the seventh, while the minimum value is expected to be near back centre middle position in the second ring.

Moreover, hardness, tensile strain at break and tear strength at break seems to be correlated to temperature. Increasing the temperature, the sulphur atoms form more crosslinks between the long rubber polymer chains. The hardness increases because the chains become more compact. The tensile strain at break decreases because the chains movement is limited and they break earlier. The tear strength decreases because the chains movement is limited, the initial cut propagates more easily and the chains break earlier. In fact, in the front of the oven, where there is the door and so the temperature is lower, the hardness reaches the lowest values, while the tensile strain at break and the tear strength at break reach the highest values. On the contrary, on the back and in the centre, where the temperature is higher, the hardness reaches the highest values, while the tensile strain at break and the tear strength at break reach the lowest values.

Finally, the post-curing effect is analysed by comparing the mechanical properties of the elastomers before and after entering the oven. As during post-curing the sulphur atoms form more crosslinks between the rubber polymer chains, the hardness and the tensile stress at break increase, while the tensile strain at break and the tear strength at break decrease. It is possible to change the duration of post-curing to change the mechanical properties.

The research carried out in this Master's thesis will be useful for the company to produce enduro motorcycle tyres instead of ring specimens, but with the same procedure.

The next steps will be to design the geometry of the tyres, to carry out some FEM simulations to analyse their behaviour and to use the results of this thesis to obtain EPDM with suitable mechanical properties. Indeed, from the laboratory tests, in particular form the tensile test, it is possible to retrieve the coefficients of the Mooney-Rivlin model which describes the behaviour of the rubber under tension and compression loads. Once the drawing of the tyre and the Mooney-Rivlin coefficients are obtained, it is possible to simulate the behaviour of the tyre under tension and compression using a FEM software.

8 References

- [1] LBN Ricerca, https://www.lbnricerca.com, 10 July 2025.
- [2] AGLA Power Transmission, https://aglapowertransmission.com, 10 July 2025.
- [3] Bottino Girardi, https://bottinogirardi.com, 10 July 2025.
- [4] "Butyl Rubber: A Techno-commercial Profile," Chemical Weekly, 3 November 2009.
- [5] R. Missel, "How to Use Tubeless Tire Sealant," *Bicycling*, 19 November 2021.
- [6] R. Rugsaj and C. Suvanjumrat, "Revolutionizing tyre engineering: Finite element analysis and design of an X-shaped spoke structure for non-pneumatic military tires," *ScienceDirect*, p. 303.
- [7] J. Jafferson and H. Sharma, "Design of 3D printable airless tyres using NTopology," *ScienceDirect*, pp. 1147-1151, 27 February 2021.
- [8] Y. Deng, Z. Wang, H. Shen, J. Gong and Z. Xiao, "A comprehensive review on non-pneumatic tyre research," *ScienceDirect*, pp. 10-20, 16 February 2023.
- [9] "Run-Flat Mousse Tyres In Detail Motorsport.com," Wayback Machine, 6 June 2011.
- [10] ISO, "ISO 48-4 Rubber, vulcanised or thermoplastic Determination of hardness Part 4: Indentation hardness by durometer method (Shore hardness)," *BSI Standards Publication*, 31 August 2018.
- [11] DIN, "DIN 53504 Testing of rubber Determination of tensile strength at break, tensile stress at yield, elongation at break and stress values in a tensile test," October 2009.
- [12] ISO, "ISO 34-1 Rubber, vulcanised or thermoplastic Determination of tear strength Part 1: Trouser, angle and crescent test pieces," *BSI Standards Publication*, 27 June 2022.
- [13] P. S. Ravishankar, "Treatise on EPDM," Rubber Chemistry and Technology, 2012.
- [14] G. Barbato, A. Germak and G. Genta, Misurare per decidere. Misure e statistiche di base, Società Editrice Esculapio, 2019.
- [15] D. C. Montgomery, Introduction to statistical quality control, John Wiley & Sons, 2020.
- [16] F. Grubbs, "Sample criteria for testing outlying observations," *Annals of Mathematical Statistics*, 18 July 1950.
- [17] Statistics How To, https://www.statisticshowto.com/grubbs-test/, "Grubbs' Test for Outliers (Maximum Normed Residual Test)," 18 July 2025.
- [18] Minitab Support, https://support.minitab.com/en-us/minitab/help-and-how-to/statistical-modeling/doe/how-to/response-surface/analyze-response-surface-design/interpret-the-results/all-statistics-and-graphs/regression-equation/, "Regression equation for Analyze Response Surface Design," *Minitab Support*, 6 August 2025.